공학박사 학위논문

Advanced Viewing-Angle and Coloration Technologies for High-Performance Liquid Crystal Displays

차세대 액정 디스플레이용 광시야각 및 칼라구현 기술에 관한 연구

2017 년 8 월

서울대학교 대학원

공과대학 전기·컴퓨터공학부

서 정 훈

Advanced Viewing-Angle and Coloration Technologies for High-Performance Liquid Crystal Displays

지도 교수 이 신 두

이 논문을 공학박사 학위논문으로 제출함
2017 년 8 월

서울대학교 대학원
공과대학 전기 · 컴퓨터공학부
서 정 훈

서정훈의 공학박사 학위논문을 인준함
2017 년 6 월

위 원 장 _____ 이 병 호 _____ (인)

부위원장 _____ 이 신 두 _____ (인)

위 원 _____ 정 윤 찬 _____ (인)

위 원 _____ 유 창 재 _____ (인)

위 원 _____ 나 준 희 _____ (인)

Abstract

In the past decades, liquid crystal display (LCDs) have been extensively studied for use in flat panel displays (FPDs) because of light weight panel, thin thickness and low power consumption. Due to their high contrast, uniform brightness, and rapid switching times compared to conventional cathode ray tubes, LCDs have achieved a significant position in the FPD industry. However, according to the development of other FPD technologies including organic light-emitting didoes, the enhancement of LCD performances such as wide-viewing angle and vivid coloration has been demanded.

In this thesis, novel image generation technologies for high performance LCD are proposed. At first, for the reduction of the gamma distortion, wide-viewing technology was demonstrated by sophisticated multi-domain configuration in which liquid crystal (LC) molecules are aligned along different polar directions at middle gray scale. In order to realize the multi-domain LC cell, a new alignment layer which can control polar LC alignment properties including the pretilt angle and the anchoring energy was developed. Uncured hydrophobic oligomers in a cross-linked polymer mold were

transferred onto a substrate to change the surface wettability of the substrate. The thermal-transfer printing, which is a contact-transfer printing method including an additional heat treatment process, accelerated the molecular diffusion of oligomers from the polymer mold onto the substrate, resulting in the increase of the amount of transferred oligomer. Consequently, the surface energy of the substrate was manipulated according to the heat treatment temperature during the thermal-transfer printing. Then, the LC alignment properties in both azimuthal and polar directions were measured through LC cell fabrication and electro-optical characterization. It was found that the polar pretilt angle and polar anchoring energy were changed in a wide-range, resulting from the adjustment of the substrate surface energy.

Based on the results described above, the reduction of the gamma distortion through the multi-domain configuration in the vertical alignment (VA) mode was demonstrated. The oligomer layer was formed onto a conventional VA alignment layer to control the polar alignment properties. The ultra-violet ozone (UVO) treatment for the enhancement of the oligomer transfer onto hydrophobic substrates was added in the fabrication process. The surface energy and anchoring energy of the stacked alignment layers depending on the UVO treatment was examined. The anchoring disparity, which is the anchoring energy difference between sub-domains as a result of the oligomer layer patterning, induced the threshold voltage difference in the sub-domains and constructed the multi-domain at applied voltages. The experimental measurements for the assessment of the gamma distortion were performed in a conventional patterned VA mode cell and proposed multi-

domain cell.

Next, for the expansion of the color space, a new type of coloration technique based on the photo-luminescent emission of the quantum dots (QDs) in an organic polymer matrix was described. Recently, QD patterning technologies based on the polymer matrix have been extensively studied to accurately express the primary color in pixel units, but suffered from the non-uniform light emission owing to uneven distribution of the QDs in the polymer matrix. Reactive mesogen (RM), which is photo-curable, transparent, and soluble in organic solvents, was used for the fabrication of uniformly distributed QDs in the RM matrix. The emission characteristics of QD-RM composites depending on the concentration ratios of QD and RM were examined. In addition, color-separated patterns of QD-RM composites on a single substrate through conventional photo-lithography processes were demonstrated.

Finally, a novel QD emissive LCD based on the color-separated pattern for high color purity was proposed. The proposed LCD consists of modulation part and emission part. LC cells acts as a role of electrically tunable lightwave retarder depending on the applied voltage. The transmitted light through the modulation part emits the photo-luminescent light from the color-separated QD pattern. The color purity and color gamut of the QD emissive LCD was measured in comparison with previous LCDs such as the color filter LCD and QD compensated LCD.

In conclusion, the applicability of proposed image generation technologies to the FPD industry was explored. The new concepts and experimental results

will lead to the development of the advanced LCD performance.

Keywords: liquid crystal, wide-viewing angle display, gamma distortion, quantum dot, quantum dot in polymer matrix, color gamut, quantum dot display.

Student number: 2012-30937

Contents

List of Figures

List of Tables

Chapter 1

Introduction

1.1 Overview of Flat Panel Displays

Flat panel displays (FPDs) are electronic viewing technologies used to enable to show contents (text, photograph, video, or other visual material) in a range of entertainment, consumer electronics, personal computer, and mobile devices, and many types of medical, transportation and industrial equipment [1]. The FPDs are far lighter and thinner than traditional cathode ray tube (CRT) television sets and are usually less than 10 centimeters (3.9 in) thick. Digital technology takes part in TV processing units and displays, with the development of flat panel displays screen sizes bigger than 42 inch, which could not be realized with CRT become feasible. The advantages of FPD over CRT can be described as larger screen size, higher resolution, smaller volume,

lower weight, compatibility with digital and high resolution video interfaces. The market for FPDs is increasing day by day.

Current market forecast of flat panel display

Figure 1.1. Flat panel display (FPD) market revenue (actual and forecast) [2].

The global FPD market has been steadily growing since 2000 as shown in Fig. 1.1 [2]. This gradual increase of the market size until 2008 results from the various advantages of FPD over the conventional CRT. The market growth have rebounded from 2009 caused by the global recession of 2009 and are showing the positive signs of longer-term sustainability until 2020. After two consecutive decline years, FPD revenues is expected to soar by 7.5 percent year-over-year in 2017 to $129 billion.

However, as might be expected, the display landscape has changed in the meantime. New display technologies, resolutions, product features, and form factors are now available. In order to determine the future direction of FPD,

many display companies are asking themselves which will be the driving forces behind this growth and which FPD technologies will hold the most promise.

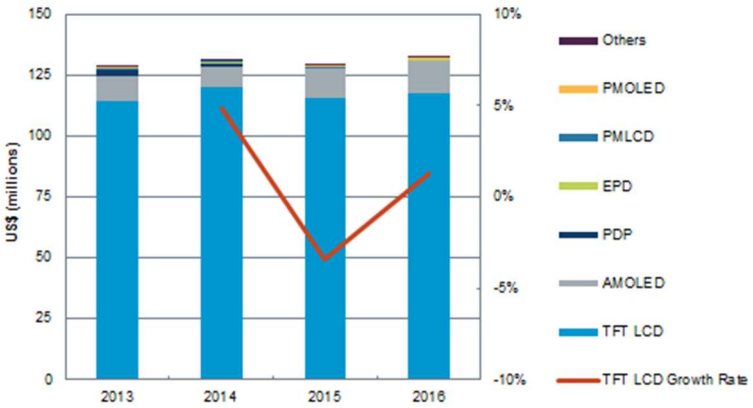

Figure 1.2. FPD market revenues depending on technologies and market growth rate of thin film transistor (TFT)-liquid crystal display (LCD) [3].

Figure 1.2 shows the market revenues of the FPD depending on technologies and the market growth rate of the thin film transistor (TFT)-liquid crystal display (LCD). Now that commercial plasma displays are no longer being manufactured, TFT-LCDs are the dominant technology have more than 80% of the market share, and earn more than $110 million as shown in Fig. 1.2. This direct-view flat-panel technology has become relatively affordable and readily available, due to the significant price erosion that has occurred over the last several years and to rapid adoption by the consumer television market.

However, the future of the TFT-LCD industry is not very optimistic. The growth rate of TFT-LCDs has been saturated and it shrink to -2.5% in 2015. The main cause of the suppression of the increase in TFT-LCD industry is the growth of the organic light-emitting diode (OLED) market based on the rapidly growing the OLED technology. Active-matrix (AM) OLED revenues reached $11.8 billion in 2015 up 36 percent from 2014 and passive-matrix (PM) OLED reached $450 million in 2015 up 22 percent from 2014. This is, the FPD industry currently locates in a transitional state between LCD technologies and OLED technologies. Now, let major FPD technologies such as LCD and OLED be discussed in following paragraph.

Liquid crystal displays

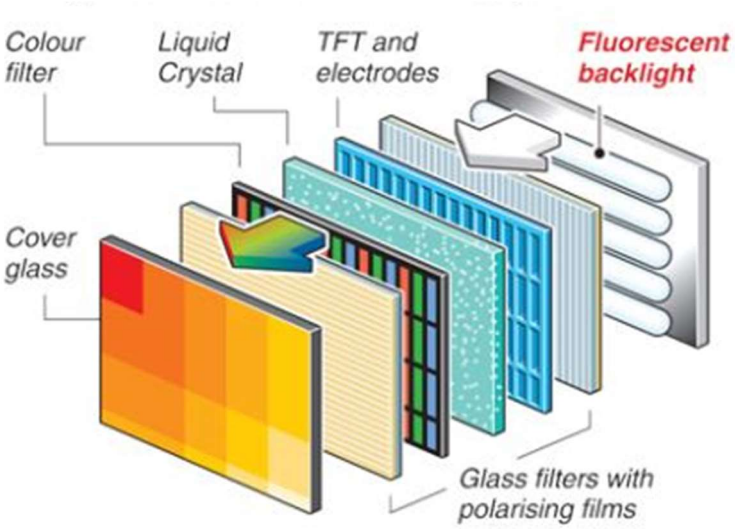

Figure 1.3. Schematic diagram of a LCD [4].

LCD is a kind of FPD technologies and an electronically modulated optical device that uses the light-modulating properties of liquid crystal material [4]. LCDs do not emit light directly, instead, produce images using a backlight or reflector in color or monochrome as shown in Fig. 1.3. Since LCDs do not use phosphors, they do not suffer image burn-in when a static image is displayed on a screen for a long time (e.g., the table frame for an aircraft schedule on an indoor sign). LCDs are, however, susceptible to image persistence. The LCDs are more energy-efficient and can be disposed of more safely and its low electrical power consumption enables it to be used in battery-powered electronic equipment more efficiently. LCDs are lightweight, compact, portable, cheap, more reliable, and easier on the eyes. LCDs use a thin layer of liquid crystal which is sandwiched between two electrically conducting plates. The top plate has transparent electrodes deposited on it, and the back plate is illuminated so that the viewer can see the images on the screen. By applying controlled electrical signals across the plates, the alignment direction of the liquid crystal can be controlled, resulting in changes in light polarizing properties. As a result, LCDs can either transmit or block the backlight. The operating mechanism of LCDs will be discussed in detail in chapter 2.1.

LCDs are categorized according to the type of the backlight unit (BLU). Conventional LCDs uses the cold cathode fluorescent backlight (CCFL) [5-7] as shown in Fig. 1.3. In recent year, LCDs using light emitting diodes (LEDs) as BLU [8, 9] instead of CCFLs have been developed for more narrow thickness. The LCD using LED BLU use the conventional TFT-LCD

technologies except BLU. Image quality is primarily based on TFT-LCD technology, independent of BLU type so that image qualities of two types LCD show the same image qualities. While TFT-LCD using LED BLU is not an intrinsic LED display in the operation principle, this display is called an LED TV in the FPD industry.

Organic light-emitting diode

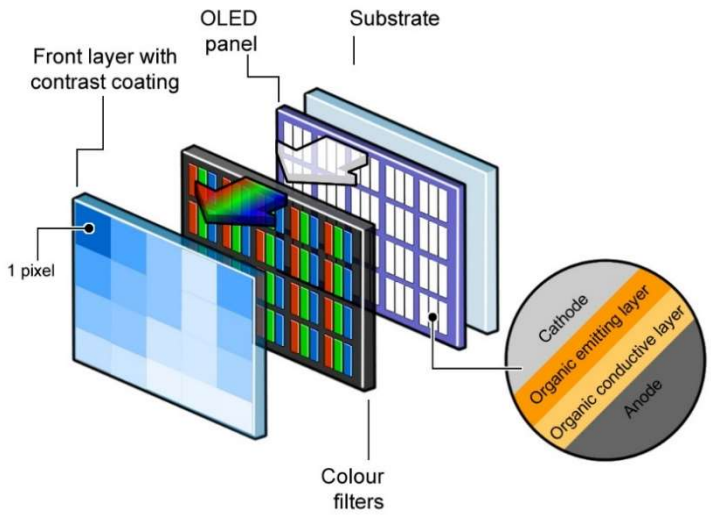

Figure 1.4. Schematic diagram of a white organic light-emitting diode (W-OLED) [10].

An OLED is a LED in which the emissive electroluminescent layer is a film of organic compound that emits light in response to an electric current [10]. This layer of organic semiconductor is situated between two electrodes; typically, at least one of these electrodes is transparent.

Depending on generation method in the primary colors including red (R), green (G), and blue (B), OLEDs can be classified into RGB OLEDs and white OLEDs (W-OLED). In the case of the RGB OLED, light emitting materials having different emission wavelengths are patterned on a single substrate to implement the primary colors. In this case, although it has an advantage of extracting a desired light of high purity, it is difficult to make the pattern on a large substrate. Therefore, W-OLED technology using a color filter and unifying the emission material without patterning process has been actively studied in the FPD industry. However, in the case of the W-OLED, since the color filter used in the same manner as the conventional LCD, the color purity has been degraded comparable to that of RGB OLED. In addition to this, there is a problem in color stability owing to the change in color coordinates depending on operating time based on unstable emission materials.

With this problem, the current FPD industry is in a transitional position between LCD and OLED technologies. Let LCD and OLED be compared in the next paragraph.

Comparison of LCDs and OLEDs

FPD can be considered to be divided into only two parts such as LCDs and OLEDs. Table 1.1 shows the comparison of LCDs and OLEDs in various fields. The biggest difference between LCDs and OLEDs is the type of the device. Since the LCD is the transmission type device, it is inferior in performance from emission type OLED to response time, power, viewing angle and contrast. The colorations in both technology show similar performance owing to color filters. However, from the lifetime to price, LCDs

	LCD	OLED
Type	Transmission type	Emissive type
Response time	30 ms	1 μs
Power	High	Low
Viewing angle	Limited	Unlimited
Contrast ratio	LCD < OLED	
Coloration	BLU & color filter	W-OLED & color filter
Lifetime	60,000 hour	25,000 hour
Fabrication process	LCD < OLED	
Price	LCD < OLED	
Flexibility	Low	High

Table 1.1. The comparison of LCDs and OLEDs.

have advantages over OLED in terms of price and products. Such a market share competition based on the gap between performance and price is expected to be maintained until the appearance of a new killer application such as a flexible or transparent display. Therefore, at present, there is a need for a technology capable of improving the performance of LCD until the OLED manufacturing cost fall to LCD cost level.

1.2 Outline of Thesis

This thesis contains five chapters. In Chapter 1, recent global trend of FPD industry and several FPD such as LCD and OLED are introduced.

In Chapter 2, the emerging technologies of the LCD industry are discussed. At first, the operating principle and mode of the LCD device are described. Among various LC modes, vertical alignment (VA) mode, which is one of the most widely used in FPD and is the subject of this thesis, is discussed about the pros and cons in compassion to other modes. The viewing angle and color generation technologies which are typical weak points of VA mode are theoretically considered and recent studies to overcome these problems are introduced.

In Chapter 3, the wide-viewing angle technique of LCD is demonstrated by multi-domain construction in which LC molecules are arranged in different polar directions at middle grey scale. In order to realize this, a new alignment layer which can control the polar anchoring energy is developed. Uncured oligomers in cross-linked polymer are transferred onto substrate to change the surface wettability of the substrate. Since oligomers are transferred onto the substrate through diffusion, the amount of transferred oligomers are changed by additional heat treatments, the thermal-transfer printing, during the oligomer diffusion. During the thermal-transfer printing, the amount of transferred oligomer according to the heat treatment temperature are examined. Then, I studied how the LC molecules are aligned in the direction

on the transferred oligomer layer through the fabrication of the LC cell. The crystal rotaion (CRM) method are used to measure the pretilt angle of LC molecules on transferred oligomer layer. The polar anchoring energy between the LC molecules and the substrate was measured by the high-electric technique. Through this, a correlation between the surface energy of the substrate and alignment properties of LCs is shown.

Next, using developed alignment layer of which the polar anchoring energy can be manipulated in a wide range, a new multi-domain LCD based on the anchoring disparity in polar direction for reducing the gamma distortion is demonstrated. The additive layer acts as a role of anchoring energy control for shifting the threshold voltage in sub-domain and is capable of spontaneously aligning the LC molecules without the change of the pretilt angle. The threshold difference compensates the difference of the phase retardation between the normal and an oblique viewing direction, which results in the reduction of the gamma distortions. The alignment property of LC on the anchoring energy control layer depending on the ultra-violet ozone (UVO) treatment for the enhancement of amount of transferred oligomer from cross-linked polymer is examined. The experimental measurement for the assessment of the gamma distortion were performed in the 4-domain cell of patterned vertical alignment (PVA) mode and 8-domian cell of proposed cell structure.

In Chapter 4, a new type of color LCD based on the photo-luminescent emission of the quantum dots (QDs) in polymer matrix is described. Various QD patterning techniques based on polymer matrix have been developed to

make primary colorations in pixel units, but color filters were needed owing to non-uniform light emission. In contrast with previous approaches, reactive mesogen (RM), which is photo-curable, transparent and molecular aligned, is used for construction of polymer matrix to completely dissolve the quantum dots. The emission characteristics of the QDs are measured by changing the concentration ratios of QD and RM. In addition, color-separated patterns on a single substrate through applying conventional photo-lithography process are demonstrated.

Next, a novel QD emissive LCD based on the color-separated QD pattern for high color purity is proposed. The QD emissive LCD consists of the VA mode LC cells and a light source on bottom of the structure. The LC cell acts as a role of tunable light modulator for the incident light from the light source depending on the applied voltage. In front of the QD emissive LCD, the photo-luminescent light of QD is emitted in certain pixels of which the source light is transmitted through LC modulator. In end of this chapter, the color purity and color gamut of QD emissive LCD was measured compared to the previous researches where the color filters and QD compensation layers are placed in front of the cell.

Finally, the summary and some concluding remarks are made in Chapter 5.

Chapter 2

Emerging Technologies of Liquid Crystal Display

2.1 Operating Principles of LCD

In LCD devices, the basic components of a LCD consist of a thin layer of LC sandwiched between a pair of polarizers. To control the optical transmission of the display element electronically, the LC layer is placed between transparent electrodes [e.g., indium thin oxide (ITO)]. The minimum thickness of a few millimetre is needed to maintain the structural integrity of the panel. The thickness of the LC layer is kept uniform by using spacers that are made of glass fibers or plastic microspheres. By applying a voltage across the electrodes, an electric field inside the LC can be obtained to control the

transmission of light through the LC cell. To achieve the display of information, a two-dimensional array of these electrodes is needed. These electrodes can be driven electrically for data input by using two sets (x, y) of parallel array of electrodes. In what follows, we will briefly describe each of the optical components.

2.1.1 Properties of LCs

Liquid crystal

LC is a mesomorphic state which is intermediate between a crystalline solid and an amorphous liquid [11], or simply means a matter in such state. It has a directional order like a crystalline solid as well as some degree of fluidity like a liquid. Today, a large number of organic compounds are known to form the LC. Generally, LCs are categorized into three types by the mechanism for the phase transition: thermotropic, lyotropic, and metallotropic. Thermotropic LCs exhibit a phase transition into the liquid crystal phase as temperature is changed. Lyotropic LCs exhibit phase transition depending on both the temperature and the concentration of the LCs in a solvent. Metallotropic LCs are composed of both organic and inorganic molecules and their phase transition depends not only on the temperature and the concentration, but also on the composition ratio of inorganic-organic molecules. Since thermotropic, rod-like materials are mainly used in the LCDs, only these LC materials will be discussed in this thesis.

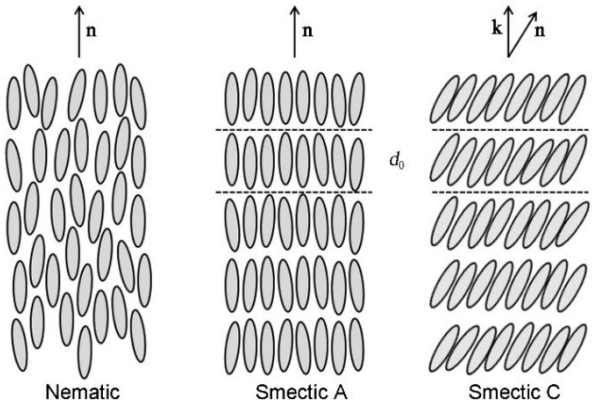

Figure 2.1. Schematic illustration of nematic, smectic A, and smectic C phases.

Since LCs have a certain order of molecular arrangement, they exhibit strong electrical and optical anisotropy which is not observed in other fluids. For instance, LCs change their orientation according to the direction of the applied electric field. The optical anisotropy of LC can be described by two local axes (long and short). Those local axes yield the different optical pathway between the polarization components along each axis. In general, sandwich-type cells consisting of two glass substrates deposited with an alignment layer and LCs between them are provided for examining the intrinsic properties of the LCs. In those LC cells, the alignment of the LC is governed by physical and chemical effects of the alignment layers so that the LC has the preferred orientations. The LC can be re-oriented by the external electric filed applied across the substrates. The reorientation of LC gives a change in the optical properties of the LC cell. This is the basic operation

principle of practical LC devices. Due to the large optical anisotropy and simplicity in electrical tuning capability, LCs have been widely used and studied in numerous fields.

The various LC phases can be characterized by the type of ordering. LCs can have two types of order: orientational order and positional order. Moreover, such orders can exist in either short-range or long-range. Most thermotropic LCs have an isotropic phase at high temperature. It means that the LC phase will be diminished by heating and eventually it changes into an isotropic phase at the temperature over clearing point. Under the lower temperature, the crystallinity of LC become stronger so that the one or more LC phase can be observed with an anisotropic orientation of molecules. Several LC phases are described in Fig. 2.1. Among these LC phases, nematic phase which has intrinsic simple structure and wide operation temperature is widely used as polarization tunable layers in LCDs.

Nematic phase

Nematic phase possesses an orientational order, but no positional order in a long range. It means that the molecular centers of mass are randomly distributed throughout the medium. In nematic phase of the rod-like LC, the long axes of molecules are aligned on average to a particular direction. Therefore, nematic phase is optically uniaxial. The average direction of LC is often called as director and it can be indicated by a global vector **n**. The degree of order in nematic phase is given by the order parameter *S* [12, 13],

$$S = \left\langle \frac{3}{2}\cos^2\theta_p - \frac{1}{2} \right\rangle \tag{2.1}$$

where θ_p is the deviation angle of individual molecules from the director. Isotropic liquids have $S = 0$ and crystalline solids with a perfect orientational order have $S = 1$. LCs in nematic phase typically have $0.5 < S < 0.7$. The order parameter of the LC decreases as the temperature increases.

Dielectric constant

Because of the orientational ordering of rod-like molecules, the smectic and nematic LCs are uniaxially symmetric, with the axis of symmetry parallel to the axes of the molecules. As a result of the uniaixial symmetry, the dielectric constants differ in value along the preferred axis ($\varepsilon_{\parallel}$) and perpendicular to this axis ($\varepsilon_{\perp}$). The dielectric anisotropy is defined as

$$\Delta\varepsilon = \varepsilon_{\parallel} - \varepsilon_{\perp} \tag{2.2}$$

The sign and magnitude of the dielectric anisotropy $\Delta\varepsilon$ are of the utmost importance in the applicability of LC material in LCDs using one of the various electro-optic effects.

Refractive index

In a glass flask, nematic LCs often appear as an opaque milky fluid. The scattering of light is due to the random fluctuation of refractive index of the sample. With no proper boundaries to define the preferred orientation, the sample consists of many domains of nematic LC. The discontinuity of the refractive index at domain boundaries is the main cause of the scattering leading to the milky appearance. Under the proper treatment (e.g., rubbing the alignment layer on the glass substrate), a slab of nematic LC can be obtained

with a uniform alignment of the director. Such a sample exhibits uniaxial optical symmetry with two principal refractive indices n_o and n_e. The ordinary refractive index n_o is for light with electric field polarization perpendicular to the director and the extraordinary refractive index n_e is for light with electric field polarization parallel to the director. The birefringence (or optical anisotropy) is defined as

$$\Delta n = n_e - n_o \tag{2.3}$$

If n_o<n_e, the LC is said to be positive birefringent, whereas if If n_o>n_e, it is said to be negative birefringent. In classical dielectric theory, the macroscopic refractive index is related to the molecular polarizability at optical frequencies. The existence of the optical anisotropy is due mainly to the anisotropic molecular structures. The optical anisotropy plays an essential role in changing the polarization state of light in LCs.

Surface alignment

By the influence of the alignment film on the substrates, LC molecular orientations are determined. These orientations are classified into two groups. The directors of the liquid crystal molecules in the homogeneous, tilted and homeotropic cases are aligned in one fixed direction, while the director of the liquid crystal molecules in the splay, twist, bend, hybrid and super-twisted nematic cases are not fixed in one direction. In the latter orientations, the liquid crystals are under stress.

The LC molecules align parallel to the substrate in the homogenous and

perpendicular to the substrates in the homeotropic alignments as shown in Fig. 2.2. Tilted alignment is an intermediate state between homogeneous and homeotropic, and the molecules are tilted at a certain pretilt angle. Actually, the tilted alignment with low pretilt angle (less than 10°) is often called homogenous. In the hybrid alignment, the liquid crystals on one substrate have homogeneous alignment and those on the other substrate homeotropic alignment.

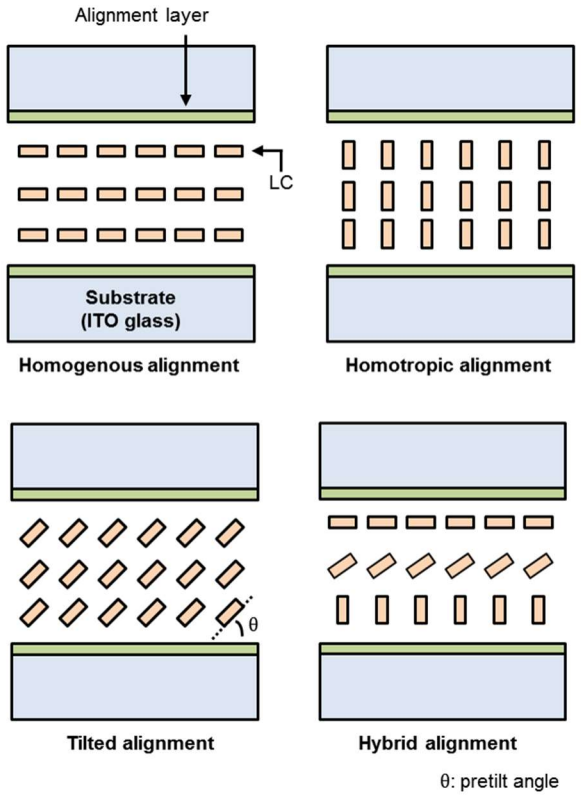

Figure 2.2. Typical orientations of nematic liquid crystals.

In order to obtain homogeneous alignment including the tilted alignment with less than about 10°, rubbed polyimide films are usually used in mass production. Non-rubbing methods such as photo-alignment and those using microgrooves have been developed. Homeotropic alignment is obtained by substrates coated with hydrophobic films such as silane compounds. Recently, polyimide films with hydrophobic side chains have been developed and used in the multi-vertical aligned nematic mode. The liquid crystal molecules near the substrate surface affect the LC orientation in the bulk (in the middle of a LC cell) by molecular-molecular interactions, and the orientation in the entire liquid crystal cell is so determined. In most cases, the interaction between the substrate surface (alignment layer) and the LC molecules near the surface is very strong. By the application of electric or magnetic fields, the alignment of LCs near the substrate is hardly changed. Such a relationship between the substrate surface and the LCs is called strong anchoring. In the case of the strong anchoring, after removing the electric or magnetic field, the LC orientation recovers to that of the initial orientation. In contrast, when LC orientation after removing the field is different from the initial orientation, the relationship is called weak anchoring.

In the following chapter, I will discuss about the LCD mode which depends on the LC molecular alignment direction. LCD modes dominate diverse electro-optical properties range from the threshold voltage, response time, power consumption, and transmittance.

2.1.2 Main LCD modes

Nowadays, LCDs based on nematic LCs are widely used for watches, calculators, cellular phones, and display monitors in personal computers, TV screens and so on. Although the LC state was discovered in 1888, it was 80 years before the first LCD was developed. In 1968, Heilmeier et al. [14] first applied the dynamic scattering effect to LCDs. After this application, many electro-optic effects of LCs were discovered and many applications to display devices were developed. The twisted nematic (TN), the most widely used LCD mode, was invented by schadt and Helfrich in 1970 [15]. TN displays provide a high contrast ratio, analog grey scale and low driving voltage. Especially, the twisted nematic LCD combined with an array of TFTs, the TN mode TFT-LCD produces a high quality full color display, and is used for high information content displays such as computer monitors and TV.

Typical display modes using nematic LCs are classified into three groups; TN mode, in-plane switching (IPS) mode, and vertical alignment (VA) mode. The important display modes from the viewpoint of applications and alignment techniques are described in more detail in the following sections.

TN mode

The TN is the most widely used LCD mode for applications ranging from watches to computer monitors. The advantages of the TN mode are high contrast ratio, ananlog grey scale and low driving voltage. Additionally, the TN mode has a wide gap margin, because the principle of the TN mode

utilizes not retardation but optical rotation. Although viewing angle and response speed are shortcomings of the TN mode, new technologies to resolve them have been developed. Multi-domain methods [16-18] and an optically anisotropic film with negative birefringence using a discotic LC [19] have improved the viewing angle of TN-LCDs. Fast response speed was attained by a narrow gap (about 2 μm) TN-LCD with a novel driving scheme for impulse-type displays [20].

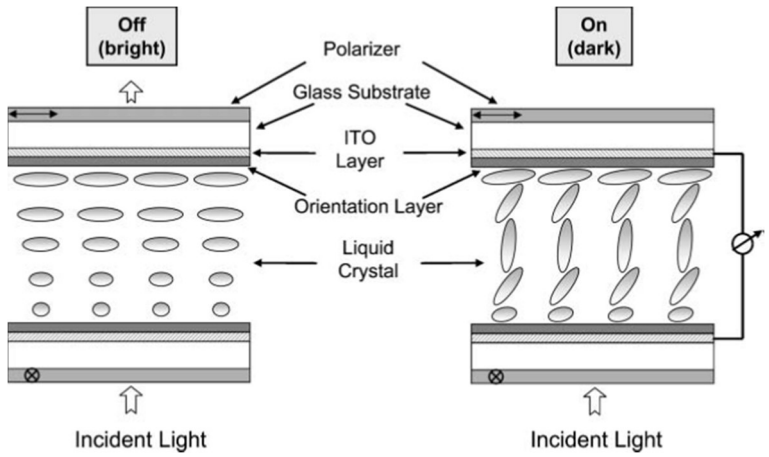

Figure 2.3. Operating principle of TN mode [16].

The basic operation of a TN-LCD in normally the white mode is illustrated in Fig. 2.3. In the inside of each glass substrate, a thin layer of indium-tin oxide (ITO) is present, which acts as a transparent electrode. Then it is coated with an alignment layer, which promotes the alignment of the LCs parallel to the glass substrate plane. Rubbed polyimide film is mostly used as the alignment layer. The rubbing directions of the alignment layers of the

upper and lower glass substrates are perpendicular and the LC molecules perform a 90° twist through the thickness of the LC cell. In the case of the normally white mod, each polarizing film is placed on the outside of the substrates, so that the transmissive axis of each polarizer is parallel to the rubbing direction of each alignment layer. The light incident on the TN display is polarized by the first polarizer and the light passes through the LC layer with its polarization direction rotated by 90°. Consequently, the polarization of the light becomes parallel to the transmissive axis of the second polarizer and the light is transmitted.

IPS mode

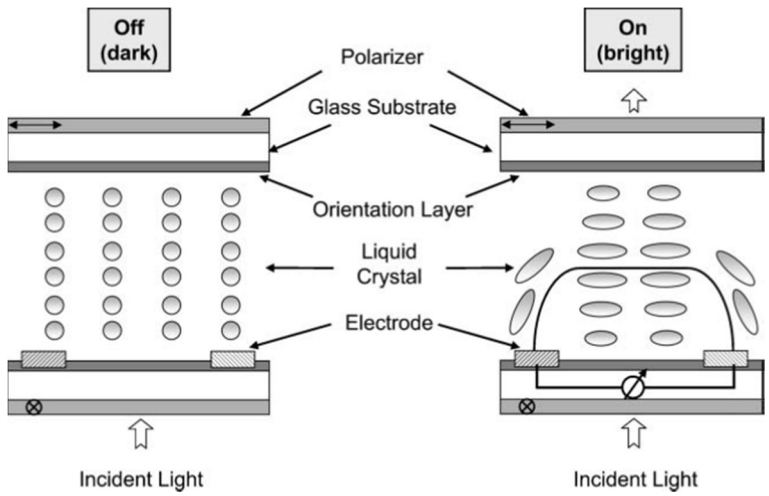

Figure 2.4. Operating principle of IPS mode [21].

The principle of the IPS mode is shown in Fig. 2.4. In typical LCDs, both substrates have electrodes and the direction of the electric field is

perpendicular to the substrates. In the IPS mode, however, only one substrate has electrodes and the electric field runs parallel to the substrates. The molecular long axes of the LC molecules are thus parallel to the substrates whether an electric field is or is not applied. In other words, the switching of the LC molecules by the electric field remains within a single plane. The strong merit of operation in the IPS mode is its wide viewing angle. Kiefer *et al*. proposed this mode in 1992 [21], and, in 1995, Oh-e *et al*. presented a wide viewing angle TFT-LCD in which the IPS mode was applied [22].

Operation in the IPS mode requires homogeneous alignment. Such homogeneous alignment is usually produced by rubbing. The effect of the pretilt angle induced by rubbing on the characteristics of the display and especially on the viewing angle is that the pretilt angle has a strong effect on the dependence of the viewing angle on the contrast ratio. When the pretilt angle is low, a high contrast ratio is obtained with a wide viewing angle. On the other hand, when the pretilt angle is high, the contrast ratio rapidly decreases as the viewing angle grows.

VA mode

The vertically aligned (VA) mode (Fig. 2.5) was introduced in 1998 [23] in a monitor display. This mode requires LC materials with negative dielectric anisotropy. The average molecular orientation (director orientation) without electric field is perpendicular to the substrate of the display. With this homeotropic orientation and crossed polarizers, the VA mode is working in the so-called normally black mode. For the incident light the liquid crystal in the off state behaves like an isotropic medium (the light "sees" only the

ordinary refractive index). As a consequence very good black states can be achieved independent of the wavelength of the light and the operating temperature. Pixel and electrode design of VA displays allow for a high aperture ratio (the fraction of transparent pixel area) resulting in a high brightness of the display. These two points are the main reason for the good contrast of VA LCDs. The first generation already achieved fast switching times of around 25 ms. Thus, the VA mode was from the beginning a very promising technology because of the combination of intrinsically good contrast values and fast switching times.

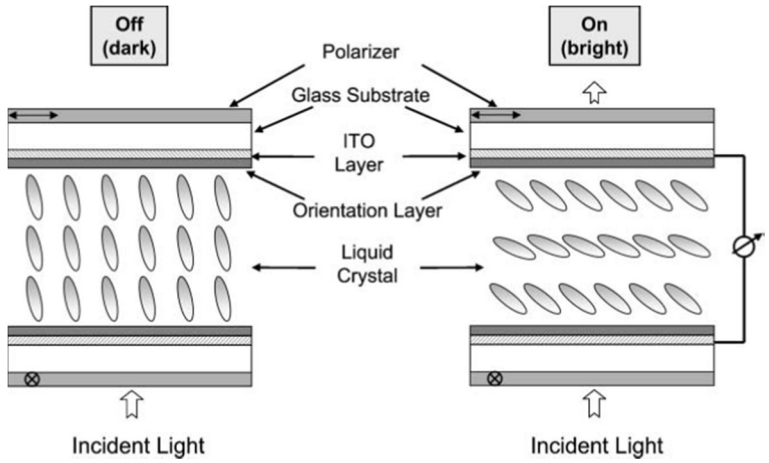

Figure 2.5. Operating principle of VA mode [23].

The grey scale switching of VA LCDs is relatively slow compared to other LCD modes like TN or IPS because of the low rate of change of transmission with voltage especially near the black state. Very recently this has been significantly improved by the so-called over-driving technique. Regarding

material properties the following basic requirements must be fulfilled. The standard TFT driver requires an operating voltage under 6 volts. As a consequence the dielectric anisotropy of the LC mixture has to be around at least 23 taking the corresponding elastic constants into consideration. The switching time from black to white of 25 ms is not sufficient to realize full moving pictures. Moreover, the slower grey scale switching (around 50 ms especially near black states) had to be improved. The required optical path is a little lower than 0.3. For currently used cell gaps this results in the optical path values for the VA mixtures of around 0.08. As it was not possible to achieve sufficiently low switching times, smaller cell gaps were introduced. 3 micron or even lower values for the cell gap require higher optical path values for the liquid crystals.

Challenging points are the controlled switching-on mechanism and grey scale switching. Since the directors are oriented homeotropically in the off state, they can be tilted randomly in any direction by the electric field. This leads to disclination lines between domains of equal orientation, thus deteriorating the optical performance. Several ideas have been developed to overcome this problem. By using an optically uniaxial polymer film or retardation film, the viewing angle dependence of the VA mode can be reduced. Concerning the usage of retardation films, there are two methods, one using only the negative refractive index [24], and the other using two films [25], one of positive refractive index and another of negative refractive index. By using two films, the viewing angle dependence can be reduced more than in the case of using only the negative refractive index.

Apart from this problem, as described above, the VA mode has a deeper-black background, a higher contrast ratio and better image quality at extreme temperatures. For this reason, The VA mode is the most widely used in the FPD industry. Therefore, in this thesis, researches are based on the VA mode LCD to solve the critical issues of the image quality. The technical requirements that LCDs must generally meet for overcoming the viewing angle problem will be discussed in chapter 2.2. In the following, the wide color gamut, which is a problem to be overcome not only in VA mode LCD but also in FPD industry as a whole, will be discussed in chapter 2.3.

2.2 Wide-Viewing Angle Technologies

As described in the previous chapter, a typical LCD mode including TN mode and VA mode causes a viewing angle dependency. In this chapter, the causes of the viewing problem and the related technologies will be discussed.

2.2.1 General description of viewing properties

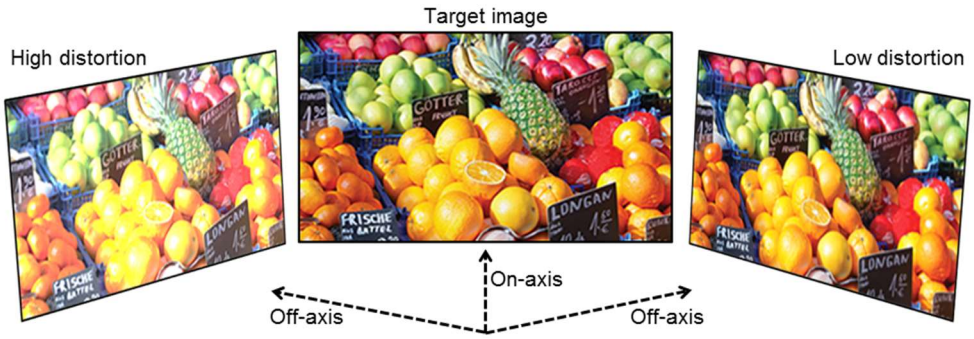

Figure 2.6. Viewing angle dependency in LCD.

As shown in Fig. 2.6., the luminance difference of the light occurs in the LCDs depending on the viewing angle. High distortion is the case when the luminance is brighter than the target luminance, low distortion is the case where the luminance is lower than the target luminance. This difference in brightness causes the desired image distortion, which has been a major problem in image quality. Since this phenomenon does not occur in OLED

display, it is a major challenge that LCD must overcome in order to maintain current position in the FPD industry. In this chapter, the cause of the viewing angle dependency will be discussed.

Viewing angle dependency

The VA mode display utilizes a homeotropic alignment, where liquid crystal molecules are perpendicular aligned in bulk to the substrate. The LC molecules are switched parallel to the substrate when an electric field is applied as shown in Fig. 2.7.

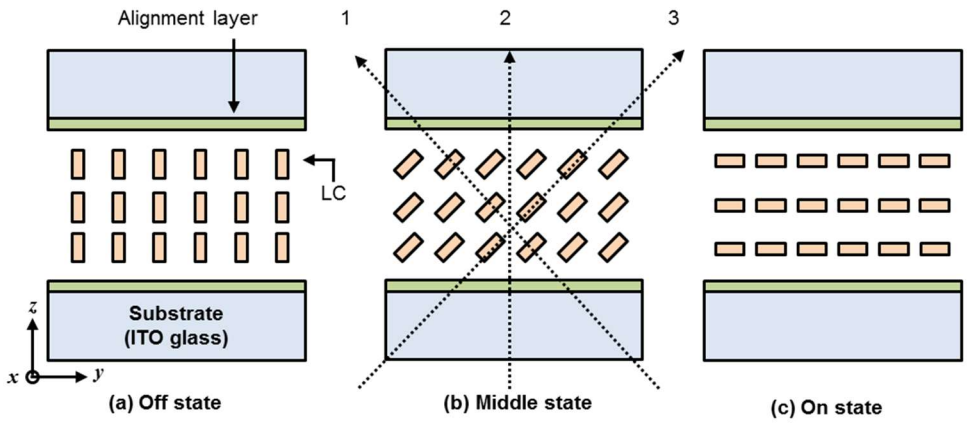

Figure 2.7. The principle of viewing angle dependency in VA mode.

When no voltage is applied as shown in Fig. 2.7(a), the LC becomes a medium with an uniaxial birefringence. In this case, when the display is observed from a vertical direction to the substrate, the display shows a dark state, because the optical axis of LC is perependicular to the substrate. When

the voltage is applied enough (Fig. 2.7(c)), polarizing plane of linearly polarized light passes through the first polarizer and the passes light is separated according to the orientation of the LC molecules. This is called optical rotation. The optical rotational behavior is maintained even if the incident direction of light is tilted.

In the middle state as shown (c) in Fig. 2.7, optical rotation exists together with birefringence. The birefringence becomes predominant with an increase in the voltage. For example, if the views from each of the direction, 1,2 and 3, are compared, the birefringence in the direction 1 is the highest and the transmission is difference in each direction.

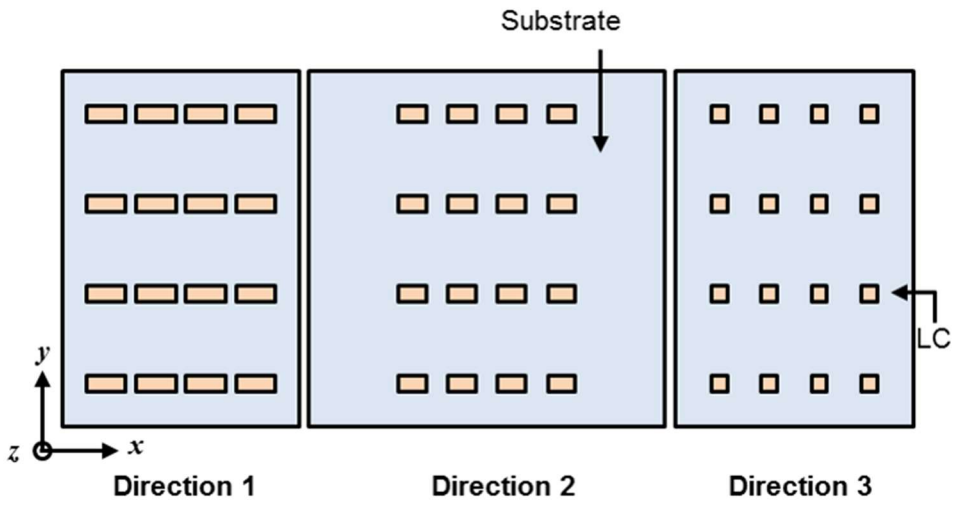

Figure 2.8. The effective LC alignment in different viewing directions.

As shown in Fig. 2.8, when birefringence is changed according to the

viewing angle, the effective light path difference that the light is actually transmitted is generated. The LCDs determines the transmittance of light using the difference in effective light path, and since the transmitted light passes through the color filter, the color changes according to the viewing angle.

Multi-domain TN mode

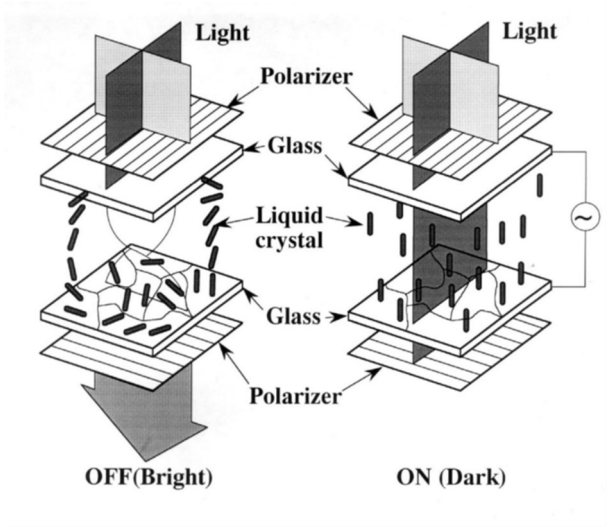

Figure 2.9. The amorphous TN method [26].

The multi-domain method gives each pixel two or more domains with a different orientational state. For example, Kobayashi et al. have proposed the amorphous TN method with multi-domain using an aligning film without rubbing for improve viewing angle of TN mode as shown in Fig. 2.9 [26]. In this method, the rubbing process of conventional TN mode was omitted. The

molecular long axis of LC molecules are parallel to the substrate and the direction of the molecular long axis is different in each domain. Therefore, the difference of the viewing direction can be reduced since the standing up direction of the molecules is random when the electric field is applied.

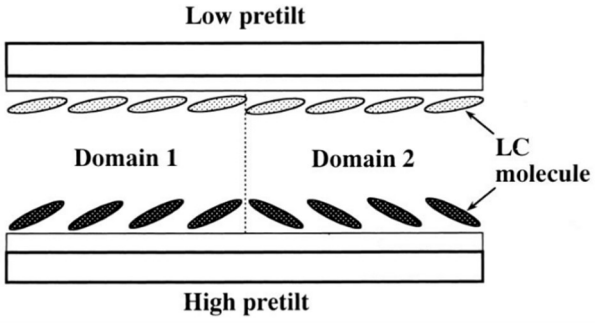

Figure 2.10. The complementary TN method [27].

Sumiyoshi et al. have proposed complementary TN method [27] which changes the standing up direction of the molecule by dividing the display pixel in orientation as shown in Fig. 2.10. In this method, a low pretilt aligning film is coated on the other substrate and each pixel is divided into two different areas with different pretilt directions. When the voltage is applied, the direction of the molecules standing up direction is opposite between the two domains and the viewing angle dependence of the TN mode is compensated.

Multi-domain VA (MVA) mode

For the vertical alignment (VA) mode, the mode called “multi-domain

vertical alignment (MVA) mode" was also proposed to compensate the viewing angle dependence of each domain by those of the adjacent domains. In the case of the dual- or multi-domain TN mod, the division is carried out, for example by alternating the rubbing direction. In one pixel, the tilt direction or the direction in which the LC molecules rise on applying an electric field in any given domain is different from that in adjacent domains. On the other hand, in case of the VA mod, their direction in which the liquid crystal molecules decline is alternated to change the direction of large viewing angle dependence in each domain. The viewing angle dependence of a domain compensates those of other domains, thereby reducing the viewing angle dependence over the whole area.

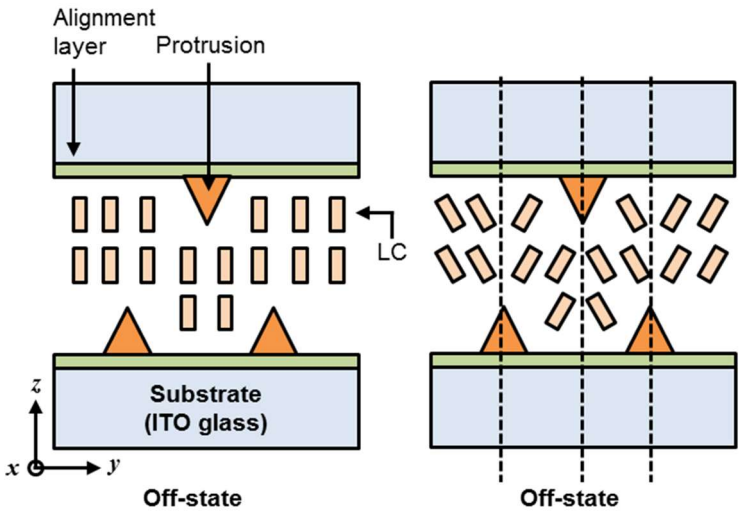

Figure 2.11. The division into domains of different alignment realized by forming protrusion on the vertical alignment layers.

In the VA mode or MVA mode, vertical alignment is realized by using polymer materials without prior rubbing treatment. Changing the subsequent rubbing direction in each division or pixel makes the processes complicated and increases the production cost. For the MVA mode, a methodology based on a completely different concept has been developed. The division into domains of different alignment is realized by forming “protrusions” on the alignment layers as shown in Fig. 2.11.

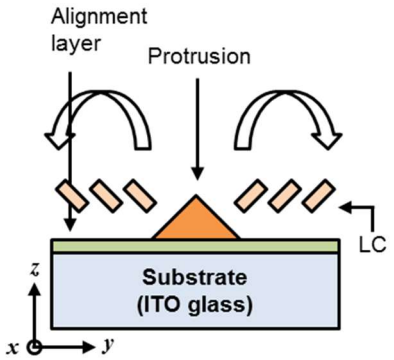

Figure 2.12. Switching of LC molecules in the MVA mode with protrusions

In Fig. 2.11, the LC molecules in different domains are shown separated by the protrusions and the molecules decline in different directions on applying an electric field. In a given domain, not only on the protrusion, but also on the alignment layer parallel to the substrates, the LC molecules decline in the same direction. Unlike the rubbing method, this method involves no complicated procedure. In LCDs operating under the MVA mode

as shown in Fig. 2.12, applying an electric field causes the LC molecules on the protrusions to begin to decline. The molecular rotation spreads in the same direction to the part parallel to the substrate. By changing the two-dimensional patterns of the protrusions, the division into plural kinds of domains can be realized. This division method introduces an alignment methodology based on the new concept that the control of alignment is realized by the polymer protrusion present on the alignment layers

The transmittance dependence on the height of the protrusion for various strengths of applied electric filed was examined [28]. This research suggested that a high protrusion and large interval can realize a high value of the transmittance. However, for intervals larger than 30 μm, no dependence can be observed. This suggests that the protrusions do not influence the LC line alignment in areas far from them.

The viewing angle dependence of the MVA-mode is wider than 160° from left to right and from up to down and the contrast is more than 10 to 1. For any viewing angle, no inversion of the grey scale can be observed. However, as the FPD industry has developed, the wide-viewing angle technologies with higher performance have become necessary.

2.2.2 Recent technologies for wide-viewing

Recently, various wide viewing angle technologies have been developed so far. Among them, the important researches are reviewed in the following paragraphs.

Optical compensation film

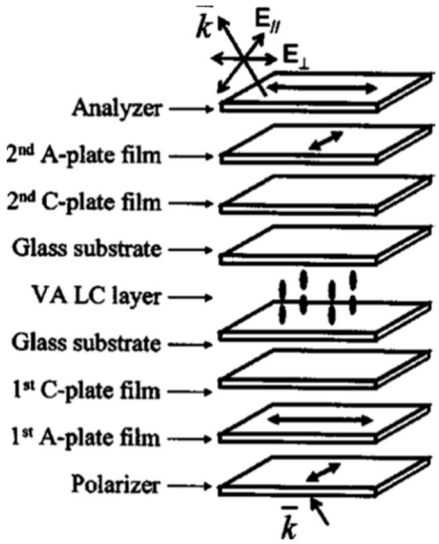

Figure 2.13. Structure of VA-LCD for optimized design using two *C*-plate and two *A*-plates [29].

As described in previous chapters, the VA LCD exhibits an excellent contrast ratio at the normal viewing direction, weak color dispersion and fast response time, however, its dark state light leakage at oblique angle is relatively large. Various studies had been conducted to overcome this problem, but the reported ~ 100:1 contrast ratio was limited to the 50° viewing cone. This insufficient for TV applications. There was need to extend the high-contrast ratio to a wider-viewing cone.

To overcome this limitation of viewing angle, Hong *et al*. proposed an optical configuration VA LCD using two *A*-plates and two *C*-plates as shown

in Fig. 2.13 [29]. They optimized the design for a four-domain VA-LCD which shows an extraordinarily high-contrast ratio over the entire 85° viewing cone. Then, VA-LCD with isocontrast ratio higher than 10000:1 over the 85° viewing cone was obtained.

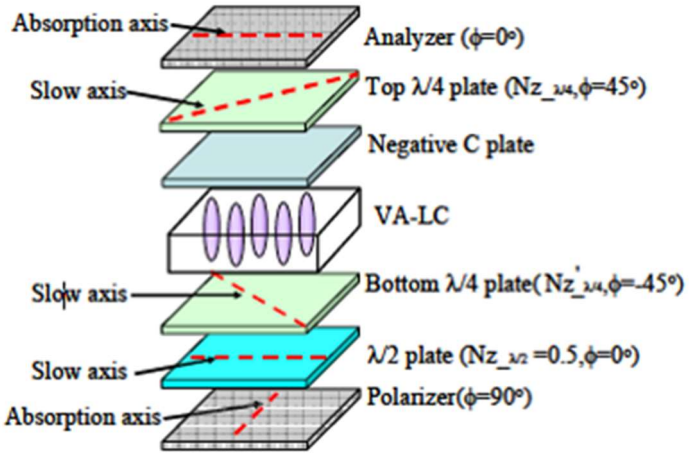

Figure 2.14. Structure of VA-LCD for compensated high-transmittance MVA-LCD [30].

Lin showed a high-transmittance circular polarizer type MVA-LCD with a wide viewing angle by using a combination of two A-plates, a C-plates, and two λ/4 plates as shown in Fig. 2.14 [30]. They propose a compensation principle for the crossed circular polarizers to widen the viewing angle of the high-transmittance MVA-LCD. The proposed compensation principle can be utilized to obtain practical compensation methods for the high-transmittance MVA-LCD. In addition, Ji *et al*., showed an optical configuration for a VA LC

cell that can improve the viewing angle and the color shift [31]. In this research, it was found that the color shift as a function of the incident angle deteriorated, especially in the blue wavelength range. Then, optical configuration for the VA LC cell that can improve the color shift and the optical viewing angle over the entire visible range using two negative *C*-plates and a single negative *A*-plate.

However, such techniques have a problem that the thickness increase of the display panel due to the additional compensation film

Collimated backlight unit

A collimated backlight unit to maintain the panel thickness while not using additional compensation film has been suggested. Since the LCD is a spatial light modulator, the viewing angle of the LCD is depending on the degree of diffuse light transmitted by the backlight unit (BLU). Because the diffuse oblique incident light rays are part of the light transmitted from the BLU, the depolarization and especially imperfection of the optical compensation film cause light leakage on the black state of LCD. The elimination of depolarized light under the scattered light illumination was a troublesome work.

In order to increase the contrast ratio and enhance the image quality of VA LCD, a light scattering film is attached on the front surface of the LCD and directional backlight that has a narrow angular luminance distribution with suppressed diffuse light is used for the LCD illumination. Kalantar proposed the concept of shping the luminance cone and making spatially uniform luminance [32]. It was found that the polarized and scattered light of a VA

LCD was mainly generated due to oblique light rays of diffusing BLU. The directional BLU was proposed in order to verify the concept on VA panels with front light scattering film, resulting in enhancing the oblique and normal contrast ratios.

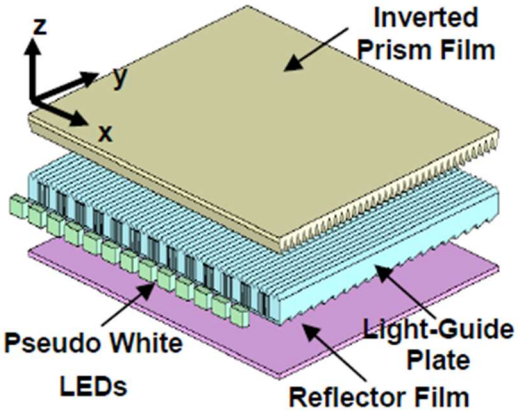

Figure 2.15. Optical structure of the directional BLU [32].

Hwang et al. developed wide-viewing display through the reduction of the residual LC phase retardation at oblique angles using an embedded diffusing unit as shown in Fig. 2.16 [33]. The backlight unit provides collimated illumination for the VA panel in such a way that the residual phase retardation experienced by the obliquely incident light is reduced. An embedded diffusing unit in the LCD panel was used for enlarging the light distribution through the VA LC layer. Compared to a conventional panel, this embedded approach provided extended isocontrast contours by more than 10° and the off-axis image distortions was improved by 50% compared to those in a film-

compensated LCD.

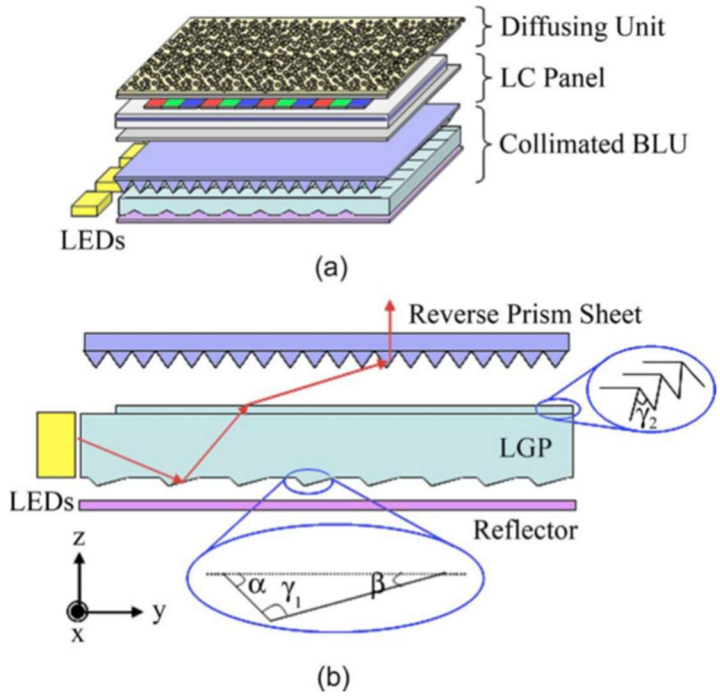

Figure 2.16. Schematic diagrams of wide viewing LCD consisting of collimated backlight unit and a diffusing unit embedded on the front polarizer [33].

However, these BLU technologies have problems that the manufacturing process is complicated and the process cost is increased due to the complicated configuration.

Advanced muti-domain

In order to overcome the drawback of the two technologies described

above, new multi-domain fabrication techniques that have been improved in conventional multi-domain techniques have been studied.

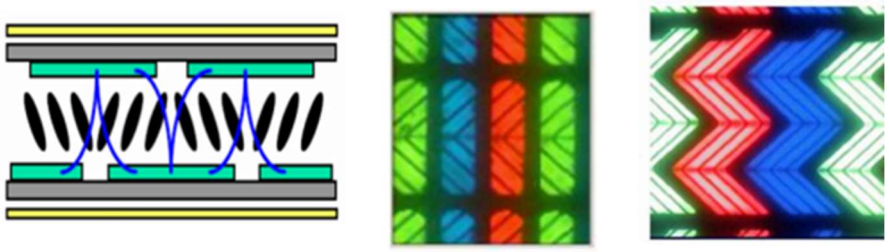

Figure 2.17. Schematic of patterned vertical alignment mode and microscopic image of fabricated PVA cell [34].

Patterned vertical alignment (PVA) modes (Fig. 2.17), where the LCs are vertically aligned in alternatively patterned pixel and common electrodes, is one of the most promising LC modes for the large-sized display applications due to high contrast ratio at a normal direction and wide viewing characteristics in the 4-domain structure without the protrusion [34]. A super-patterned vertical alignment mode (S-PVA) mode (Fig. 2.18) was developed to further improve the viewing angle of the PVA mode [35]. It is a technology to form 8-domains by doubling the multi-domain in the middle state, gray scale, by using additional transistors. Different voltages are applied to the two transistor in the middle gray level to align the LC molecules in the different polar directions to form multi-domains.

However, there is a problem that the driving circuit becomes complicated and the aperture ratio becomes reduced due to the additional transistor.

Therefore, a technique for constructing an extended multi-domain such as 8-domian using a single transistor is needed for wide-viewing angle LC display.

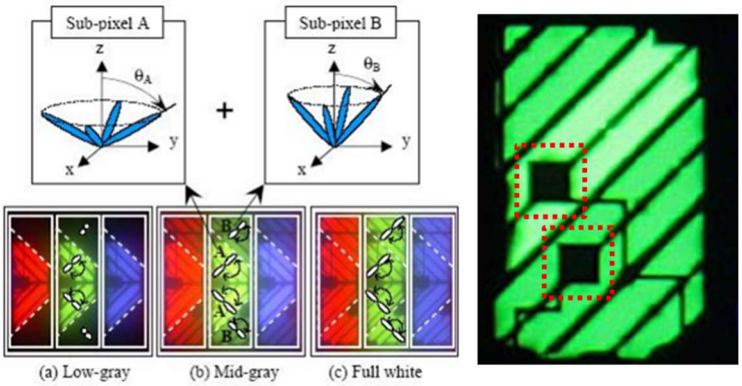

Figure 2.18. Schematic of super-patterned vertical alignment mode and microscopic image of fabricated S-PVA cell [35].

2.3 Coloration Technologies

As described in the previous chapter, a typical FPDs including LCDs and OLEDs causes a low color purity and narrow color gamut in comparison to natural coloration. In this chapter, the causes of the coloration problem and the related technologies will be discussed.

2.3.1 Coloration in flat panel displays

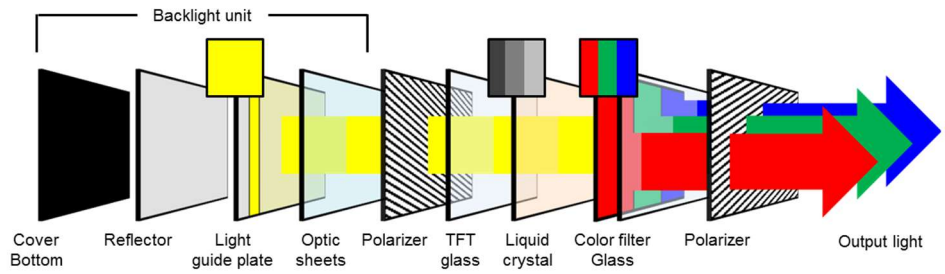

Figure 2.19. Schematic of coloration principle of conventional LC cell.

The structure of a typical LCD panel is shown in Fig. 2.19. Among these many optical components in the panel, there are three parts that are closely related to actual color reproduction. First, the backlight existing in the backlight unit is one of the most important parts. Since the light from this backlight unit coms out of the panel past the various optical components, what

kind of light is in the light source is ultimately a very important factor in determining the output light. Then, the grey scale of the light is determined in LC cells. Finally, the modulated light passes through color filters to reproduce the color, which determines the color here. As a result, except for the LC cell that determines the grey scale of the light, the backlight and color filters determine the color purity of the LCD. Such a coloration method is the same not only for the LCDs but also for the white OLED (W-OLED) currently on the TV market. In the case of W-OLED, it is nothing more than replacing the backlight and the LC cell with the W-OLED, and coloration eventually uses the same color filters.

Usually, the un-planar boundary condition such as protrusion induces the tilt change of LCs. It is mainly due to the monotonic directional preference of the surface structure. At interface between LC and RM, the interaction occurs in different manner. Here, aligning capability of the patterns of the RM film formed on the bottom substrate of LC cell will be studied. Next, the limitations of this approach and the efforts to overcome them will be discussed.

Principle of the coloration

To understand the significance of these narrow primary peaks, consider how light is generated and applied in the LCDs. First, light source in today's conventional LCD backlight unit is an array of LEDs. Because these gallium nitride (GaN)-based LEDs typically emit blue light, they are treated with a phosphor-usually yttrium aluminum garnet (YAG)-LED so they produce a white light.

Second, this white light shines through color filters in the LCD panel. This filter is composed of thousands or millions of red, green, and blue subpixels. The light passing through each of these subs-pixels is controlled to produce each pixel's color.

Typically, the BLU's white light is not centered to the primary red, green, and blue wavelengths. Instead, the white light has significant concentrations of non-primary wavelengths (such as orange or yellow) that leak through the color filter; as a result, the spectral output is not saturated. In a conventional color filter, for example, a red subpixel will transmit a band of wavelengths greater than 570 nm (a mix of yellow, orange, and red). This mix prevents the LCD from producing a pure red as shown in Fig. 2.20.

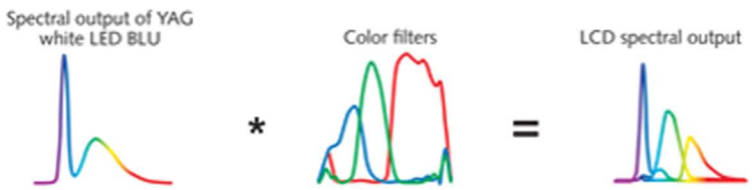

Figure 2.20. Principle of the coloration in LCD.

Color space

A color space is a specific organization of colors. In combination with physical device profiling, it allows for reproducible representations of color, in both analog and digital representations. A color space may be arbitrary, with particular colors assigned to a set of physical color swatches and corresponding assigned names or numbers such as with the Pantone collection,

or structured mathematically, as with NCS System, Adobe RGB or singular RGB(sRGB). However, a color model with no associated mapping function to an absolute color space is a more or less arbitrary color system with no connection to any globally understood system of color interpretation. When defining a color space, the usual reference standard is the CIELAB or CIEXYZ color spaces, which were specifically designed to encompass all colors the average human can see. Since "color space" identifies a particular combination of the color model and the mapping function, the word is often used informally to identify a color model. However, even though identifying a color space automatically identifies the associated color model, such a usage is incorrect in a strict sense. For example, although several specific color spaces are based on the RGB color model, there is no such thing as the sRGB color space.

Colors can be created in printing with color spaces based on the CMYK color model, using the subtractive primary colors of pigment (cyan (C), magenta (M), yellow (Y), and black (K)). To create a three-dimensional representation of a given color space, we can assign the amount of magenta color to the representation's X axis, the amount of cyan to its Y axis, and the amount of yellow to its Z axis. The resulting 3-D space provides a unique position for every possible color that can be created by combining those three pigments.

Colors can be created on computer monitors with color spaces based on the RGB color model, using the primary RGB colors. A three-dimensional representation would assign each of the three colors to the X, Y, and Z axes.

Note that colors generated on given monitor will be limited by the reproduction medium, such as the phosphor (in a CRT monitor) or filters and backlight (LCD monitor). Another way of creating colors on a monitor is with an HSL or HSV color space, based on hue, saturation, brightness (value/brightness).

CIE color space

The CIE color spaces were defined quantitative links between physical pure colors (i.e. wavelengths) in the electromagnetic visible spectrum, and physiological perceived colors in human color vision. The mathematical relationships that define these color spaces are essential tools for color management, important when dealing with color inks, illuminated displays, and recording devices such as digital cameras.

The CIE 1931 RGB color space and CIE 1931 XYZ color space were created by the International Commission on Illumination (CIE) in 1931 [36, 37]. The experimental results were combined into the specification of the CIE RGB color space, from which the CIE XYZ color space was derived. The CIE 1931 color spaces are still widely used, as is the CIE 1976 color space.

Due to the distribution of cones in the eye, the tristimulus values depend on the observer's field of view. To eliminate this variable, the CIE defined a color-mapping function called the standard (colorimetric) observer, to represent an average human's chromatic response within a 2° arc inside the fovea. This angle was chosen owing to the belief that the color-sensitive cones resided within a 2° arc of the fovea. Thus the CIE 1931 Standard Observer function is also known as the CIE 1931 2° Standard Observer. A more modern

but less-used alternative is the CIE 1964 10° Supplementary Standard Observer. For the 10° experiments, the observers were instructed to ignore the central 2° spot. CIE recommend that 1931 Standard Observer is suitable for a viewing angle of 4° or less and 1964 Standard Observer is suitable for a viewing angle of more than 4°. For the measurement equipment used in this study, the measured viewing angle was less than 4° so that the experiment and analysis were conducted using "2° standard observer". All corresponding values have been calculated from experimentally obtained data using interpolation. The standard observer is characterized by three color matching functions.

The derivation of the CIE standard observer from color matching experiments is given below, after the description of the CIE RGB space. The CIE's color matching functions $\bar{x}(\lambda)$, $\bar{y}(\lambda)$ are $\bar{z}(\lambda)$ the numerical description of the chromatic response of the observer as shown in Fig. 2.21. They can be thought of as the spectral sensitivity curves of three linear light detectors yielding the CIE tristimulus values *X*, *Y* and *Z*. Collectively, these three functions are known as the CIE standard observer.

$$X = \int_{\lambda} L(\lambda)\bar{x}(\lambda)d\lambda \tag{2.4}$$

$$Y = \int_{\lambda} L(\lambda)\bar{y}(\lambda)d\lambda \tag{2.5}$$

$$Z = \int_{\lambda} L(\lambda)\bar{z}(\lambda)d\lambda \tag{2.6}$$

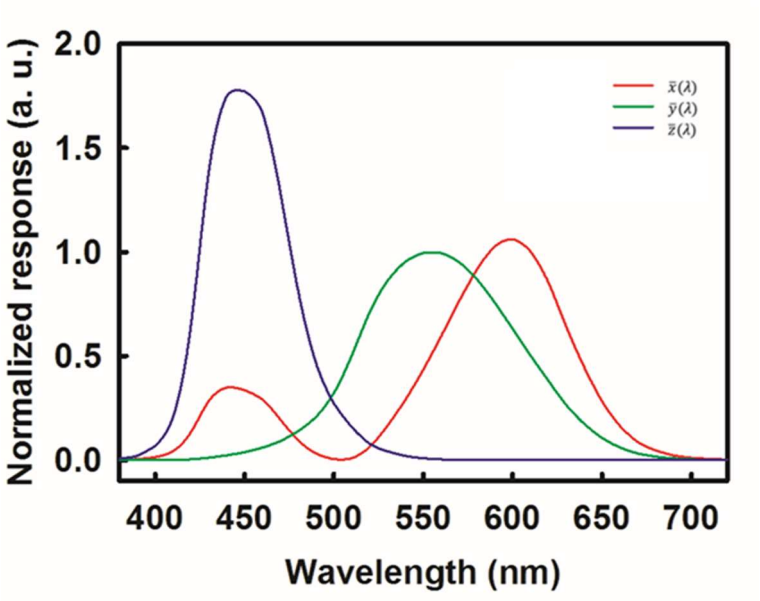

Figure 2.21. The color matching functions of 1931 standard observer [38].

Other observers, such as for the CIE RGB space or other RGB color spaces, are defined by other sets of three color-matching functions, and lead to tristimulus values in those other spaces.

Since the human eye has three types of color sensors that respond to different ranges of wavelengths, a full plot of all visible colors is a three-dimensional figure. However, the concept of color can be divided into two parts: brightness and chromaticity. For example, the color white is a bright color, while the color grey is considered to be a less bright version of that same white. In other words, the chromaticity of white and grey are the same while their brightness differs.

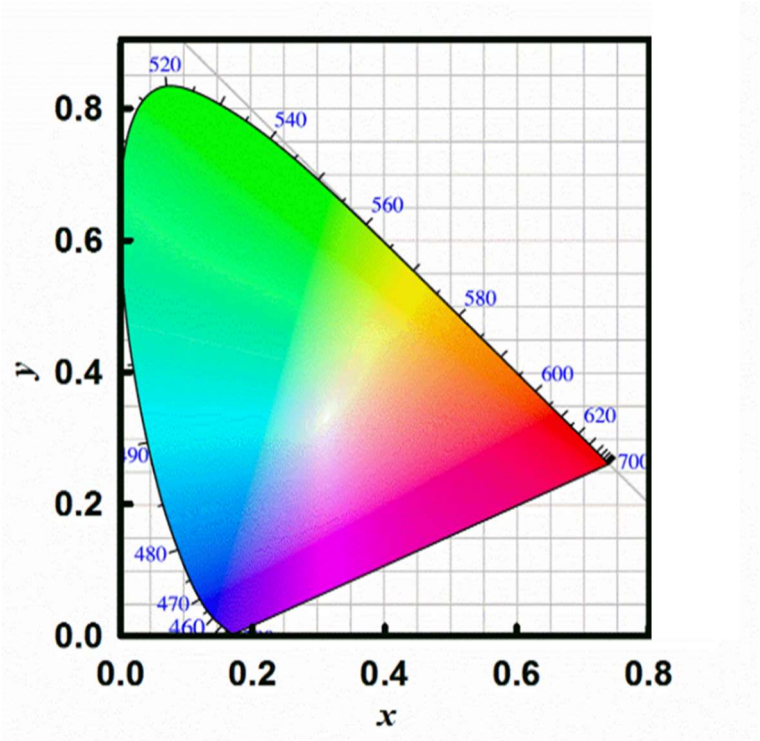

Figure 2.22. The CIE 1931 color space chromaticity diagram.

The CIE 1931 color space was deliberately designed so that the Y parameter is a measure of the luminance of a color. The chromaticity of a color is then specified by the two derived parameters x and y, two of the three normalized values being functions of all three tristimulus values X, Y, and Z:

$$x = \frac{X}{X + Y + Z} \tag{2.7}$$

$$y = \frac{Y}{X + Y + Z} \tag{2.8}$$

$$z = \frac{Z}{X + Y + Z} \tag{2.9}$$

The derived color space specified by x, y, and Y is known as the CIE xyY color space and is widely used to specify colors in practice.

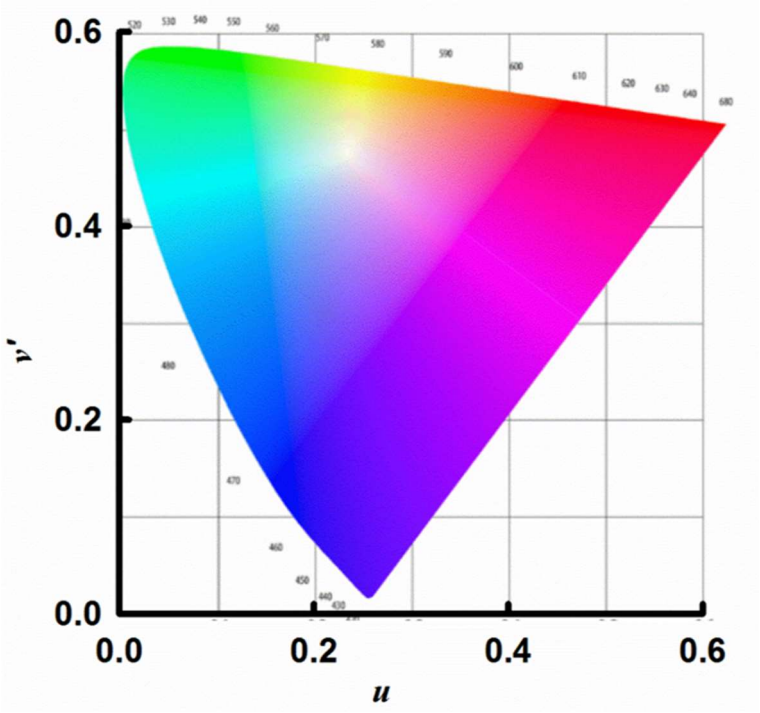

Figure 2.23. The CIE 1976 color space chromaticity diagram.

Recently, CIE 1976 color space, which express color coordinates more accurately. Has been developed and used in color expression. The chromaticity of a color is then specified by the two derived parameters *u'* and *v'*, two of the three normalized values being functions of all three tristimulus

values X, Y, and Z:

$$u' = \frac{4X}{X + 15Y + 3Z} \tag{2.10}$$

$$v' = \frac{9Y}{X + 15Y + 3Z} \tag{2.11}$$

2.3.2 Recent technologies for wide color gamut

As described above, since the conventional coloration method in LCDs has its limitations, various studies have been conducted recently. Among them, researches to expand the color gamut by applying the QDs have been made in earnest. This is due to the special optical properties of the QDs, which will be described in this chapter.

Quantum dot

QDs are very small semiconductor particles, only several nanometres in size, so small that their optical and electronic properties differ from those of larger particles. They are a central theme in nanotechnology. Many types of quantum dot will emit light of specific frequencies if electricity or light is applied to them, and these frequencies can be precisely tuned by changing the dots' size, shape and material, giving rise to many applications.

The nanoscale semiconductor materials tightly confine either electrons or electron holes. Quantum dots are also sometimes referred to as artificial atoms, a term that emphasizes that a quantum dot is a single object with bound,

discrete electronic states, as is the case with naturally occurring atoms or molecules [39]. Quantum dots exhibit properties that are intermediate between those of bulk semiconductors and those of discrete molecules. Their optoelectronic properties change as a function of both size and shape. Larger QDs (radius of 5–6 nm, for example) emit longer wavelengths resulting in emission colors such as orange or red. Smaller QDs (radius of 2–3 nm, for example) emit shorter wavelengths resulting in colors like blue and green, although the specific colors and sizes vary depending on the exact composition of the QD [40]. Because of their highly tunable properties, QDs are of wide interest. Potential applications include transistors, solar cells, LEDs, diode lasers and second-harmonic generation, quantum computing, and medical imaging [41]. Additionally, their small size allows for QDs to be suspended in solution which leads to possible uses in inkjet printing and spin-coating [42]. These processing techniques result in less-expensive and less time consuming methods of semiconductor fabrication.

In semiconductors, light absorption generally leads to an electron being excited from the valence to the conduction band, leaving behind a hole. The electron and the hole can bind to each other to form an exciton. When this exciton recombines (i.e. the electron resumes its ground state), the exciton's energy can be emitted as light. This is called fluorescence. In a simplified model, the energy of the emitted photon can be understood as the sum of the band gap energy between the highest occupied level and the lowest unoccupied energy level, the confinement energies of the hole and the excited electron, and the bound energy of the exciton (the electron-hole pair):

As the confinement energy depends on the quantum dot's size, both absorption onset and fluorescence emission can be tuned by changing the size of the quantum dot during its synthesis. The larger the dot, the redder (lower energy) its absorption onset and fluorescence spectrum. Conversely, smaller dots absorb and emit bluer (higher energy) light. Recent articles have begun to suggest that the shape of the quantum dot may be a factor in the coloration as well, but as yet not enough information is available. Furthermore, it was shown that the lifetime of fluorescence is determined by the size of the quantum dot. Larger dots have more closely spaced energy levels in which the electron-hole pair can be trapped. Therefore, electron-hole pairs in larger dots live longer causing larger dots to show a longer lifetime. To improve fluorescence quantum yield, quantum dots can be made with "shells" of a larger bandgap semiconductor material around them. The improvement is suggested to be due to the reduced access of electron and hole to non-radiative surface recombination pathways in some cases, but also due to reduced auger recombination in others.

Several methods are proposed for using quantum dots to improve existing LED design, including QD-LED displays and QD White LED (QD-WLED) displays. Because Quantum dots naturally produce monochromatic light, they can be more efficient than light sources which must be color filtered. QD-LEDs can be fabricated on a silicon substrate, which allows them to be integrated onto standard silicon-based integrated circuits or micro-electro-mechanical systems. QDs are valued for displays, because they emit light in very specific gaussian distributions. This can result in a display with visibly

more accurate colors. A conventional color LCD is usually backlit by CCFLs or conventional white LEDs that are color filtered to produce red, green, and blue pixels. An improvement is using conventional blue-emitting LEDs as the light sources and converting part of the emitted light into pure green and red light by the appropriate quantum dots placed in front of the blue LED or using a quantum dot infused diffuser sheet in the backlight optical stack. This type of white light as the backlight of an LCD panel allows for the best color gamut at lower cost than a RGB LED combination using three LEDs.

Quantum dot enhanced backlight on chip/edge type

In the on-chip geometry, the QD material is coated onto the LED emissive surface, within the LED package. This means that a minimum of area is coated with QD material, on order of a few square millimeters (less for small area LED chips). This is a large positive in terms of quantity of material consumed and hence the material cost, but also on the production scale required to service the display industry. However, the conditions which the QD material must survive are the most extreme. Typical LEDs operate at junction temperatures of 85–12°C, and the act of down conversion inherently involves a loss of energy due to Stokes' shift that translates to heat. Thus a QD material might operate at ～150°C in an on-chip environment. In addition, a 1W LED radiating 600 mW of optical power over 1 mm^2 would expose the QD material to 60 W/cm^2 of blue light flux. Many see both the temperature and flux of operation only increasing over time as LED technology improves, and so 100 W/cm^2 might soon be a reasonable operating specification for on-chip QD material. Finally, it is our assumption that all first generation QD

materials in displays will incorporate some sort of packaging to exclude water vapor and oxygen from affecting the QDs, and providing hermetic packaging at the individual LED level is widely seen as challenging, given the space and cost constraints, already on the LED package. In addition, whatever the cost of this packaging, an on-chip application will bear this cost for each LED in the system, whereas the other two geometries have only one packaging step per display

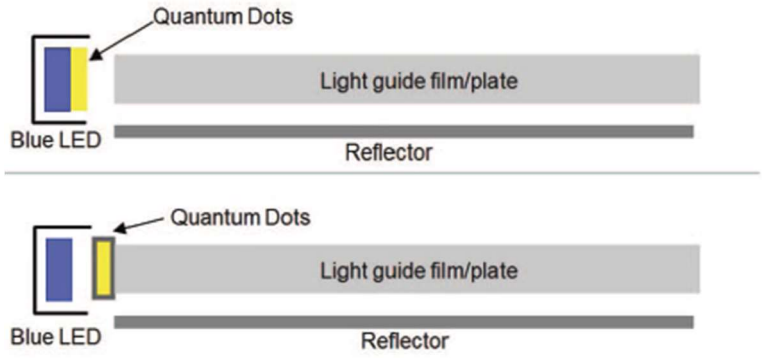

Figure 2.24. Depiction of the On-chip type, where the QDs are placed within the LED package which is coupled to the light guide and On-edge type, where the QDs are placed in between the LED packaged and the light guide plate.

On-edge solutions largely sit in between the on-chip and on-surface solutions in terms of material usage, and operating conditions. The coating area is much larger than that found in the on-chip scenario, but orders of magnitude smaller than that of on-surface. The operating conditions are also

much harsher than on-surface, but orders of magnitude lower than required by on-chip. It is for this reason that for some sizes of display, on-edge is likely to be the first geometry to emerge commercially.

Quantum dot enhanced backlight on surface type

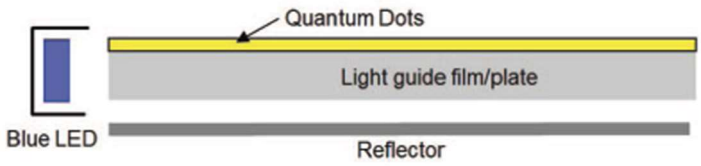

Figure 2.25. Depiction of the On-surface, where the QDs are in a thin film over the entire display area.

On-surface QD solutions will place the QDs at the latest possible stage of the backlight before the light enters the LC module. Thus, for every square inch of display area, QDs will be coated over the same number of square inches. Thus, the material utilized for the same down-conversion effect is at a maximum, with implications to both cost and need for production scale. For example, a 42” diagonal TV might consume about a gram of QD material, and hence hundreds of metric tons of material would be necessary to serve the entire TV segment of the display industry. However, as a result of doing the same work with more material, the demands on the material are much lighter. A reasonable brightness TV might only put 1–10 mW/cm^2 of optical flux through the QD material, a number so low that the Stokes’ shift temperature rise is essentially non-existent. In addition, because the QD are spatially

removed from the LED heat source, the operating temperature specification of the QDs in this configuration may be very close to room temperature.

However, in such these BLU studies, the QDs are randomly dispersed in target point, resulting in loss of the transmission through the color filters. Since the BLUs of the all sub-pixel pass both the red and green QDs, the light emitted by the green QD is lost through the red color filter and the light emitted by the red QD is lost through the green color filter. Moreover, the light emitted by the green and red QD is lost through the blue color filter. For this reason, studies have been researched to pattern and position primary color QDs for each color filters in sub-pixel.

Color-separated quantum dot pattern

As described above, studies have been researched to fabricate the color-separated QD pattern to match the transmittance band of the color filter and the QDs. Liu *et al*. proposed a well arrange QDs array, which is excited by blue backlight, was fabricated to spatially separated the red, green and blue color [43]. This QD array was further placed onto traditional color filter array, by matching the corresponding color filter pixel, in order to eliminate the blue light cross talk. In this case, the energy efficiency of this QD active color filter array no longer depends on its geometric arrangement and Absorption properties, but depends on the quantum yield of QDs. Furthermore, 90% Adobe color gamut can be achieved. One advantage of this fabrication method is synthesizing the QDs array onto the substrate directly, without the requirement of dissolving the QDs into other media. This technique may provide a new method to obtain higher color separation efficiency in LCD

than the traditional color filter matrix by enhancing the quantum yield of QDs.

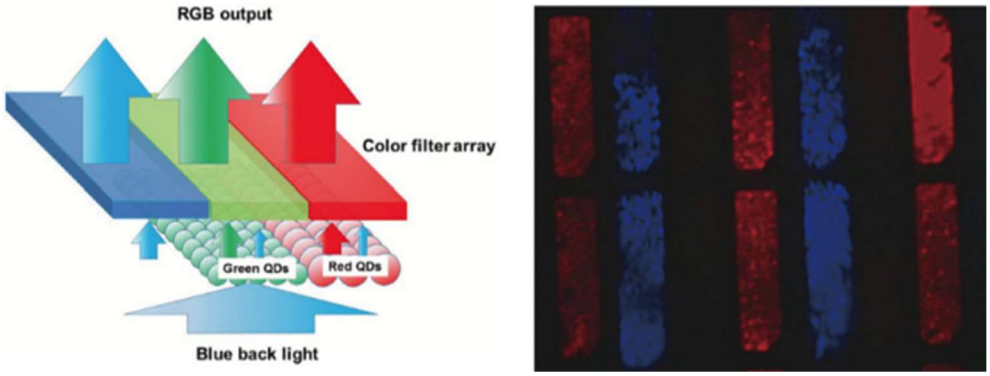

Figure 2.26. Scheme of QD enhanced active color filter array and microscopic image of QD enhanced active color filter array [43].

H.-J. Kim *et al*. developed QD nanocrystal dispersed in photoresist film and applied to W-OLED to improve optical power of red color through down-converting of blue and green light [44]. To integrate to W-OLED display panel, the QD dispersed photoresist film was prepared in a thickness of 2 μm with high concentration of QDs up to 30 wt%. QDs were dispersed successfully in photoresist with a matching of nonpolar characteristic for the ligands of QDs and PR as well as a careful mixing process of QDs and PR dispersed solutions. They also realized the patterning of QD dispersed PR film with a stripe pattern of 60 μm width without a residual layer. The experimental measurement after passing through a 30 wt% QD dispersed PR film and a color filter in W-OLED shows the enhancement of 40.2% in the

optical power of re color compared to that from a conventional W-OLED without QD dispersed photoresist film.

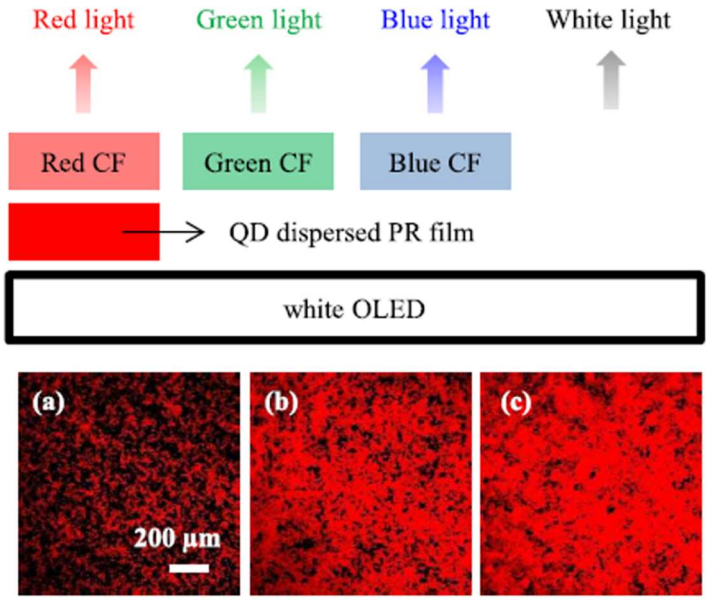

Figure 2.27. Scheme illustration for applying the QD dispersed PR film to white OLED displays and confocal microscopy images of the QD dispersed PR film [44].

Then, H.-J. Kim *et al*. proposed an optically efficient structure and fabricated to realize high brightness OLED display based on a W-OLED prepared with the air-gapped bridges on the QD patterns [45]. Compared with a conventional W-OLED display, in their experiments, the optical intensity of the proposed OLED display shows the enhancement of 58.2% in the red color and 16.8% in the green color after applying the air-gapped bridge structure on

QD patterns of 20 wt.% concentration. This enhancement comes from the two facts that the QD patterns down-convert unnecessary blue or blue/green light to the required green or red light and the air-gapped bridges increase the color conversion efficiency of QDs by optical recycling using total internal reflection at the interface. In addition, the color gamut of the proposed OLED display increases from 65.5 to 75% due to the narrow emission spectra of QDs. However, these studies also require color filters due to blue-crosstalk, resulting in the loss of transmittance.

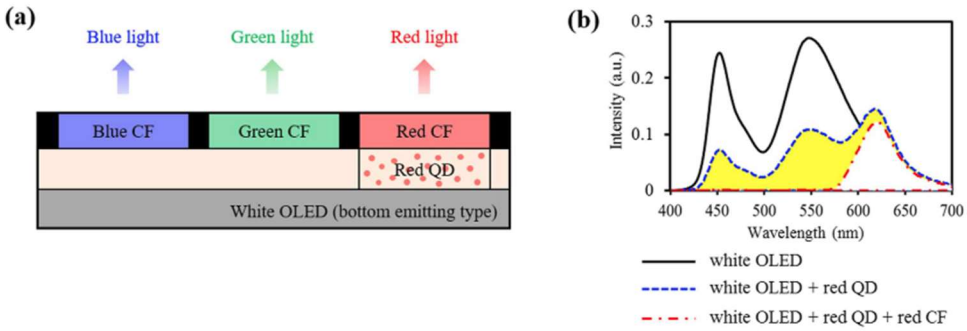

Figure 2.28. Schematic illustration of W-OLED with red QD pattern and the measured intensity spectra of W-OLED and w/o red QD and red color filter [45].

In this chapter, the emerging LCD technologies was discussed. The viewing angle and color purity problem must be solved in order to compete with OLED, which is the next generation display.

In the case of the wide viewing angle problem, a problem arising from the principle of the operation of the LCD is caused by the difference in effective

optical path depending on the viewing angle. In order to overcome this problem, a multi-domain technique in which LC molecules are arranged in different directions in one pixel has been applied. Recently, techniques such as optical path compensation film and a collimated backlight have been applied to obtain a sider viewing angle. However, due to the use of additional optical films, the thickness of the panel increases, and the circuit complexity of the backlight unit increases to use collimated light as the backlight. Therefore, techniques for widening the viewing angle using advanced multi-domain technology are attracting attention. In the S-PVA mode, a maximum 8-domain is formed using additional transistor, which greatly improves the viewing angle. However, it has drawbacks such as reduced aperture ratio and increased circuit complexity due to additional transistors.

In the case of color purity, there is a problem that the red and green light are weak due to the transmission band mismatch between the conventional YAG LED backlight and the color filters. In order to overcome this problem, recently QD have been applied to color reproduction. Various QD application BLUs ranging from on-edge, on-chip and on-surface types have been proposed. However, in the case of such these backlight application techniques, the QD are randomly dispersed and all light is enhanced to red and green, resulting in the loss of the transmittance through the actual color filters. To overcome this problem, a LCD method using a color-separated QD pattern has been proposed. By placing QDs corresponding to the color filters, the loss of the transmittance can be minimized and a wide color gamut can be realized. However, such a structure also is not able to avoid the loss of the

transmittance because color filters is essentially required due to blue crosstalk.

In subsequent chapters, therefor, new technologies and display devices that enable to intrinsically solve the above two problems will be proposed.

Chapter 3

Enhancement of Viewing Angle of LCD by Multi-Domain

3.1 Control of Molecular Alignment by Thermo-Transfer Printing

Prior to fabrication of the wide-viewing LCDs, this chapter will discuss the development of LC alignment layer to manipulate the anchoring properties including the pretilt angle and anchoring energy of the LC molecules. The anchoring control layer proposed this chapter is a key element in the later-described wide viewing display technology.

3.1.1 Introduction

The alignment of liquid crystal (LC) molecules has been extensively studied for understanding delicate interfacial interactions between the LC and various solid substrates [46–48] as well as for constructing diverse electro-optical (EO) devices such as gratings [49–51], waveguides [52–54] and information displays [55–57]. In general, the alignment state of the LC molecules is characterised by the anchoring energy and the pretilt angle on the substrate surface with anisotropic interactions that produce the easy axis of the LC orientation. Besides the anchoring strength, the pretilt angle greatly influences the response time [58], the threshold voltage and the EO transmittance [59, 60] of the LC cell. Moreover, it plays a primary role in determining the optimised EO mode in various LC cell configurations [61, 62]. Several methods of producing the pretilt angle of the LC on the substrate, for example, SiOx oblique deposition [63], inhomogeneous surfaces using mixed planar and vertical alignment materials [64], ion beam (IB) irradiation along various directions [65], and the photo-alignment by ultraviolet light [66] have been reported so far. They provide a limited range of the pretilt angle and exhibit often a discontinuous change of the pretilt angle of the LC. Even the stacked planar and vertical alignment [67] achieve the relatively wide range of pretilt angle and continuous change of pretilt angle of the LC, it has a problem that patterning is difficult to apply the display application. Recently, it was demonstrated that a modified poly(dimethylsiloxane) (PDMS) surface by the IB irradiation [68, 69] or the hybrid polymer network [70] can be used for

changing the pretilt angle from the PDMS's intrinsic vertical alignment (90°) [71] to the planar alignment (0°). However, it is still not possible to vary the pretilt angle of the LC in a continuous manner.

This chapter describe how the surface anchoring properties of the LC are controlled by adjusting the amount of the PDMS oligomers transferred onto the substrate from a bulk PDMS plate using a thermo-transfer printing method that was developed previously [72]. The heat treatment during contact printing is found to precisely control the surface energy of the PDMS-modified surface in a simple and cost-effective way. As a result, the pretilt angle of the LC is continuously varied on the PDMS-modified surface from the homogeneous (or planar) to the homeotropic (or vertical) alignment. Moreover, the relationships among the surface hydrophobicity, the pretilt angle and the polar anchoring energy are also discussed.

3.1.2 Thermo-transfer printing for surface modification

In this study, I try to control the alignment direction of LC moleclues by controlling the surface energy of the substrate as shown in Fig. 3.1. As described above, depending on the surface energy of the substrate, the alignment state of the LC molecules can be determined by the LC-substrate interaction and the LC-LC interaction. If the LC-LC interaction is stronger than the LC-substrate interaction, the LC molecules will maintain homeotropic alignment. The opposite case will have homogenous alignment.

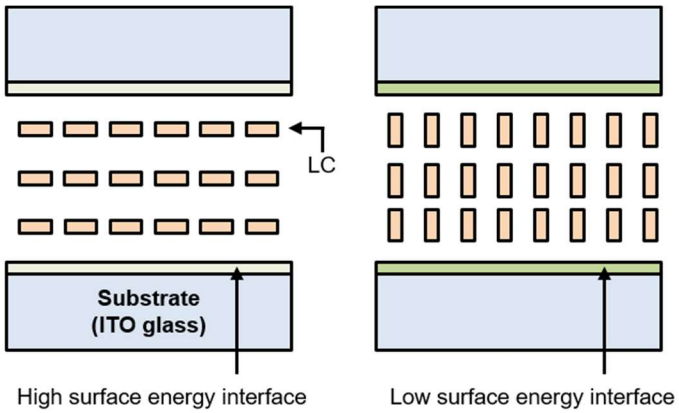

Figure 3.1. Schematic of LC alignment principle according to the surface energy of the substrate.

For this purpose, it is essential to control the surface energy of the substrate. In order to control the surface energy without changing the alignment layer material, the thermal-transfer printing technique was used in this study. Figure 3.2 shows the process of the thermal-transfer printing. Uncured oligomers in cross-linked polymer were transferred onto substrate to change the surface wettability of the substrate. The amount of transferred oligomers was changed by additional heat treatments, the thermal-transfer printing, during the diffusion of oligomer from cross-linked polymer onto substrate. During the thermal-transfer printing, the amount of transferred oligomer will be manipulated according to the heat treatment temperature.

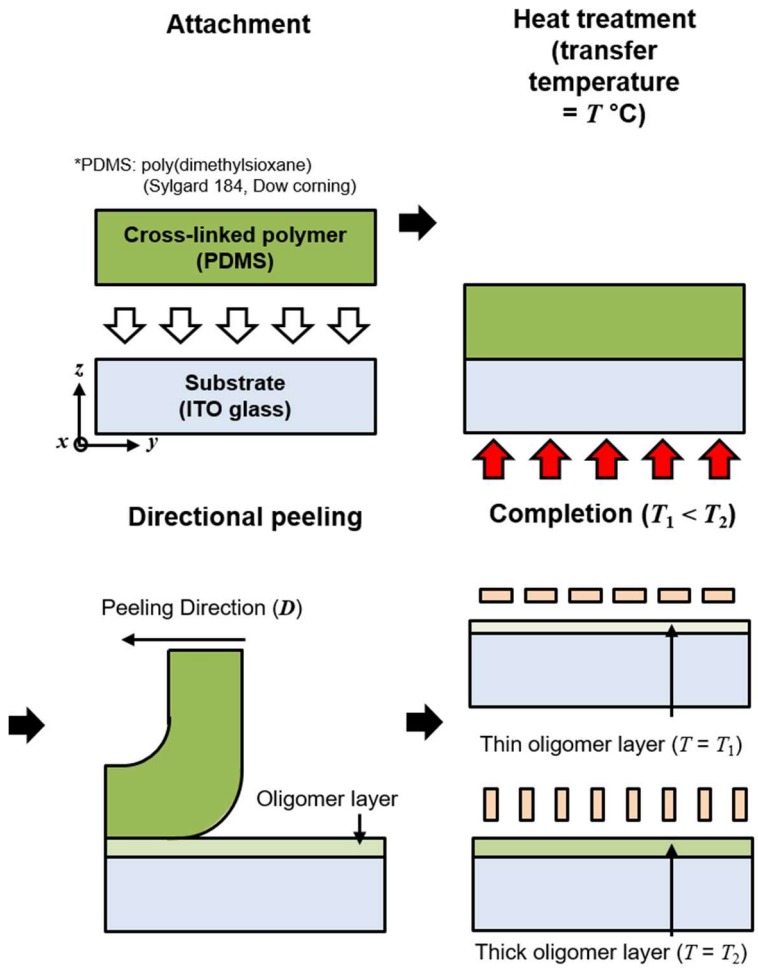

Figure 3.2. Schematic of the thermal-transfer printing process.

3.1.3 Fabrication process

The PDMS (Sylgard 184, Dow Corning) plate used in this study was made of a mixture of the PDMS precursor and a curing agent at the weight ratio of 10:1. The PDMS mixture was stirred for 5 min and placed in a vacuum

chamber at room temperature for 1 hour to remove air bubbles. It was then poured into an enclosed container and heated at 70°C for 24 hours to produce the PDMS plate. In constructing the LC cells, indium-thin-oxide coated glass substrates were first sonicated in acetone for 30 min and in deionised water for 10 min in sequence. After each cleaned glass substrate was dried with nitrogen gas, the PDMS plate was placed on it as shown in Fig. 3.3(a). The glass substrate in conformal contact with the PDMS surface was heated at the transfer temperature of T°C in the range from 25°C to 200°C for the heating time of t min. The PDMS plate was then detached from the glass substrate along the peeling direction D. After the detachment of the PDMS plate, the PDMS oligomer layer (with the thickness of h_p) was formed on the substrate as shown in Fig. 3.3(b). Figure 3.3(c) shows a schematic diagram of our LC cell, consisting of two PDMS-modified substrates by thermo-transfer printing, where the pretilt angle Θ is shown in the inset. The LC cell was assembled such that the peeling directions in two substrates were antiparallel to each other. The cell thickness h_c was maintained using glass spacers of 6 μm for the microscopic observation of the alignment texture and voltage-transmittance curve characterisation of the LC cell. For the measurement of the pretilt angle and the polar anchoring energy, a 50 μm-thick LC cell was used. The nematic LC (E7, Merck) was injected into the cell by capillary action at 80°C in the isotropic state. The filled LC cell was then cooled down to room temperature under ambient atmosphere. As shown in the inset of Fig. 3.3(c), the PDMS-modified substrate is capable of generating the pretilt angle with respect to the peeling direction as reported previously [73]. In the peeling off process, the

peeling off speed of the polymer mold not affect the LC alignment properties. The material parameters of E7 are as follows: the ordinary refractive index n_o = 1.522, the extraordinary refractive index n_e = 1.746, the splay elastic constant K_{11} = 11.7 pN and the bend elastic constant K_{33} = 19.5 pN [74].

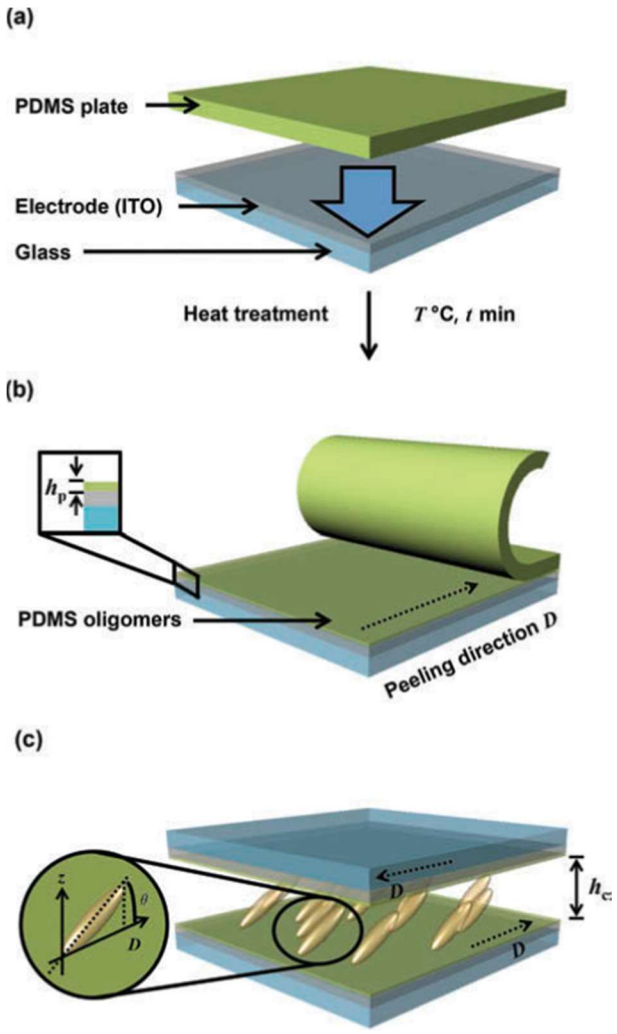

Figure 3.3. Illustration of the thermo-transfer printing process and the PDMS-modified surface [75].

3.1.4 Experimental results and discussions

Surface properties of PDMS-modified substrates

The hydrophobic characteristics of the PDMS-modified surface prepared under the heat treatment for 5 min is first determined. It was found that for longer than 5 min of the heat treatment, no conformal contact between the glass substrate and the PDMS plate was made since the thermo-mechanical force on the PDMS plate, inducing the bending stress, became to surpass the adhesion required for the conformal contact. The water contact angle and the surface energy of the PDMS-modified surface are shown as a function of the transfer temperature in Figure 2(a). Note that the surface energy (γ) was calculated from the measured water contact angle (θ_c) using the relationship between them in the following [76].

$$\cos\theta_c = -1 + 2\sqrt{\frac{\gamma}{\gamma_{lv}}}e^{-\beta(\gamma_{lv}-\gamma)^2} \tag{3.1}$$

where γ_{lv} and β are the liquid–vapour surface energy for water (72.8 mJ/m^2) and an empirically derived parameter of 1.247 × 10–4 (mJ/m^2)$^{-2}$, respectively.

From Fig. 3.4(a), it was found that the surface energy of the PDMS-modified surface decreases monotonically from 65.2 to 21.9 mJ/m^2 with increasing the transfer temperature. Note that at the transfer temperature of 200°C, the water contact angle on the PDMS-modified surface was essentially the same as that on the bulk PDMS which is hydrophobic. This means that our

thermo-transfer printing method indeed enables to modify the PDMS surface from hydrophobic to substantially hydrophilic.

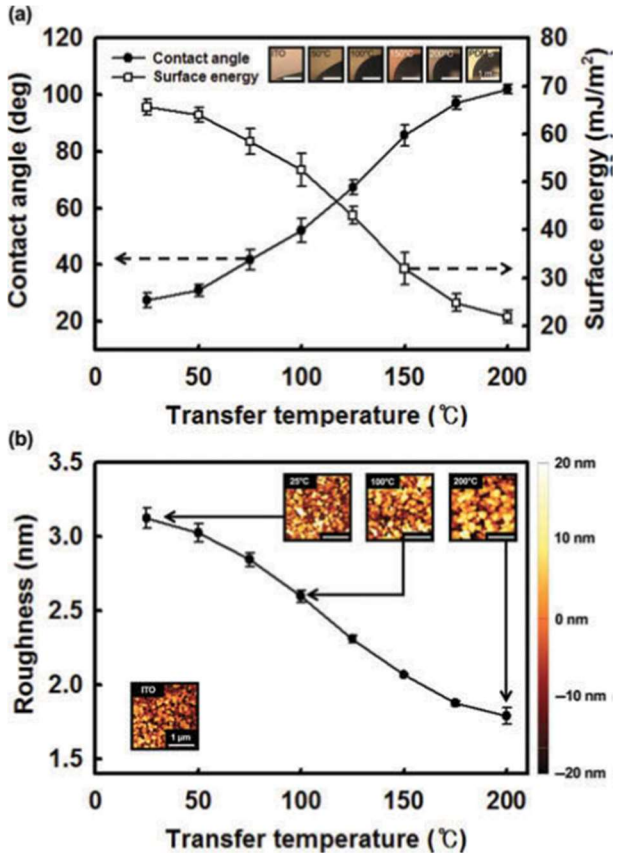

Figure 3.4. The surface properties of the PDMS-modified surface (a) The contact angle of water on the surface and the corresponding the surface energy (b) The average roughness of the PDMS-modified surface [75].

In order to describe the surface morphology of the PDMS-modified

surface, the measurements by an atomic force microscopy (AFM) (AE-100, Park Systems) were performed. Figure 3.4(b) shows the average surface roughness together with the AFM image of the PDMS-modified surface as a function of the transfer temperature. Due to the increase of the amount of the transferred PDMS oligomers onto the substrate, the grain size increases while the surface roughness decreases monotonically with increasing the transfer temperature. Note that the transfer of the PDMS oligomers from the bulk PDMS to the substrate is accelerated by the thermal energy absorbed during the heat treatment [76]. The transferred PDMS oligomers make the substrate surface be hydrophobic. The thickness of the transferred PDMS layer was estimated to be about 10 nm [77].

Alignment direction of LCs on the PDMS-modified substrates

We now discuss the alignment properties of the LC cells, each of which was assembled with the PDMS-modified surface prepared at the transfer temperature of 75°C, 100°C, 125°C or 150°C. The nominal cell thickness of each LC cell was 6 μm. Figure 3.5(a)–(d) show the optical microscopic textures of the LC cells, observed with a polarising optical microscope (Optiphoto2-Pol, Nikon) under crossed polarisers, which correspond to the transfer temperatures of 75°C, 100°C, 125°C and 150°C. For given transfer temperature, two microscopic images were taken when the peeling direction made angles of 0° and 45° with respect to one of the crossed polarisers, respectively.

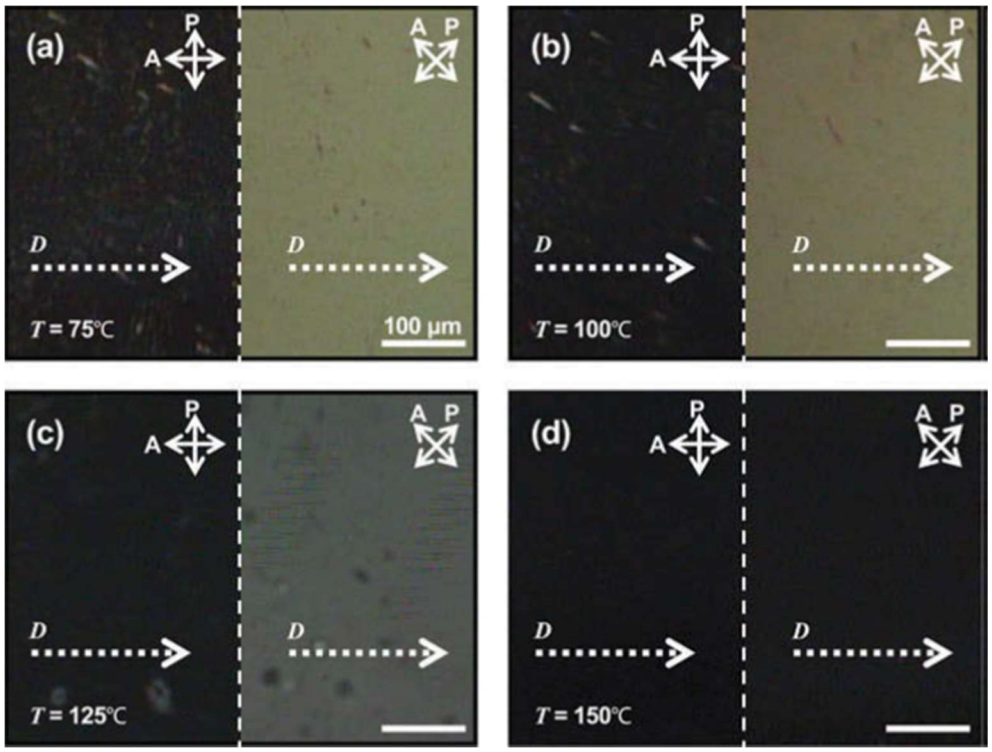

Figure 3.5. The microscopic textures of the LC observed under the cross polarizers [75].

The light transmission for the angle of 45° decreases with increasing the transfer temperature and nearly vanishes at the transfer temperature of 150°C in Figure 3.5(d), suggesting that the LC alignment becomes homeotropic in the plane of the substrate. This is consistent with the fact that in the antiparallel geometry of the LC cell, highly tilted LC molecules towards the polar direction produce low transmittance even when the direction of the azimuthal alignment makes an angle of 45° with respect to one of the crossed polarisers [78]. Except for a few defects seen in small regions, the LC

molecules were well aligned as shown in Fig. 3.5. The observed defects may be attributed to the non-uniformity of the transferred layer of the PDMS oligomers produced incidentally during the manual removal of the PDMS plate. An automated detachment process is desirable to achieve the uniformity of the PDMS layer for the LC alignment.

Electro-optical properties of LC cells

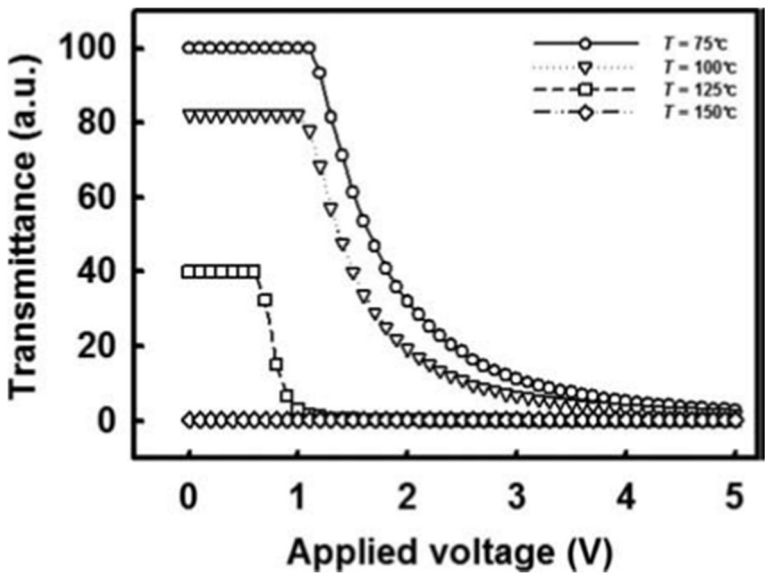

Figure 3.6. The voltage-transmittance curves of the LC cells, fabricated with the PDMS-modified surfaces at different transfer temperatures [75].

Figure 3.6 shows the voltage–transmittance curves of the LC cells, fabricated with the PDMS-modified surfaces at different transfer temperatures,

under the applied voltage in a square form with the frequency of 1 kHz. The light source was a He–Ne laser with the wavelength of 632.8 nm. The input polarisation was set to be an angle of 45° with respect to the peeling direction and perpendicular to the analyser in the normally white mode. As shown in Figure 3.6, the transmittance in the bright state and the threshold voltage of the LC cell were found to increase with decreasing the transfer temperature. At the transfer temperature of 150°C, no transmission was observed, suggesting that the LC molecules were aligned nearly vertically. The magnitude of the transmittance depends on the orientation of the LC director whereas the threshold voltage is related to the polar anchoring energy [79]. This indicates that the EO properties of the LC cell are strongly affected by the transfer temperature.

Pretilt angle

More quantitatively, we determine the pretilt angle and the polar anchoring energy of the LC as a function of the surface energy of the PDMS-modified surface. The LC cells of 50 μm thick were used for the measurements of the pretilt angles by the crystal rotation method [80]. The pretilt angle is directly related to the symmetric point (ψ_x) in the transmittance. The theoretical transmittance (I_{trans}) can be expressed in terms of the cell gap (h_c), the rotation angle (ψ), the wavelength (λ) of the incident light, the pretilt angle (Θ) and two refractive indices (n_o and n_e) of the LC as follows:

$$\theta = \cos^{-1}\left(\frac{\sin\psi_x}{n_o}\right) \tag{3.2}$$

$$I_{trans} = \frac{1}{2}\sin^2\left\{\frac{\pi}{\lambda}\cdot h_c \cdot f(\theta,\psi)\right\} \tag{3.3}$$

$$f(\theta,\psi) = \frac{{n_o}^2 - {n_e}^2}{n^2}\sin\theta\cos\theta\sin\psi$$

$$+\frac{n_o n_e}{n^2}(n^2 - \sin^2\psi)^{\frac{1}{2}} - ({n_o}^2 - \sin^2\psi)^{\frac{1}{2}} \tag{3.4}$$

$$n^2 = {n_o}^2\cos^2\theta + {n_e}^2\sin^2\theta \tag{3.5}$$

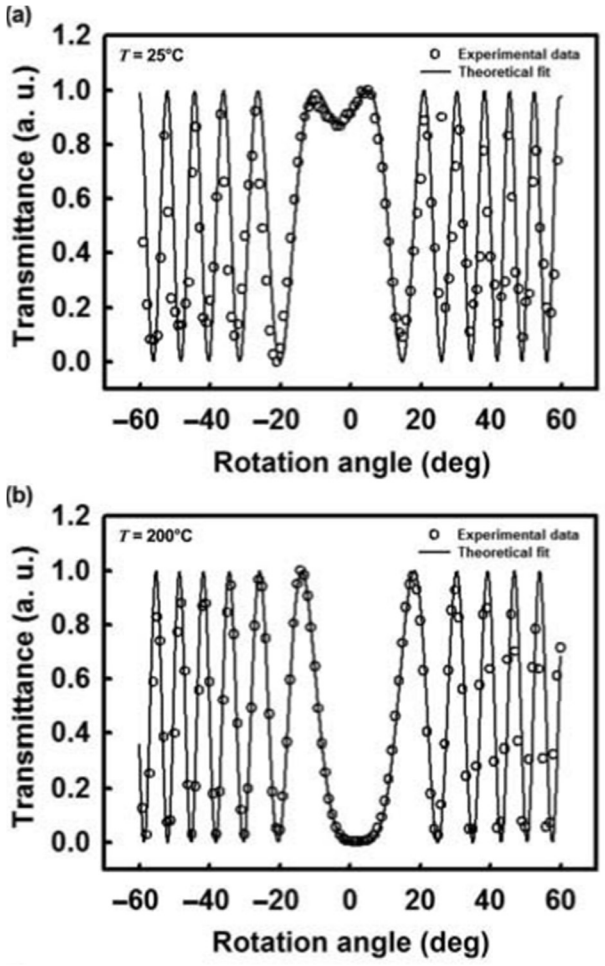

Figure 3.7. The transmittance and the pretilt angle of the LC cell as a function of the rotation angle for the transfer temperatures [75].

Figure 3.7(a) and (b) show two typical examples of the transmittance (experimental and theoretical) as a function of the rotation angle for the transfer temperature of T = 25°C and 200°C, respectively. The symmetric points in the measured transmittance were estimated to be $\psi_x = -3.1°$ in Fig.

3.7 (a) and 1.9° in Fig. 3.7(b). The corresponding pretilt angles, calculated from Eq. (3.2), were 3.5° for T = 25°C and 87.6° for T = 200°C. It should be noted that the theoretical curves obtained from Equation (3.3) agree well with the experimental data for the two cases as shown in Fig. 3.7(a) and (b).

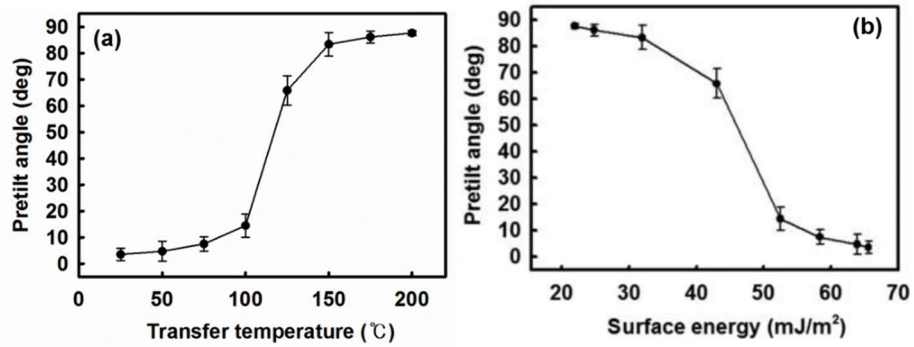

Figure 3.8. The preilt angle of the LC on the PDMS-modified surface as a function of (a) the transfer temperature and (b) the surface energy.

In Fig. 3.8, the pretilt angle on the PDMS-modified surface was shown as a function of the surface energy obtained in Fig. 3.4 (a). Although there is an abrupt change in a certain range (between 15° and 65°), the pretilt angle decreases monotonically from about 90° to 0° with increasing the surface energy from about 15 to 70 mJ/m^2. It is clearly that a hydrophobic surface promotes the homeotropic alignment of the LC molecules. As described previously [81], the competition between the LC–LC interactions and the LC–substrate interactions determines the equilibrium orientation of the LC molecules. In our case, the nature of a rather continuous change in the

wettability difference among the PDMS-modified surfaces leads to the monotonic change of the pretilt angle by the transfer temperature of the PDMS oligomers.

Polar anchoring energy

Finally, let how the polar anchoring energy of the LC depends on the surface energy of the PDMS-modified surface be investigated. The polar anchoring energy of the LC was measured using the high electric technique [82] based on the simultaneous measurements of the capacitance (C) and the optical phase retardation (R) as a function of applied voltage (V). The polar anchoring energy (W_θ) can be determined from the linear fit of the data of R/R_0, plotted in $1/CV$, where R_0 is the maximum phase retardation of the LC in the high voltage regime well above the Frederiks threshold (in the range from 6 to 16 V in our case). The linear function between R/R_0 and $1/CV$ is expressed as follows:

$$\frac{R}{R_0} = \frac{J_0}{CV} - \frac{2K_{11}}{h_c W_\theta}(1 + \kappa \sin^2\theta) \tag{3.6}$$

$$\kappa = \frac{K_{11} - K_{33}}{K_{11}} \tag{3.7}$$

where J_0 is a constant. Typical plots of the experimental data of R/R_0 as a function of $1/CV$ were shown in Fig. 3.9 (a) and (b) for the transfer temperature of T = 25°C and 200°C, respectively. From the intercepts in the y-axis, $-0.7 \pm 0.1 \times 10^{-3}$ for T = 25°C and $-2.2 \pm 0.2 \times 10^{-3}$ for T = 200°C, together with the measured values of the pretilt angle, the magnitudes of the

polar anchoring energy were calculated to be (670 ± 50) μJ/m^2 for T = 25°C and (330 ± 24) μJ/m^2 for T = 200°C from Eq. (3.6).

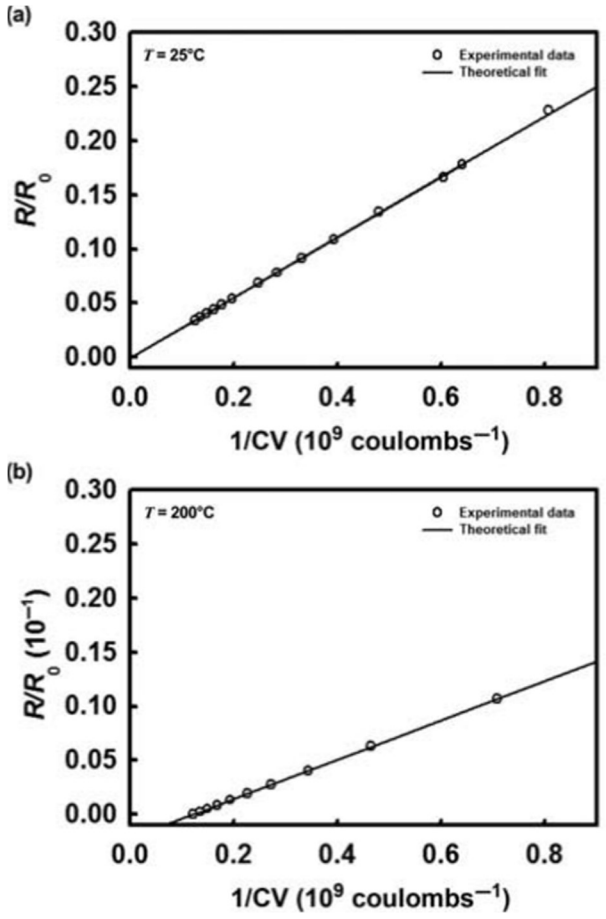

Figure 3.9. The plots of R/R_0 as a function of 1/CV in the high voltage regime (between 6 and 16 V) for the transfer temperatures [75].

Figure 3.10 shows the polar anchoring energy for the LC as a function of

the surface energy of the PDMS-modified surface. It was found that the polar anchoring energy is linearly proportional to the surface energy, suggesting that the LC orientation can be well controlled by the macroscopic surface wettability. The surface energy of the substrate is generally believed to have no direct correlation with the anchoring energy of the LC [83], but the relationship between them has been found in a recent work [84]. This is consistent with our results that the interactions between the substrate and the LC molecules become strong as the surface energy increases.

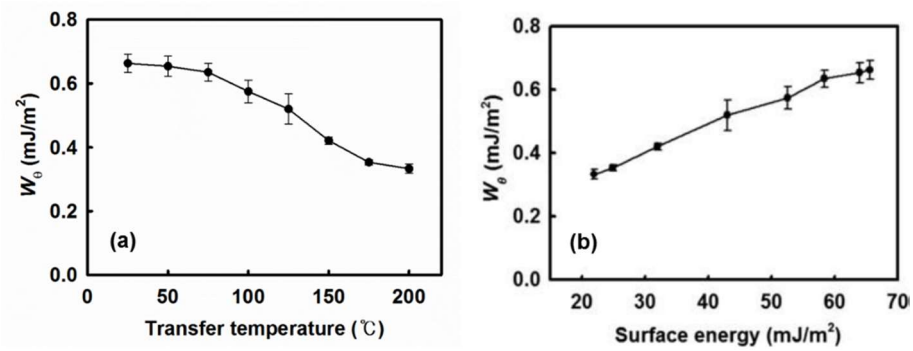

Figure 3.10. The polar anchoring energy for the LC as a function of (a) the transfer temperature and (b) the surface energy of the PDMS-modified surface.

3.1.5 Summary

A new approach to the LC alignment, called the thermo-transfer printing, which is capable of varying the surface energy of a substrate have been

demonstrated. According to the transfer temperature, the pretilt angle of the LC can be varied continuously from the homogeneous to the homeotropic alignment. The change of the surface energy of the PDMS-modified surface is dictated by the amount of the PDMS oligomers transferred from a bulk PDMS plate to the substrate during thermo-transfer printing. Such PDMS oligomers play a critical role on the variations of the pretilt angle as well as the polar anchoring energy of the LC in a wide range. If the surface wettability is controlled by a uniform method such as the thermal evaporation instead of the uneven peeling method proposed in this study, it can be applied to the display technology. In addition to, the control of the pretilt angle in a continuous manner presented here will be applicable for devising a variety of optical devices based on liquid crystalline materials in complex architecture with different optical configurations.

3.2 Wide-Viewing by Anchoring Disparity

Using the LC molecular alignment layer developed in the previous chapter, I will discuss wide-viewing LCDs in this chapter. I intend to reduce the gamma distortion by expanding the multi-domains through a new multi-domain fabrication method using the anchoring disparity.

3.2.1 Introduction

The invariance of the color uniformity at oblique viewing angles has been one of the critical challenges in LCDs where the gamma distortions in the off-axis results primarily from the difference in the effective optical pathway among different viewing directions. A simple way of reducing the gamma distortions is the use of an extra birefringence film to compensate for the phase retardation change depending on the viewing direction [85, 86]. Another one relies on the pixel-division into sub-domains with different directions of the LC alignment through either the use of patterned electrodes or the modification of the alignment layer [87-91]. In the pixel-division approach, the gamma distortions can be further reduced using multiple driving transistors [92-95], the variations of the anchoring energy [96, 97], structured electrodes [98-100], or the difference of the surface anchoring energy [101, 102]. Among them, the use of the difference of the surface anchoring energy provides a reliable and effective way of reducing the gamma distortions by

means of the shift of the threshold voltage. However, existing techniques for constructing multi-domains using anchoring energy differences have been suffered to apply to wide-viewing angle LCD fabrication due to the difficulty of patterning techniques for fabricating multi-domains and the small difference in the anchoring energy.

In this chapter, a new approach to the reduction of the gamma distortions by the introduction of the anchoring disparity using the anchoring energy control layer will be demonstrated. The underlying concept is based on the voltage division by the anchoring disparity which is capable of shifting the threshold voltage in sub-domain by sub-domain as well as spontaneously aligning the LC with maintaining the pretilt angle of the sub-domains. The anchoring disparity was constructed through the thermos-transfer printing of the PDMS by simple micro-contact printing under the ultra-violet oxygen (UVO) treatment. It was found that the UVO exposure time for the pre-treatment of the cross-linked polymer plays a crucial role in the control of the transferred oligomer onto substrate for the change of the LC molecular alignment properties. For the assessment of the off-axis image quality, the experimental measurements were performed to obtain the gamma curves in the vertical alignment configuration with 4-domain electrodes.

3.2.2 Anchoring disparity by thermo-transfer printing

Figure 3.11 shows the basic operation principle of the multi-domain fabrication technology using the anchoring disparity. The anchoring energy

control layer developed above chapter is placed on the vertical alignment layer and LC molecules aligned as shown in Fig. 3.11(a). In this state, the anchoring control layer is patterned to place two sub-domains having different anchoring energies in one pixel.

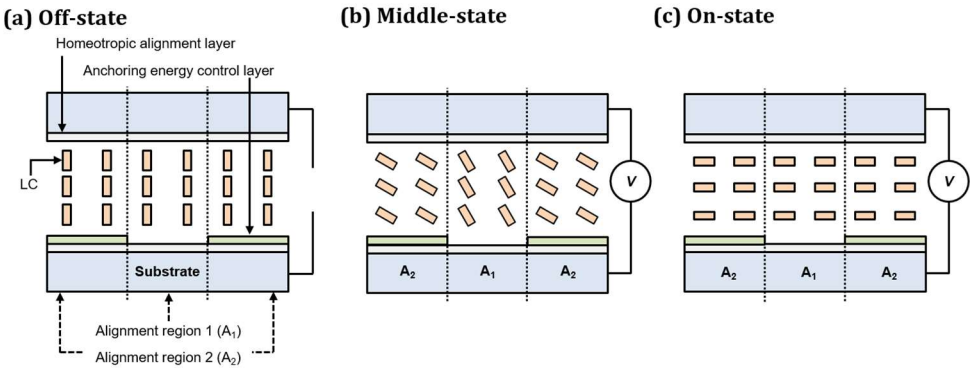

Figure 3.11. Schematic of the multi-domain based on the anchoring disparity.

The patterned anchoring control layer basically aligns the LC molecules vertically so that both the off-state and the on-state, there is no disclination line between sub-domains. In this case, since the anchoring energy difference between the sub-domains is present in the middle-state, applied moderate voltage, the LC molecules in the middle state have different polar tilted angles to form a multi-domain. Therefore, if the multi-domain is fabricated by applying this technique, conventional multi-domain is enable to be expanded more than twice.

In order to investigate the actual characteristics of the anchoring energy

control layer before applying it to practical multi-domain fabrication technology, the following experiment was conducted. Figure 3.12 shows the fabrication process of the anchoring energy control layer and the LC cells for the measurement of the anchoring characteristics of the LCs on the anchoring energy control layer.

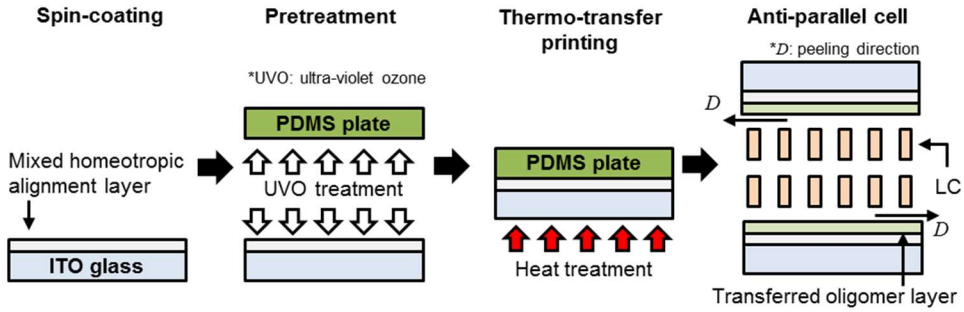

Figure 3.12. Illustration of fabrication process of the anchoring energy control layer using the thermo-transfer printing.

In constructing the LC cells, indium-thin-oxide coated glass substrates were first sonicated in acetone for 30 min and in deionised water for 10 min in sequence. After each cleaned glass substrate was dried with nitrogen gas, mixed homeotropic alignment layer was spin-coated at 3000 rpm for 30 s. The mixed alignment layer was a mixture of homeotropic alignment layer (AL22620, JSR) and homogeneous alignment layer (SE-6414, Nissan) for the enhancement of the amount of transferred PDMS oligomer. The PDMS (Sylgard 184, Dow Corning) plate used in this study was made of a mixture of the PDMS precursor and a curing agent at the weight ratio of 10:1. The

PDMS mixture was stirred for 5 min and placed in a vacuum chamber at room temperature for 1 hour to remove air bubbles. It was then poured into an enclosed container and heated at 70°C for 24 hours to produce the PDMS plate. The ultra-violet ozone (UVO) treatment was applied to both the substrate for pre-treatment time t and the PDMS plate for 45 s to increase the amount of PDMS oligomer transferred. After the pre-treatment, the substrate in conformal contact with the PDMS surface was heated at the transfer temperature of 200°C for the heating time of 5 min. The PDMS plate was then detached from the glass substrate along the peeling direction D. After the detachment of the PDMS plate, the PDMS oligomer layer was formed on the substrate. Finally, the LC cell was assembled such that the peeling directions in two substrates were antiparallel to each other. The cell thickness h_c was maintained using glass spacers of 5 μm for the microscopic observation of the alignment texture and voltage-transmittance curve characterisation of the LC cell. The nematic LC (MLC-2038, Merck) was injected into the cell by capillary action at 80°C in the isotropic state. The filled LC cell was then cooled down to room temperature under ambient atmosphere. The material parameters of MLC-2038 are as follows: the ordinary refractive index n_o = 1.4816, the extraordinary refractive index n_e = 1.5848, the splay elastic constant K_{11} = 13.8 pN and the bend elastic constant K_{33} = 18.1 pN. The LC textures were observed using a polarized optical microscope (POM) (Potiphot-Pol, Nikon).

Surface properties of anchoring energy control layer

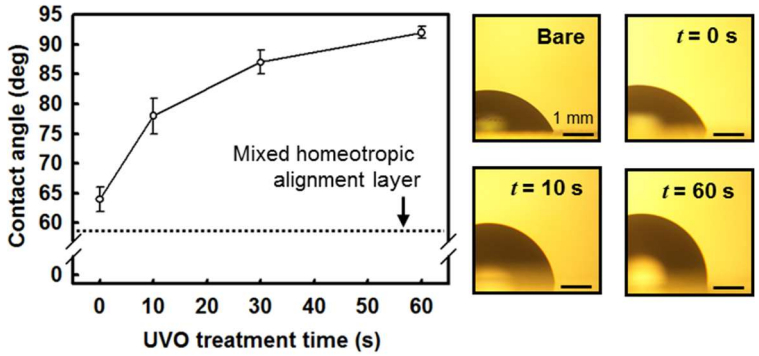

Figure 3.13. The contact angle of water on the surface according to the UVO treatment time.

From Fig. 3.13, it was found that the contact angle of the water on the anchoring energy control layer increase monotonically from 59 to 92° with increasing the pre-treatment time, UVO treatment time *t*. Note that at the without the pre-treatment, the water contact angle on the anchoring energy control layer was essentially the same as that on the bulk mixed homeotropic alignment layer. This means that the pre-treatment using UVO indeed enables to modify the PDMS surface to hydrophobic.

More quantitatively, we determine the polar anchoring energy of the LC as a function of the pre-treatment time. The polar anchoring energy of the LC was measured using the high electric technique [82] based on the simultaneous measurements of the capacitance and the optical phase retardation as a function of applied voltage as in the previous chapter.

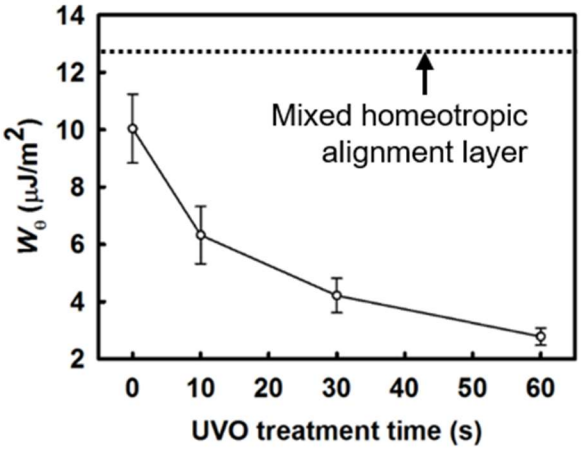

Figure 3.14. The polar anchoring energy on the anchoring energy control layer according to the UVO treatment time.

Figure 3.14 shows the polar anchoring energy for the LC as a function of the UVO treatment time. It was found that the polar anchoring energy is decreased in a wide range, suggesting that the anchoring energy control layer can be well controlled by the macroscopic surface wettability. Based on the results obtained in chapter 3-1, the predicted variation of the polar anchoring energy was 0.6 μJ/m^2 which was smaller than actual experimental variation. This is considered to be due to the experimental differences in the alignment layers, LC molecules, and polymer used as the anchoring energy control layer

Electro-optical properties of LC cells

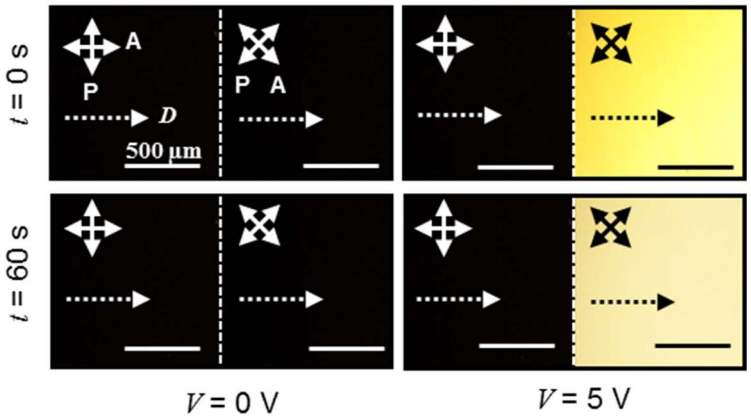

Figure 3.15. Microscopic texture of the LCs on the anchoring energy control layer corresponding to the pre-treatment time and applied voltage.

Figure 3.15 shows the microscopic images of the LCs on the anchoring energy control layer according to the pre-treatment time and applied voltage. As expected, uniform dark images in which the LC molecules were all vertically aligned in off-state and all homogenous aligned in on-state regardless of the pre-treatment time were measured. Especially, in the on-state, it was possible to measure the well-aligned LC molecules along the PDMS plate peeling direction *D*. Based on this results, the voltage-transmittance curves were measured according to the pre-treatment time as shown in Fig. 3.16.

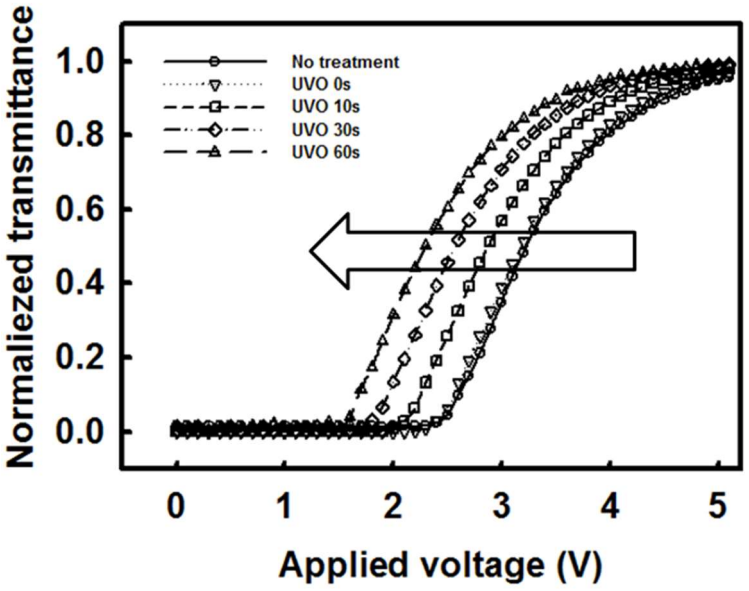

Figure 3.16. Voltage-transmittance curves corresponding to the pre-treatment time.

The voltage–transmittance curves of the LC cells, fabricated with the anchoring energy control layers at different pre-treatment times, under the applied voltage in a square form with the frequency of 1 kHz. The light source was a He–Ne laser with the wavelength of 632.8 nm. The input polarisation was set to be an angle of 45° with respect to the peeling direction and perpendicular to the analyser in the normally white mode. As shown in Fig.3.16, the transmittance in the bright state and the threshold voltage of the LC cell was found to decrease from 2.7 V to 1.7 V. It is consistent that threshold voltages decrease as the decrease of the polar anchoring energy. The function between the threshold voltage and polar anchoring energy is

expressed as follows:

$$V_{th} = \frac{\pi}{(h_c + 2K_{33}/W_\theta)}\sqrt{\frac{K_{33}}{\varepsilon_0|\Delta\varepsilon|}}\,d \tag{3.8}$$

where V_{th} is the threshold voltage, $\Delta\varepsilon$ is the dielectric anisotropy.

However, the threshold voltage varied from 1 V, which is wider than 0.5 V, the range predicted based on the anchoring energy change. As a result, it can be predicted that the pretilt angle of LC molecule has changed. However, as can be seen from the previous microscopic image, there is little difference in the dark state.

In the case of the response time, the functions between the decay time, rising time and polar anchoring energy are expressed as follows;

$$\tau_d = \frac{\gamma_1 h_c}{2W_\theta} \tag{3.9}$$

$$\tau_r = \frac{\gamma_1}{\left|\varepsilon_0|\Delta\varepsilon|E^2 - 2\,W_\theta/h_c\right|} \tag{3.10}$$

where γ_1 is the rotational viscosity. Therefore, according to decrease of the anchoring energy, the decay time is expected to increase, but the rising time is expected to decrease. Because of this, it is expected to that the total response time of the LC devices will not be affected according to anchoring energy change.

Such the reduction of the threshold voltage affects the instability in operating the devices comparison to previous research [96] which uses RM

layers as the voltage dividing layer. However, this approach cause the increase in the power consumption in operation. In contrast, the proposed technique has a strength in terms of the power consumption compared with the voltage dividing layer.

3.2.3 Fabrication of 8-domains

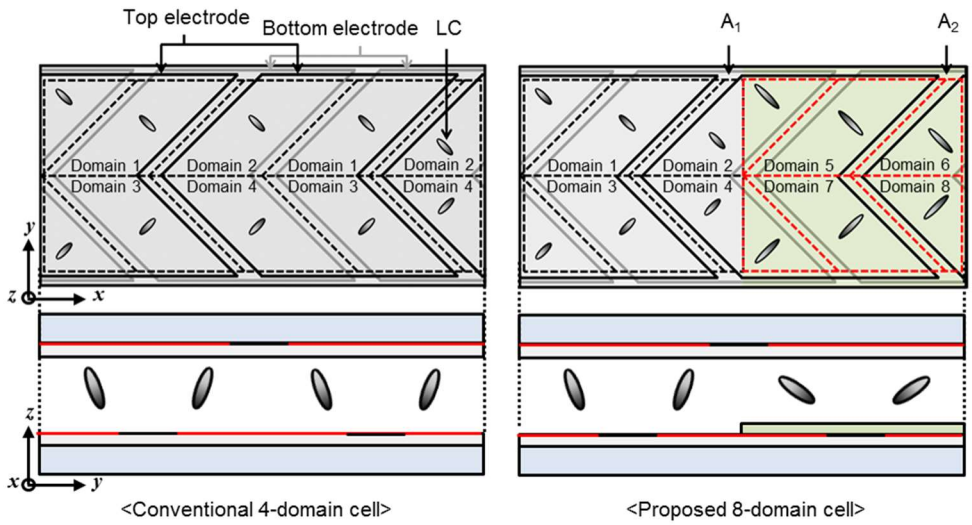

Figure 3.17. The schematic illustration of the top and side view of the LC unit cell (a) without the anchoring disparity (4-domain) and (b) with the anchoring disparity (8-domain).

The 8-domain cell was fabricated through the anchoring disparity based on the anchoring energy control layer which was verified through the experiments in previous chapter. Figures 3.17(a) and 3.17(b) show the show

the top and side views of two unit cells without the anchoring disparity (4 domains) and with the anchoring disparity (8 domains), respectively, in the PVA configuration with simple chevron electrodes [103, 104].

Using the chevron electrode, the LC cell with the patterned anchoring energy control layer (t = 60 s) was fabricated as shown in Fig. 3.18. In fabricating the LC cells, ITO-coated glass substrates were spin-coated with a mixed homeotropic alignment material at the rate of 3000 rpm for 30 s and post-annealed at 150˚C for 1 h. The PDMS (Sylgard 184, Dow Corning) plate was made in same method in Chap. 3.2.2. The ultra-violet ozone (UVO) treatment was applied to both the substrate for pre-treatment time 60 s and the PDMS plate for 45 s to increase the amount of PDMS oligomer transferred. After the pre-treatment, the substrate in conformal contact with the PDMS surface was heated at the transfer temperature of 200°C for the heating time of 5 min. The PDMS plate was then detached from the glass substrate along the peeling direction D. Finally, the LC cell was assembled such that the top substrate which was spin-coated with homeotropic alignment layer (AL60702) at 3000 rpm, 30 s. The cell thickness h_c was maintained using glass spacers of 5 μm for the microscopic observation of the alignment texture and voltage-transmittance curve characterisation of the LC cell. The nematic LC (MLC-2038, Merck) was injected into the cell by capillary action at 80°C in the isotropic state. The filled LC cell was then cooled down to room temperature under ambient atmosphere. The voltage-dependent transmittance was measured as a function of the polar angle (θ) using a spatial photometer (EZcontrast 160R, ELDIM). Here, the voltage-dependent transmittance from

the LC cell without the anchoring disparity was also measured as a reference. After that, gamma curves were obtained from the both cells.

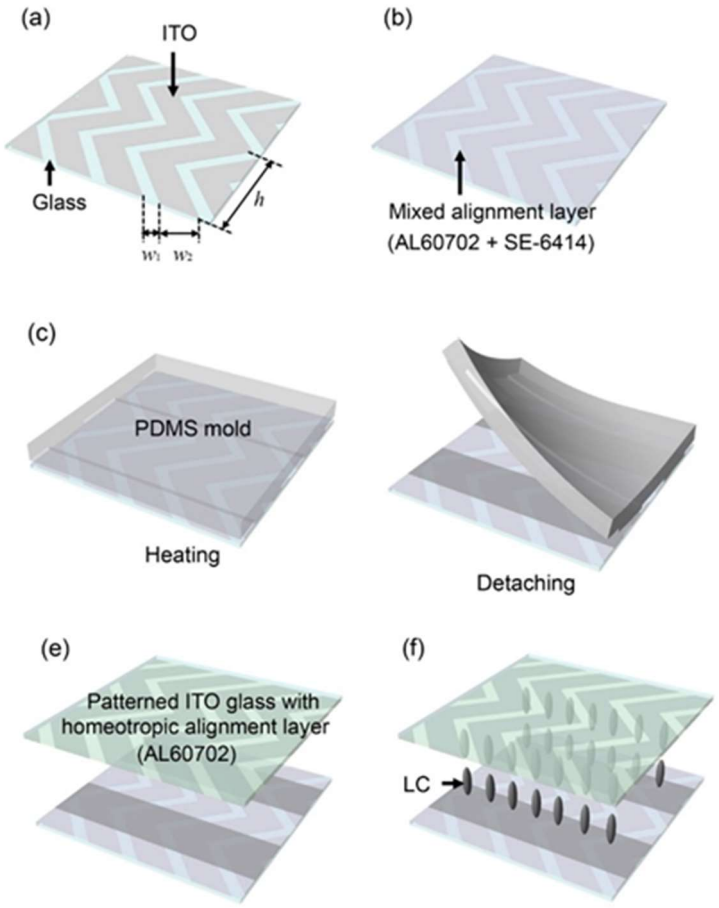

Figure 3.18. Schematic diagram showing the fabrication process of the PVA LC cell based on the anchoring disparity.

3.2.4 Experimental results and discussions

Microscopic images

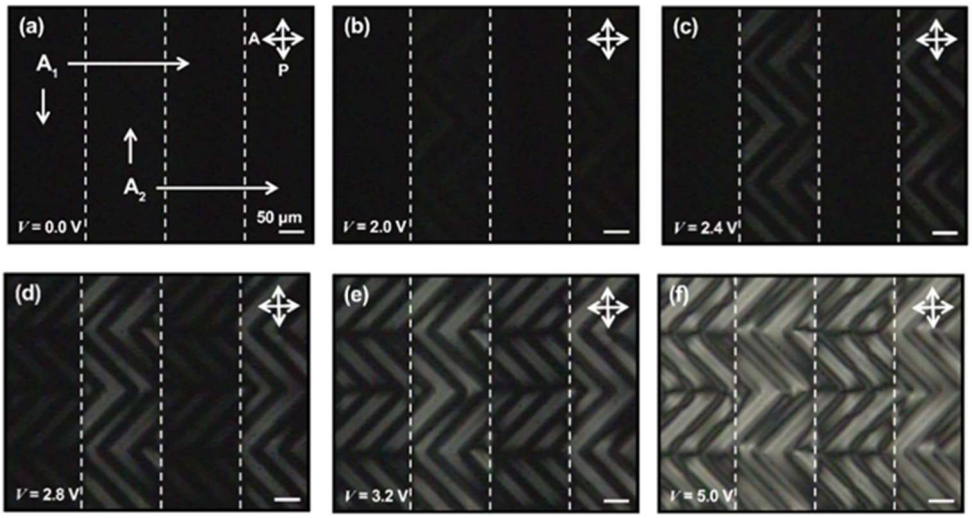

Figure 3.19. Microscopic images of the PVA LC cell with the anchoring disparity at various applied voltages of 0, 2.0, 2.4, 2.8, 3.2, and 5.0 V.

Figure 3.19 shows the microscopic textures of the LC cell with periodic anchoring energy control layers, observed using the POM under crossed polarizers, at different values of the applied voltage (0, 2.0, 2.4, 2.8, 3.2, and 5.0 V). The pre-treatment time of the PDMS mold was determined to be t = 60 s. Under no applied voltage, a highly uniform dark state was obtained. As the applied voltage was gradually increased, the remaining surfaces and sub-

domains on the anchoring energy control layer were successively appeared due to the difference in the threshold voltage between them by the principle of the voltage division.

Gamma distortion

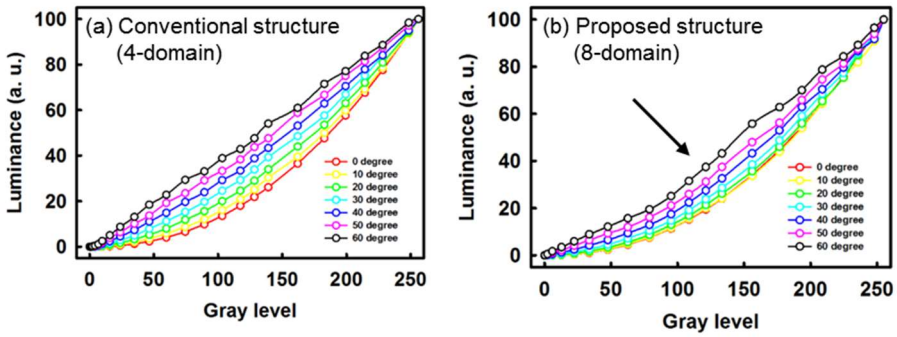

Figure 3.20. Experimental results for the luminance as a function of the input grey level for (a) conventional 4-domain and (b) proposed 8-domain.

Figures 3.20(a) and (b) show the experimental results for the gamma curves of the LC cells with 4-domain cell and 8-domainm, respectively. Clearly, in the presence of the anchoring disparity, the reduction of the gamma distortion was profound at large viewing angles. This result is quite desirable since the human eye is more sensitive to change in dark. It was also observed that the relief of gamma shift becomes more distinct at the higher value of the polar angle. It means that the variation of the optical phase retardation depending on the polar angle was successfully diminished by the two different

tilt angles of LC in the presence of an applied voltage. In other words, by the use of the anchoring disparity, the gamma shift, particularly at large viewing angles becomes greatly diminished so that the color uniformity at different viewing angles will be preserved.

3.2.5 Summary

In this chapter, it was demonstrated that the new concept of the LCD which enables to reduce gamma distortion at off-axis by construction of the anchoring disparity based on the anchoring energy control layer onto the homeotropic alignment surface. The anchoring energy control layer plays a role of the capacitive element in series to divide the applied voltage, providing the sub-domain with the different threshold voltages. In contrast to the conventional multi-domain LCD based on the anchoring energy, the wide-range change of the anchoring energy and the large shift of the threshold voltage were realized by the control of the pre-treatment time with the thermo-transfer printing. The experimental results for the gamma curves of the fabricated LC cell with the anchoring disparity were the reduction of the gamma distortion in comparison to conventional 4-domain LC cell. This simple approach is directly applicable for constructing in various types of the LCD modes with high image quality.

Chapter 4

Novel Quantum Dot-Based LCD for High Color Purity

4.1 Color-Separated Pattern of QDs

In this chapter, color-separated pattern of QD for the enhancement of color purity in FPD. The possibilities of wide color gamut display than conventional QD based color reproduction technology will be demonstrated by patterning quantum dots based on a polymer matrix.

4.1.1 Introduction

In the past decades, the LCDs have been extensively studied for use in flat apnel displays because of lightweight panel, thin thickness and low power consumption [14-16, 21, 23]. In order to improve image performances of LC display, much effort has been made in developing a variety of LC operating characteristics such as viewing angle, threshold voltage and response time [85,87,92]. Among various operating characteristics, color reproduction with high quality is essential for constructing LCDs since conventional color filters and LED backlight severely deteriorate the color gamut and reduce the total amount of the transmittance. As promising candidates, QDs have been widely studied for such compensation layer in backlight unit owing to the unique selective emissive characteristics arising from the intrinsic narrow emission band according to material and size [105-107]. Recently, in order to minimize the transmission loss occurring in the color filter, blue LED and color-separated QD pattern techniques based on a polymer matrix for positioning the QDs in front of the panel according to color of the color filters have been extensively studied [43-45]. However, the coloration without the color filters is still challenging due to the blue light cross-talk since QD patterns does not absorb the backlight completely, and the QDs are not uniformly distributed in the polymer matrix.

In this chapter, a novel color-separated QD pattern in the polymer matrix was demonstrated. In contrast with previous approaches, reactive mesogen, which is photo-curable, transparent and molecular aligned, was used for construction of polymer matrix to completely dissolve the quantum dots. The emission characteristics of the QDs were measured by changing the

concentration ratios of QD and RM. In addition, red, green, and blue patterns on a single substrate through applying conventional photo-lithography process were demonstrated. Next, a novel QD emissive LCD based on the color-separated QD pattern for high color purity was proposed. The QD emissive LCD consisted of the VA mode LC cells and a light source on bottom of the structure. The LC cell acted as a role of tunable light modulator for the incident light from the light source depending on the applied voltage. In front of the QD emissive LCD, the photo-luminescent light of QD was emitted in certain pixels of which the source light is transmitted through LC modulator. The color purity and color gamut of QD emissive LCD was measured compared to the previous LCD structure in which the color filters and QD compensation layers was placed in front of the cell.

4.1.2 Fabrication of color-separated QD patterns

In constructing the color-separated QD pattern, glass substrates were first sonicated in acetone for 30 min and in deionised water for 10 min in sequence. After each cleaned glass substrate was dried with nitrogen gas, the homeotropic alignment layer (AL22620, JSR) was spin-coated at 3000 rpm for 30 s and post-annealed at 150˚C for 1 h.

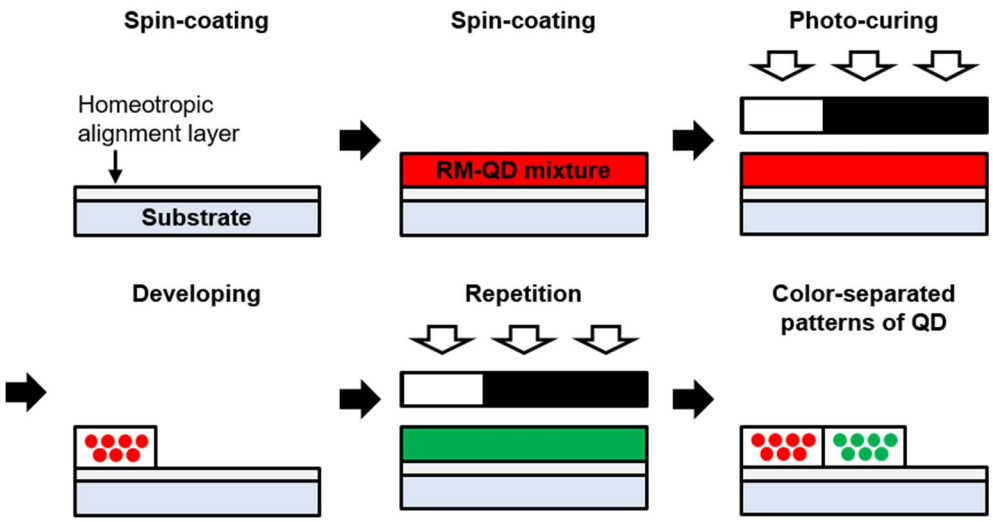

Figure 4.1. Illustration of fabrication process of the color-separated QD pattern based on the polymer matrix.

A mixture of the hoemotropic RMs in propylene glycol monomethyl ether acetate solution (RMS03-015, Merck) and red QDs in toluene (NSQDs-HOS(T)-620, Nanosqure) was then spin-coated at rate of 3000 rpms for 30 s on the alignment layer without the rubbing process and softly annealed at 75°C for 60 s to remove the solvent The RM-QD mixture layer was photo-polymerized with the photomask under the UV at the intensity of 20 mW/cm^2 for 120 s. The un-polymerized RM-QD mixtures were removed by PGMEA (Sigma Aldirich Korea) and fully dried at 75°C. Then the same procedures were applied to a RM-green QDs (NSQDs-HOS(T)-530, Nanosquare) mixture and RM-blue QDs (NSQDs-OS(T)-440, Nanosqure) mixture. Not that the emission wavelength peaks of red QDs, green QDs, and blue QDs were 620 nm, 530 nm, and 440 nm, respectively.

4.1.3 Experimental results and discussions

Emission properties of QD-RM layer

First, the emission characteristics of the RM-QD layer according to the QDs and RM concentration were measured under the ultra-violet (UV) light which has the emission wavelength peak at 365 nm and the intensity of 20 mW/cm^2.

As shown in Fig. 4.2, the emission of the QD layer gradually increases according to the increment of the QD concentration. Moreover, unlike conventional patterning techniques based on polymer matrix, QDs emit very uniform light even at low concentrations because the QDs are dispersed uniformly inside the RM matrix. It is noted that when the concentration of the QDs exceeds a certain concentration, cracks occur on the RM-QD layer owing to the aggregation of the QDs breaks the alignment of the RM polymer matrix.

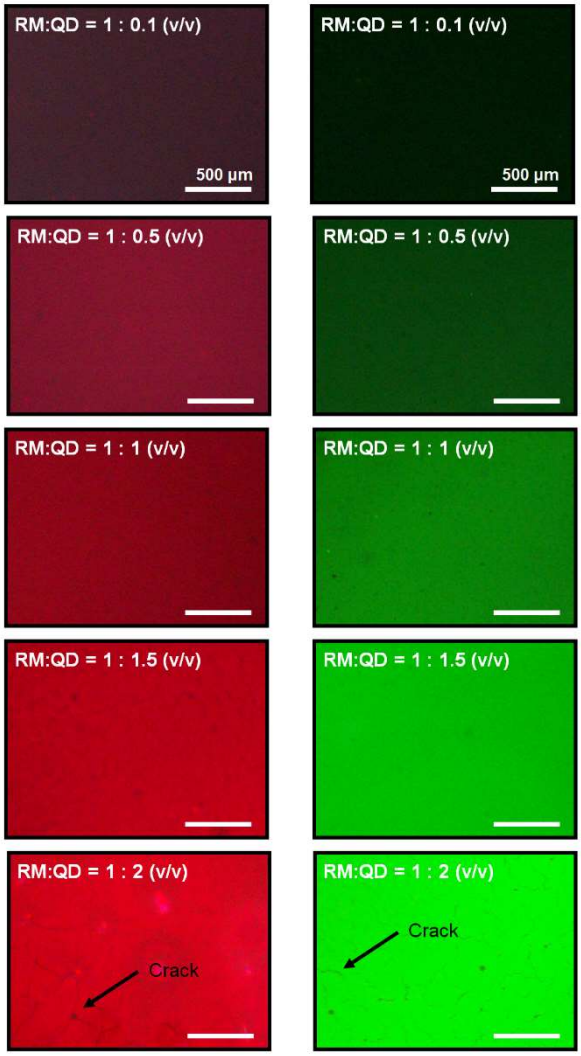

Figure 4.2. Microscopic images of the RM-QD layer corresponding to the QD conenctration in RM-QD mixture under UV lights.

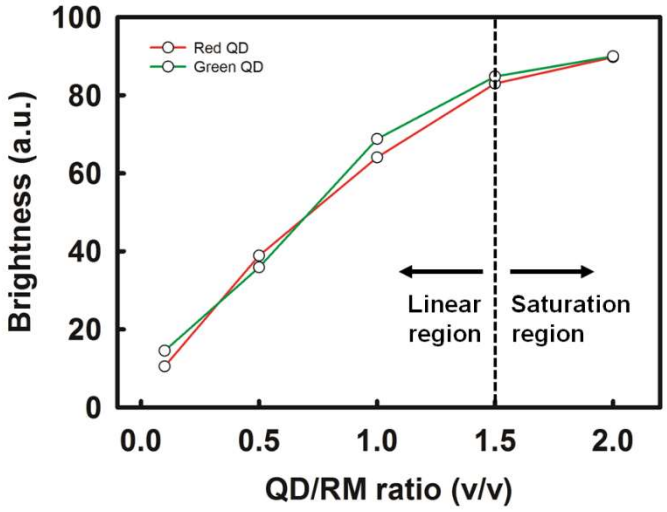

Figure 4.3. The Brightness of RM-QD layer according to QD/RM ratio.

As a result of measuring the brightness for more quantitative measurement, the brightness linearly increased according to the concentration up to the QD/RM concentration of 1.5. As described in Fig. 4.2, due to the occurrence of cracks in RM-QD layer, the brightness of QD is saturated at later concentrations.

Color separated pattern of QDs

Based on these results, the QD-RM layer was patterned on the same substrate through dual patterning using photo-mask. Figure 4.4 shows the microscopic image of the red QD pattern, green QD pattern and both colors pattern on a single substrate through the dual patterning process.

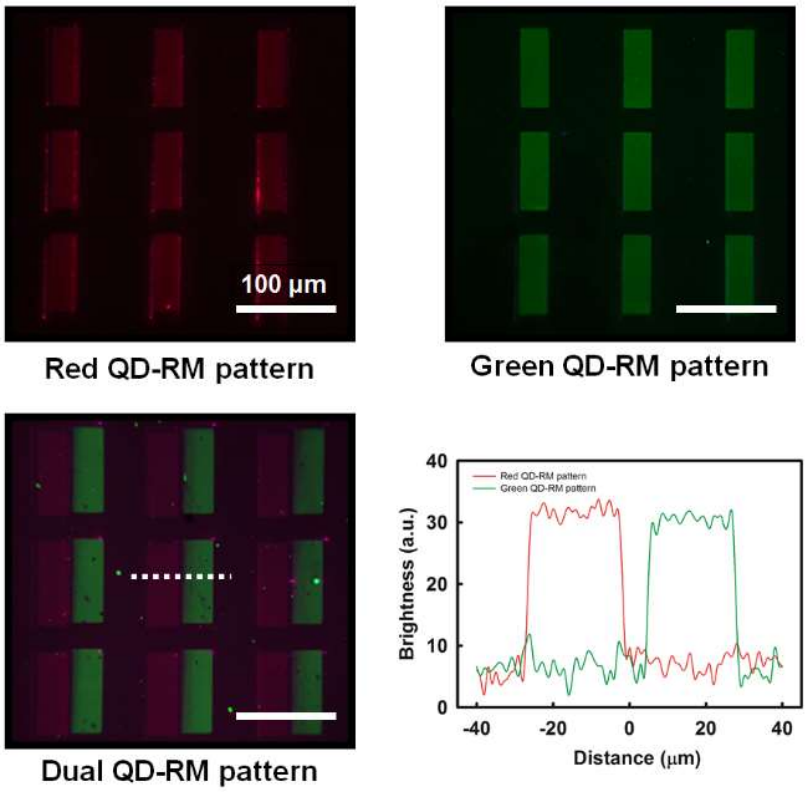

Figure 4.4. The color-separated pattern of QD through dual patterning process.

As observed from the Fig. 4.4, it can be noted that the pattern was formed very uniformly without any crack, and the emission properties remains constantly even in the continuous dual patterning process. In addition, the emission properties of red and green QDs can be controlled to be the same brightness by controlling the ratio of the QD and RM. In this case, the ratio of the red QDs and RM is 0.5 and the ratio of green QDs and RM is 1 owing to a difference in photo-luminance effect between red QDs and green QDs.

4.2 QD Emissive LCD

In this chapter, a new QD emissive LCD display for the enhancement of color purity based on the color-separated pattern of quantum dots developed in previous chapter was proposed. The color purity and the color gamut in comparison to the conventional LCD, QD compensation LCD, and proposed QD emissive LCD will be discussed.

4.2.1 Device concept

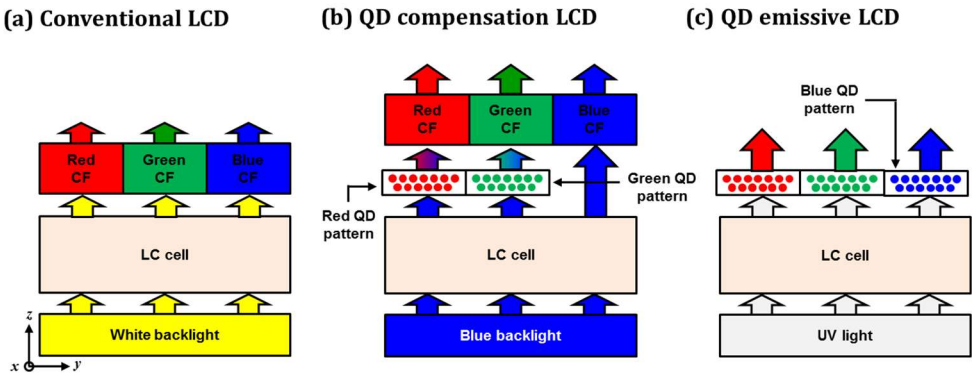

Figure 4.5. Schematic illustration of the coloration in (a) conventional LCD using white LED and color filters, (b) QD compensation LCD using blue LED, and (c) proposed QD emissive LCD using UV backlight.

As described above, conventional LCDs implement colors using conventional color filters and the white backlight as shown in Fig. 4.5(a). In the case of QD compensation LCD, the separated QD pattern is placed between the color filter and the LC cell to improve the transmittance of red and green light using the down-conversion. In this study, I intend to implement color using only the emission of the QD without color filters in order to essentially eliminate the reduction of the transmittance during passing the color filters. For proposed LCD configuration, ultra-violet (UV) light was used in this study.

4.2.2 Fabrication of QD-based LCD

In constructing the color-separated QD pattern, the same method as in the previous chapter was used. In fabrication of the LC cell, glass substrates were first sonicated in acetone for 30 min and in deionised water for 10 min in sequence. After each cleaned glass substrate was dried with nitrogen gas, the homeotropic alignment layer (AL22620, JSR) was spin-coated at 3000 rpm for 30 s and post-annealed at 150˚C for 1 h. After rubbing process on the alignment layer, anti-parallel LC cell was fabricated with 5-μm cell spacer. The color-separated QD patterns were placed on the VA-LC cell and the cell was driven with a UV light of 365 nm wavelength (Ocean Optics) as a backlight.

4.2.3 Experimental result and discussions

Electro-optical properties of QD emissive LCD

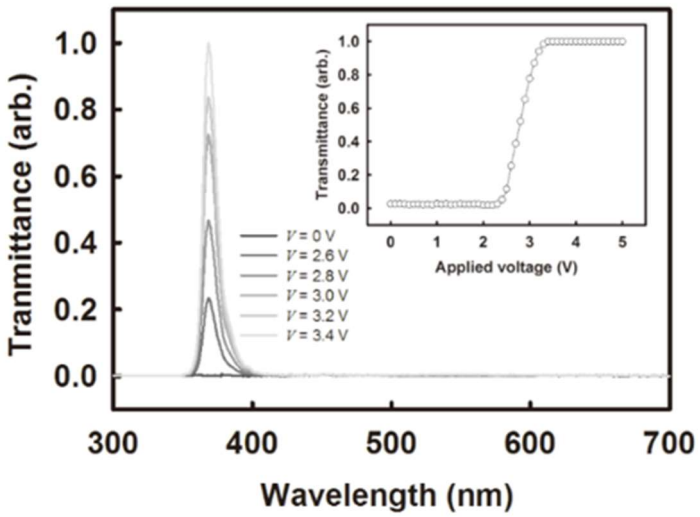

Figure 4.6. The voltage-transmittance curves of the VA LC cell for QD emissive LCD under the 365 nm UV light.

Figure 4.6 shows the voltage–transmittance curves of the LC cells, fabricated with homeotropic layers, under the applied voltage in a square form with the frequency of 1 kHz. The input polarisation was set to be an angle of 45° with respect to the rubbing direction and perpendicular to the analyser in the normally black mode. For measuring the emission, a ultra-violet light source and UV-Vis. fiber optic spectrometer (S2000, Ocean Optics) were used. As shown in inset of Fig. 4.6, the transmittance of the LC cell was found to

increase with increasing the applied voltage as normal VA mode under the white light. It should be noticed that no change of wave-shape and peak shift occurs during applying the voltage. It is expected that QD emission will be possible through this new LCD structure which uses the UV backlight.

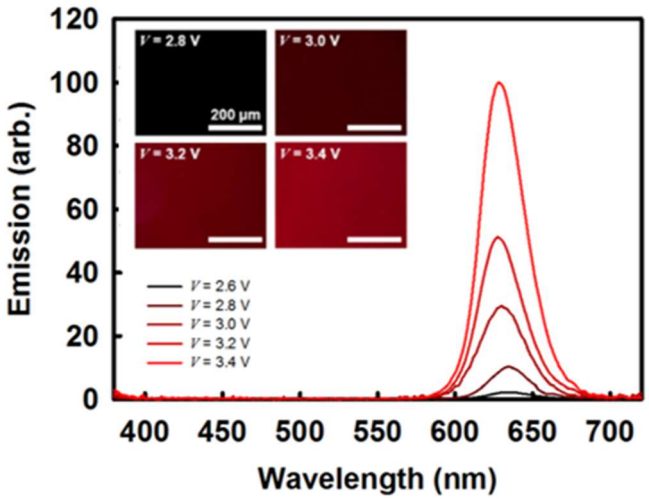

Figure 4.7. The voltage-emission curves of the red QD-RM layer on the VA mode LC cell and the 365 nm UV light.

Figure 4.7 shows the voltage-emission curves of the red QD-RM layer on the VA mode LC cell, under the same way in previous experiments. As shown in inset of Fig. 4.7, the emission of the red QD-RM layer was found to increase with increasing the applied voltage as increase of the transmittance of the UV light. Moreover, wave shape of the emission light from the red QD maintained the narrow bandwidth shape from 2.8 V to 3.4 V of the applied

voltages. It is noted that proposed LCD devices have higher color purity than conventional LCDs which uses the color filter and white light.

Coloration properties of QD emissive LCD

The color reproduction was measured by replacing the QD-RM layer based on the previously fabricated LCD device.

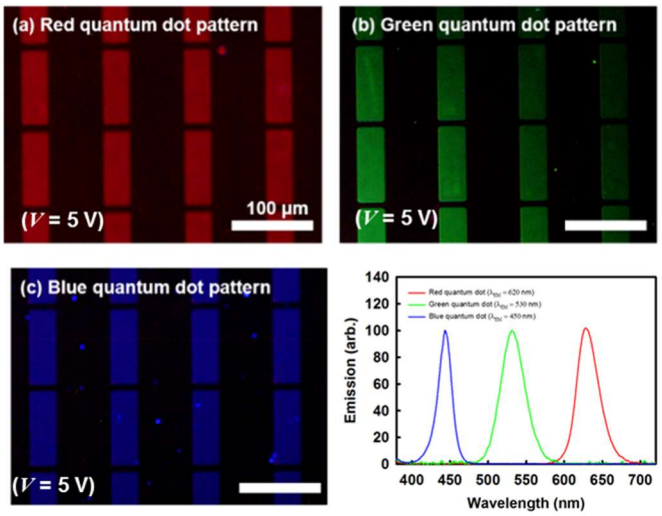

Figure 4.8. Microscopic images of the (a) red QD emission, (b) green QD emission, and (c) blue QD emission on the proposed LCD devices.

Figure 4.8 shows the microscopic images of the primary colors emission properties including red, green, and blue based on patterned QD in RM matrix. The red, green, and blue colors all operate normally in on-state, and the color purity was also very narrow as shown in the graph.

Finally, color coordinate of the proposed QD emissive LCD was calculated for comparing to conventional LCD and QD compensation LCD. For calculation of the color coordination, computer program (Matlab, MathWorks) was used with the emission properties at on-state and color matching functions.

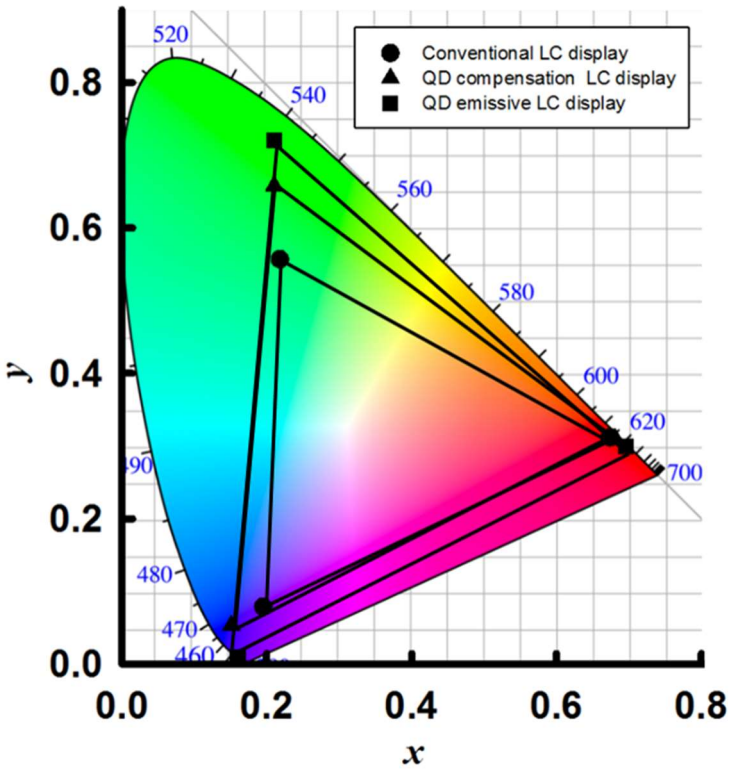

Figure 4.9. Color coordinate of the conventional LCD, QD compensation LCD, and proposed QD emissive LCD in CIE 1931.

Figure 4.9 shows the expansion of the color space in comparison to conventional LCDs. Especially, in the case of the green, it should be noticed that the large shift of green coordinate compared to the conventional LCDs contributes to expansion of the color gamut.

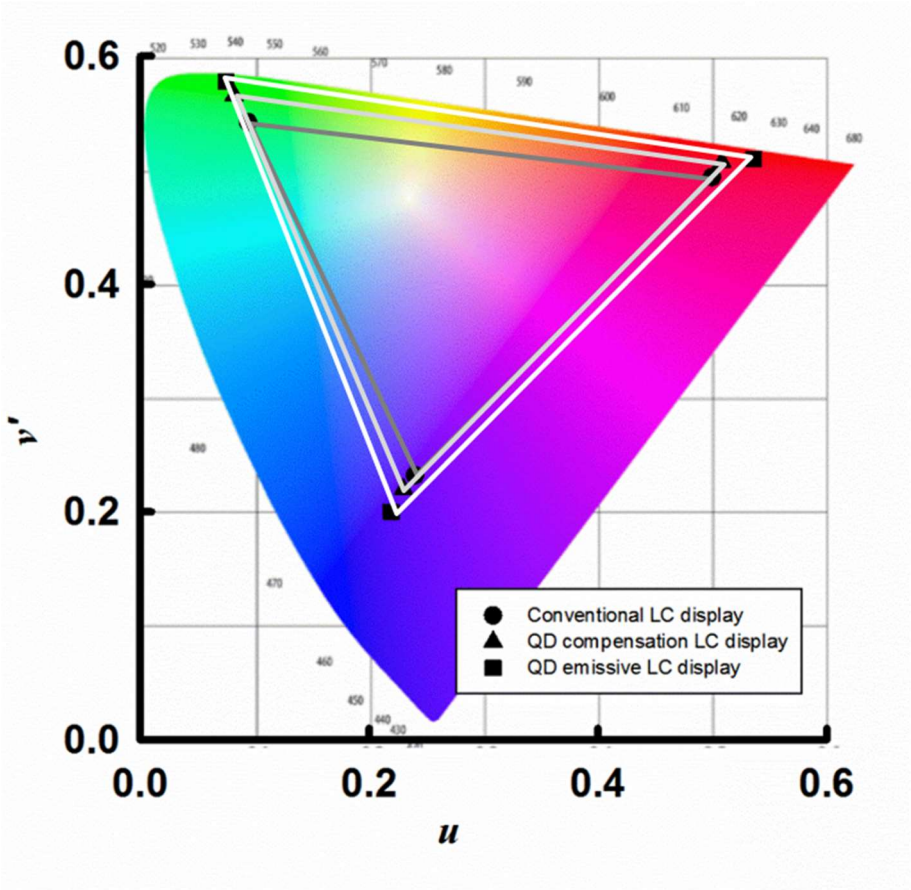

Figure 4.10. Color coordinate of the conventional LCD, QD compensation LCD, and proposed QD emissive LCD in CIE 1976.

Based on the previous measurements and calculations, Fig. 4.10 shows the color coordinates of three display devices on the CIE 1976. Even the large green shift in CIE 1931 decreased, the color gamut widened in overall primary color because the CIE 1976 represents a more uniform color space than the CIE 1931.

For measurement of the color space more quantitatively, table 4.1 shows the results of the calculated color coordinate from fabricated reference LCD devices in the CIE 1931 color space and CIE 1976 color space. In CIE 1931 color space, calculated color space area of QD emissive LCD was significantly extended compared to the conventional LCD and QD compensation LCD as reference devices. Compared with the conventional LCD, it increased to about 63.1% and increased to about 20.4% compared with QD compensation LCD.

In CIE 1976, calculated color space area of QD emissive LCD was significantly extended compared to the conventional LCD and QD compensation LCD as reference devices. Compared with the conventional LCD, it increased to about 20.9% and increased to about 10.3% compared with QD compensation LCD.

(x, y)	Conventional LCD	QD Compensation LCD	QD emissive LCD
Red (CIE1931)	(0.674, 0.312)	(0.681, 0.310)	(0.696, 0.299)
Green (CIE1931)	(0.218, 0.557)	(0.215, 0.658)	(0.210, 0.720)
Blue (CIE1931)	(0.195, 0.079)	(0.151, 0.053)	(0.160, 0.010)
Area (CIE1931)	0.112	0.152	0.183
Red (CIE1976)	(0.499, 0.494)	(0.508, 0.507)	(0.536, 0.517)
Green (CIE1976)	(0.094, 0.542)	(0.082, 0.566)	(0.075, 0.577)
Blue (CIE1976)	(0.240, 0.232)	(0.234, 0.221)	(0.219, 0.199)
Area (CIE1976)	0.112	0.122	0.137

Table 4.1. The color coordinate of the different type LCD in CIE 1931 and CIE 1976.

4.2.4 Summary

In this chapter, a new concept of QD emissive LCD based on the color-separated QD patterns was proposed. In contrast to the conventional QD patterning method based on a polymer matrix, the RM is capable of dissolving the QD very uniformly and serves as a transparent polymer matrix for minimizing the loss of the light transmittance. The remarkable high emission and color uniformity is mainly due to the separation of the element for the color generation and that for the intensity control, which has not been made so far. The color gamut of QD emissive LCD was expanded compared with conventional LCD and QD compensation LCD. This QD emissive LCD approach will provide a new method of achieving the high image quality of the LCD.

Chapter 5

Concluding Remarks

In this thesis, new types of LCDs for the reduction of the gamma distortion and the expansion of color gamut were proposed. The key concept described in this thesis is the development of the LCD configuration by utilizing the additional layers based on the thermo-transfer printing and color-separated QD patterns.

In Chapter 1, several example of flat panels including LCD, LED display, PDP, and OLED which construct FPD industries were briefly introduced. Especially, the LCD have played a major role to date, and have been expected to play a pivotal role in the future industry.

In Chapter 2, the emerging technologies in LCD to survive in the FPD market were discussed. Wide-viewing angle technology and coloration are the most important technologies to overcome the intrinsic problems in LCD panel. A variety of techniques have been developed for the viewing angle

dependency, which is based on the difference in effective optical path, but still have many problems. Also, the color reproduction technique using white light and conventional color filer have suffered from the essential problems.

To overcome the viewing angle dependency, in chapter 3, the wide-viewing angle technique of LCD was demonstrated by multi-domain construction in which liquid crystal (LC) molecules are arranged in different polar directions at middle grey scale. In order to realize this, a new alignment layer which can control the polar anchoring energy was developed. Uncured oligomers in cross-linked polymer were transferred onto substrate to change the surface wettability of the substrate. The amount of transferred oligomers was changed by additional heat treatments, the thermal-transfer printing, during the diffusion of oligomer from cross-linked polymer onto substrate. During the thermal-transfer printing, the amount of transferred oligomer was manipulated according to the heat treatment temperature. Then, the LC alignment properties including the pretilt angle and anchoring energy were changed in a wide-range from homogenous alignment to homeotropic alignment as the adjustment of the substrate surface energy.

Based on the results, a new multi-domain LCD based on the anchoring disparity in polar direction for reducing the gamma distortion was demonstrated. The additive layer acted as a role of anchoring energy control for shifting the threshold voltage in sub-domain and was capable of spontaneously aligning the LC molecules without the change of the pretilt angle. The threshold difference compensated the difference of the phase retardation between the normal and an oblique viewing direction, which can

reduce the gamma distortions. The alignment property of LC on the anchoring energy control layer depending on the UVO exposure time for the enhancement of amount of transferred oligomer from cross-linked polymer was changed. The experimental measurement for the viewing angle showed that the 8-domian cell of proposed cell structure reduced the gamma distortions in compared with the 4-domain cell without the change of the aperture ratio and circuit complexity.

In Chapter 4, a new type of color LCD based on the photo-luminescent emission of the quantum dots (QDs) in polymer matrix was described. In contrast with previous approaches, reactive mesogen, which is photo-curable, transparent and molecular aligned, was used for construction of polymer matrix to completely dissolve the quantum dots. The emission characteristics of the QDs were manipulated by changing the concentration ratios of QD and RM. In addition, uniform red, green, and blue patterns on a single substrate through applying conventional photo-lithography process were demonstrated.

Finally, a novel QD emissive LCD based on the color-separated QD pattern for high color purity was proposed. The QD emissive LCD consisted of the VA mode LC cells and a light source on bottom of the structure. The LC cell acted as a role of tunable light modulator for the incident light from the light source depending on the applied voltage. In front of the QD emissive LCD, the photo-luminescent light of QD was emitted in certain pixels of which the source light is transmitted through LC modulator. The color purity and color gamut of QD emissive LCD was enhanced compared to the previous LCD structure in which the color filters and QD compensation layers

were placed in front of the panels.

In conclusion, the applicability to the FPD industry was explored for the control of the viewing-angle and coloration. The new concept of device and experimental results provided here will lead to the development of the advanced LCD devices for high performance. In conclusion, the novel concept of LCD configurations was explored for the enhancement of LCD performance. Based on the experimental results of the unique LCD modes, new types of wide viewing technologies as well as coloration technologies were demonstrated. This versatile approach will give great impact on the research fields of the advanced LCD and FPD industry.

Bibliography

[1] T. J. Nelson and J. R. Wullert II, *Electronic information display technologies* (World Scientific Publishing, MA, 1997).

[2] IHS markit, "IHS display long-term demand forecast tracker 2015", UK (2016).

[3] IHS markit, "IHS display long-term demand forecst tracker 2016", UK (2017).

[4] P. Yeh, and C. Gu, *Optics of liquid crystal displays* (Wiley, New york, 2006).

[5] S. K. Kim, H. S. Han, Y. J. Woo, and G. H. Cho, *IEEE Transactions on Industrial Electronics* **53**, 707 (2006).

[6] C. H. Lin, *IEEE Transactions on Industrial Electronics* **52**, 1881 (2006).

[7] S. J. Choi, K. C. Lee, and B. H. Cho, *IEEE Transactions on Industrial Electronics* **53**, 707 (2006).

[8] M. Rico-Secades, A. J. Calleja, J. Ribas, E. L. Corominas, J. M. Alonso, J. Cardesin, and J. Garcia-Garcia, *IEEE Transactions on Industrial Applications* **41**, 1386 (2005).

[9] G. Moschopoulos and P. Jain, *IEEE Transactions on Industrial Electronics.* **52**, 23 (2005)

[10] J. H. Burroughes, D. D. C. Bradley, A. R. Brown, R. N. Marks, K. Mackay, R. H. Friend, P. L. Burns, and A. B. Holmes, *Nature* **347** 539 (1990).

[11] P.-G. d. Gennes and J. Prost, *The physics of liquid crystals,* 2nd ed. (Clarendon Press, Oxford, 1993).

[12] P. J. Collings, *Liquid crystals: nature's delicate phase of matter* (Princeton University Press, Princeton, 2002).

[13] V. Chigrinov, ASID'04 Tutorial notes (2004).

[14] G. H. Heilmeier, L. A. Zanoni and L. A. Barton, *Proceeding of IEEE* **56**, 1162 (1968).

[15] M. Schadt and W. Helfirch, *Applied Physcis Letter* **18**, 127 (1971).

[16] Y. Toko, T. Sugiyama, K. Katoh, Y. Iimura and S. Kobayshi, *SID Digest*, 622 (1993).

[17] A. Lien and R. A. John, *SID Digest*, 269 (1993).

[18] K. W. Lee, A. Lien, J. H. Stathis and S. H. Paek, Japanes

Journal of Applied Physcis **36**, 3591 (1997).

[19] M. Okazaki, K. Kawata, H. Nishikawa and M. Negoro, *Polymer Advaned Thechology* **11**, 398 (2000).

[20] T. Nose, M. Suzuki, D. Sasaki, M. Imai and H. Hayama, *SID Digest*, 994 (2001).

[21] R. Kiefer, B. Weber, F. Windschied and G. Baur, *Proceeding of Japan Display*, 577 (1995).

[22] M. Oh-e, M. Ohta. S. Aratani and K. Kondo, *Proceeding of Asia Display*, 427 (1995).

[23] K. Ohmuro, S. Kataoka, T. Sasaki and Y. Koike, *SID Digest*, 845 (1997).

[24] S. Yamauchi, M. Aizawa, J. F. Clerc, T. Uchida and J. Duchen, *SID Digest*, 378 (1989).

[25] K. Koike, S. Takaoka, T. Sasaki, H. Chida, H. Tuda, A Takeda and Ohmuro, *Proceeing of AM-LCD*, 25 (1997).

[26] S. Kobayashi, *Syposium of the Japanese Association of Liquid Crystal Scientists*, 1 (1994).

[27] K. Sumiyoshi, K. Takatori, Y. Hirai and S. Kaenko, *Journal of SID* **2**, 31 (1994).

[28] A. Takeda, *EKISHO* **3** 117 (1999).

[22] S. Ohmuro, S. Kataoka, T. Sasaki and Y. Koike, *SID Digest*, 1221 (2010).

[23] J. Guo, H. Wu, F. Chen, L. Zhang, W. He, H. Yang, and J. Wei, *Journal of Materials Chemistry* **20**, 4094 (2010).

[24] M. E. McConney, V. P. Tondiglia, J. M. Hurtubise, L. V. Natarajan, T. J. White, and T. J. Bunning, *Advanced Materials* **23**, 1453 (2011).

[25] A. Y.-G. Fuh, Z.-H. Wu, K.-T. Cheng, C.-K. Liu, and Y.-D. Chen, *Optics Express* **21**, 21840 (2013).

[26] K. M. Lee, V. P. Tondiglia, M. E. McConney, L. V. Natarajan, T. J. Bunning, and T. J. White, *ACS Photonics* **1**, 1033 (2014).

[27] X. Zhu, Z. Ge, and S.-T. Wu, *Journal of Display Technology* **2**, 2 (2006).

[28] B.-J. Mun and G.-D. Lee, *Molecular Crystals and Liquid Crystals* **595**, 92 (2014).

[29] Q. Hong, T. X. Wu, X. Zhu, R. Lu, and S.-T. Wu, *Applied Physics Letters* **86**, 121107 (2005).

[30] C.-H. Lin, *Optics Express* **16**, 13276 (2008).

[31] S.-H. Ji, J. W. Moon, B. Kang and G.-D. Lee, *Journal of the Korean Physical Society* **55**, 4 (2009).

[32] K. Kalantar, *SID Digest*, 604 (2011).

[33] S. Hwang, J. Min, M.-G. Lee, K. Choe, H.-Y. Choi, Y.-T. Kim, S.-M. Cho, and S.-D. Lee, *Optical Engineering* **48**, 114001 (2009).

[34] K. H. Kim, S. B. Park, J. K. Song, S. Kim and J. H. Souk, *Proceeding of Asia Display*, 383 (1998).

[35] J. Ma, Y.-C. Yang, Z. Zheng, J. Shi, and W. Cao, *Displays* **30**, 185 (2009).

[36] T. Smith and J. Guild, *Transations of the Optical Society* **30**, 73 (1928).

[37] W. D. Wright, *Transactions of the Optical Society* **30**, 141 (1928).

[38] International Commission on Illumination, "Selected Colorimetric Tables", http://www.cie.co.at/index.php (accessed June, 2017).

[39] R. C. Ashoori, *Nature* **379**, 413 (1996).

[40] C. B. Murray, C. R. Kagan, and M. G. Bawendi, *Annual Reviewi of Materials Research* **30**, 545 (2000).

[41] H. Y. Ramirez, J. Florez, A. S. Camacho, *Physics Chemistry and Chemical Physics* **17**, 37 (2015).

[42] S. Coe-Sullivan, J. S. Steckel, W.-K. Woo, M.G. Bawendi, and V. Bulovid, *Advanced Functional Materials* **15**, 1117 (2005).

[43] Y. Liu, J. Lai, X. Li, Y. Xiang, J. Li, and J. Zhou, *IEEE Photonics Journal* **9**, 6900207 (2017).

[44] H.-J. Kim, M.-H. Shin, H.-G Hong, B.-S. Song, S.-K. Kim, W.-H. Koo, J.-G. Yoon, S.-Y. Yoon and Y.-J. Kim, *Journal of Display Technology* **12**, 6 (2016).

[45] H.-J. Kim, M-H. Shin, J.-S. Kim, S.-E. Kim and Y.-J. Kim, *Scientific Reports* **7**, 43063 (2017).

[46] D. W. Berreman, *Physics Review Letter* **28**, 1683 (1997).

[47] J. M. Geary, J. W. Goodby, A. R. Kmetz, and J. S. Paterl, *Journal of Applied Physics* **62**, 4100 (1987).

[48] W. M. Gibbons, P. J. Shannon, S. T. Sun, and B. J. Swetling, *Naure* **351**, 49 (1991).

[49] B. Wen, R. G. Petschek, and C. Rosenblatt, *Applied Optics* **41**, 1246 (2002).

[50] C. J. Yu, D. W. Kim, J. Kim, and S. D. Lee, *Optics Letter* **30**, 1995 (2005).

[51]J. Kim, J. H. Na, and S. D. Lee, *Optics Express* **20**, 3034 (2012).

[52] H. Okada, P. J. Bos, and H. Onnagawa, *Japanese Journal of Applied Physics* **37**, 2576 (1998).

[53] M. Marangoni, R. Osellame, R. Rampni, M. Buscaglia, and T. Bellini, *Journal of Applied Physcis* **95**, 5972 (2004).

[54] H. R. Kim, Y. W. Lee, S. J. Kim, D. W. Kim, C. J. Yu, B. Lee, and S. D. Lee, *Ferroeelctrics* **95**, 5972 (2004).

[55] M. Schadt, and H. Seiberle, *Nature* **381**, 212 (1996).

[56] S. Varghese, S. Narayanankutty, C. W. M. Bastiaanse, G. P. Crawford, and D. J. Broer, *Advanced Materials* **16**, 1600 (2004).

[57] J. H. Na, H. Li, S. C. Park, and S. D. Lee, *Journal of Information Display* **12**, 191 (2011).

[58] X. Nie, H. Xianyou, R. Lu, T. X. Wu, and S. T. Wu, *Journal of Display Technology* **3**, 280 (2007).

[59] C. M. Waters, E. P. Raynes, and V. Brimmell, *Moleuclar Crystals and Liquid Crystals* **123**, 303 (1985).

[60] E. J. Acosta, M. J. Towler, and H. G. Walton, *Liquid Crystals* **27**, 303 (2007).

[61] P. J. Bos, and K. R. Koechler Beran, *Molecular Crystals and Liquid Crystals* **113**, 329 (1984).

[62] T. Miyashita, Y. Tmaguchi, and T. Uchida, *Japanes Journal of Applied Physics* **34**, L177 (1995).

[63] J. L. Janning, *Applied Physics Letter* **21**, 173 (1972).

[64] F. S. yeung, J. Y. Ho, Y. W. Li, F. C. Xie, O. K. Tsui, P. Sheng and H. S. Kwok, *Applied Physcis Letter* **88**, 051910 (2006).

[65] J. B. Kim, K. C. Kim, H. J. Ahn, B. H. Hwang, D. C. Hyun, and H. K. Baik, *Applied Physcis Letter* **90**, 043515 (2007).

[66] V. G. Chigrinov, V. M. Kozenkov, and H. S. Kwok, *Photoalignment of liquid crystalline materials: physics and application* (Wiely, New York, 2008).

[67] H. Pae, Y. Choi, D. W. Kim, and S. D. Lee, *Molecular Crystals and Liqudic Crystals* **492**, 237 (2008)

[68] B. H. Hwang, C. J. Choi, M. K. Jo, J. B. Kim, H. M. Choe, S. S. Chae, Y. S. Kim, and H. K. Baik, *Langmuir* **26**, 5072 (2010).

[69] S. Yang, J. J. Lee, H. J. Lee, Y. G. Kang, Y. J. Kim, H. Y. Jung, and D. S. Seo, *Liquid Cyrstals* **39**, 71 (2012).

[70] D. Ahn, Y. C. Jeong, S. Lee, J. Lee, Y. Heo, and J. K. Park, *Optics Express* **17**, 19 (2012).

[71] Y. T. Kim, J. H. Hong, T. Y. Yoon and S. D. Lee, *Appied Physcis Letter* **88**, 263501 (2006).

[72] S. Kim, Y. S. Ryu, J. H. Suh, C. M. Keum, Y. Shon, and S. D. Lee, *Journal of Nanoscience and Nanotechonology* **14**, 6069 (2014).

[73] Y. Kawata, and Y. Mori, *Japanese Journal of Applied Physcis* **35**, L40 (1996).

[74] E. P. Raynes, C. V. Brown, and J. F. Stromer, *Applied Physcis Letter* **82**, 13 (2003).

[75] J.-H. Suh, J. Kim, Y.-S. Ryu, Y. Sohn, and S.-D. Lee, *Liquid Crystals* **42**, 1236 (2015).

[76] S. Yunus, C. Looringhe, C. Poleunis, and A. delcorte, *Surface Interaface* **39**, 922 (2007).

[77] L. Yang, N. Shirahata, G. Saini, F. Zhang, L. Pei, M. C. Asplund, D. G. Kurth, K. Ariga, K. Sautter, T. Nakanishi, V. Smentkowsky, and M. R. Linford, *Larmuir* **25**, 5674 (2009).

[78] S. M. Kim, Y. M. Koo, and J. D. Kim, *Molecular Cyrstals and Liquid Crystals* **263**, 437 (1995).

[79] B. Zhang, F. K. Lee, O. Tsui, and P. Sheng, *Physics Review Letter* **91**, 215501 (2003).

[80] G. Baur, V. Witttwer, and D. W. Berreman, *Physics Letter A* **56**, 142 (1976).

[81] L. T. Creagh, and A. R. Kmetz, *Molecular Crystals and Liquid Crystals* **24**, 59 (1973).

[82] Y. A. Nastichin, R. D. Polak, and S. V. Shiyanovskii, *Applied Physics Letter* **75**, 202 (1999).

[83] T. Uchida, and T. Seki, *Liquid crystlas: applications and uses* (World Scientific, Singapore, 1992).

[84] S. J. Hwang, T. A. Chen, K. R. Lin, and S. C. Jeng, *Applied Physcis B* **107**, 151 (2012).

[85] X. Zhu, Z. Ge, and S.-T. Wu, *Journal of Display Technology* **2**, 2 (2006).

[86] B.-J. Mun and G.-D. Lee, *Molecular Crystals and Liquid Crystals* **595**, 92 (2014).

[87] M. Oh-e and K. Kondo, *Applied Physics Letters* **67**, 3895 (1995).

[88] S. Lee, S. Lee, and H. Kim, *Applied Physics Letters* **73**, 2881 (1998).

[89] Y. Tak, W. Park, M. Kim, J. Lee, N. Kim, and J. Souk, *SID Symposium Digest of Technical Papers* **33**, 1281 (2002).

[90] Y.-J. Lee, S. I. Jo, J.-H. Kim, and C.-J. Yu, *Japanese Journal of Applied Physics* **49**, 030209 (2010).

[91] J.-H. Na, H. Li, S. C. Park, and S.-D. Lee, *Journal of Information Display* **12**, 191 (2011).

[92] S. S. Kim, B. H. Berkeley, K. H. Kim, and J. K. Song, *Journal of the Society for Information Display* **12**, 353 (2004).

[93] J. Ma, Y.-C. Yang, Z. Zheng, J. Shi, and W. Cao, *Displays* **30**, 185 (2009).

[94] S. B. Park, J.-K. Song, Y. Um, and K.-H. Kim, *IEEE Electron Device Letters,* **31**, 987 (2010).

[95] K. C. Tien, C. H. Liao, M. H. Wu, W. C. Wei, C. C. Shih, W. H.

Hsu, and J. J. Su, *SID Symposium Digest of Technical Papers* **45**, 1481 (2014).

[96] J.-H. Lee, H. Jin, J.-W. Kim, K.-H. Kim, B. W. Park, T.-H. Yoon, H. Kim, K.-C. Shin, and H. S. Kim, *Journal of Applied Physics* **112**, 054107 (2012).

[97] J.-H. Suh, J. Kim, Y.-S. Ryu, Y. Sohn, and S.-D. Lee, *Liquid Crystals* **42**, 1236 (2015).

[98] H. Y. Kim, G. R. Jeon, D.-S. Seo, M.-H. Lee, and S. H. Lee, *Japanese Journal of Applied Physics* **41**, 2944 (2002).

[99] Y. H. Kwon, J. I. Baek, J. C. Kim, and T. H. Yoon, *Journal of Information Display* **8**, 17 (2007).

[100] J.-W. Kim, D. H. Song, K.-H. Kim, S.-T. Shin, and T.-H. Yoon, *Applied Optics* **52**, 5256 (2013).

[101] J.-H. Lee, H. Jin, J.-W. Kim, K.-H. Kim, B. W. Park, T.-H. Yoon, H. Kim, K.-C. Shin, and H. S. Kim, *Journal of Applied Physcis* **112**, 054107 (2012).

[102] J.-H. Lee, Y. E. Choi, J. H. Lee, B. H. Lee, W. I. song, K.-U. Jeong, G.-D. Lee, and S. H. Lee, *Journal of Physics D: Applied physics* **46**, 485503 (2013).

[103] C. S. Lee, H. J. Yoon, S. I. Yoon, S. H. Yoon, M. S. Jung, D. W. Kim, and T. Won, *SID Symposium Digest of Technical Papers* **36**, 982 (2005).

[104] S. J. Hwang, S. M. Kim, Y. J. Lim, S. H. Lee, G.-D. Lee, J.-J. Lyu, and K. H. Kim, *Current Applied Physics* **9**, 556 (2009).

[105] J. Lee, V. C. Sundar, J. R. Heine, M. G. Bawendi, and K. F. Jensen, *Advanced Materials* **12**, 1102 (2000).

[106] H. S. Jang, H. Yang, S. W. Kim, J. Y. Han, S.-G. Lee, and D. Y. Jeon, *Advanced Materials* **20**, 2696 (2008).

[107] H. C. Yoon, H. Kang, S. Lee, J. H. Oh, H. Yang, and Y. R. Do, *Applied Materials and Interfaces* **8**, 18189 (2016).

Publication

1. International paper

1. **J.-H. Suh**, I.-H. Lee, S. Kang and S.-D. Lee, “Color-separated patterns of quantum dots for high color purity brightness in liquid crystal display”, (*Journal of Display Technology*, in preparation).

2. S.-U. Kim, B.-Y. Lee, **J.-H. Suh**, J. Kim, J.-H. Na and S.-D. Lee, “Reduction of gamma distortions in liquid crystal display by anisotropic voltage-dividing layer of reactive mesogens”, *Liquid Crystals* **44**, 364 (2017).

3. S.-U. Kim, J. Kim, **J.-H. Suh**, J.-H. Na, and S.-D. Lee, “Concept of active parallax barrier on polarizing interlayer for near-viewing autostereoscopic displays”, *Optics Express* **24**, 25010 (2016).

4. Y.-S. Ryu, N. J. Wittenberg, **J.-H. Suh**, S.-W. Lee, Y. Sohn, S.-H. Oh, A. N. Parikh and S.-D. Lee, “Continuity of

monolayer-bilayer junctions for localization of lipid raft microdomains in model membranes", *Scientific Reports* **6**, 26823 (2016).

5. H.-L. Park, B.-Y. Lee, S.-U. Kim, **J.-H. Suh**, M.-H. Kim, and S.-D. Lee, "Importance of surface modification of a microcontact stamp for pattern fidelity of soluble organic semiconductors", *Journal of Micro/Nanolithography Mems and MOEMS* **15** 013501 (2016).
6. Y.-S. Ryu, **J.-H. Suh**, M.-H. Kim, Y. Sohn, and S.-D. Lee, "Dynamic manipulation of charged lipids in model membrane for bio-microarrays", *Journal of Nanoscience and Nanotechnology* **16**, 6355 (2016).
7. *(cover image)* **J.-H. Suh**, J. Kim, Y.-S. Ryu, Y. Sohn, and S.-D. Lee, "Control of surface anchoring properties of liquid crystal by thermo-transfer printing of siloxane oligomers", *Liquid Crystals* **42**, 1236 (2015).
8. J. Kim, **J.-H. Suh**, B.-Y. Lee, S.-U. Kim and S.-D. Lee, "Optically switchable grating based on dye-doped ferroelectric liquid crystal with high efficiency", *Optics Express* **23**, 12619 (2015).
9. **J.-H. Suh**, S.-W. Lee, Y.-S. Ryu, Y. Sohn and S.-D. Lee, "Coarsening nature of liquid-ordered domain in model membrane", *Molecular Crystals and Liquid Crystals* **600**, 81 (2014).

10. Y.-S. Ryu, I.-H. Lee, **J.-H. Suh**, S. C. Park, S. Oh, L. R. Jordan, N. J. Wittenberg, S.-H. Oh, N. L. Jeon, B. Lee, A. N. Parikh, and S.-D. Lee, "Reconstituting ring-rafts in bud-mimicking topography of model membranes", *Nature Communications* **5**, 4507 (2014).

11. S. Kim, Y.-R. Ryu, **J.-H. Suh**, C.-M. Keum, Y. Sohn, and S.-D. Lee, "Biocompatible patterning of proteins on wettability gradient surface by thermo-transfer printing", *Journal of Nanoscience and Nanotechnology* **14**, 6069 (2014).

2. Domestic paper

1. **J.-H. Suh,** J. Kim, S.-U. Kim, B.-Y. Lee, and S.-D. Lee, "Reduction of gamma distortions of liquid crystal display by anchoring disparity in vertical alignment", (*Journal of Information Displays*, in preparation).

2. E.-S. Yu, S.-U. Kim, **J.-H. Suh**, J. Kim, J.-H. Na and S.-D. Lee, "The domain mixing effect on the electro-optical properties of liquid crystals using polyimide doped with reactive mesogen", *Journal of Information Displays* **17**, 125 (2016).

3. (Invited) J. Kim, S.-U. Kim, B.-Y. Lee, **J.-H. Suh** and S.-D. Lee, "Lenticular lens array based on liquid crystal with a polarization-dependent focusing effect for 2D-3D mage applications", *Journal of Information Displays* **16**, 11 (2015).

3. International proceedings

1. H.-L. Park, B.-Y. Lee, S.-U. Kim, **J.-H. Suh**, M.-H. Kim, and S.-D. Lee, "Importance of surface modification of a micro-contact stamp for pattern fidelity of soluble organic semiconductors", *Proceeding of SPIE* **9568**, 956815 (2015).

4. International Conference

1. S. Kang, **J.-H. Suh**, B.-Y. Lee, C. Kim, and S.-D. Lee, "Optical Micro-Resonators Based on Reactive-Mesogen Doped with Quantum-Dots for Color Elements", *The 6th SLCP* (Tianjin, China, 2017)

2. H. Kim, H.-L. Park, S.-U. Kim, **J.-H. Suh**, B.-Y. Lee and S.-D. Lee, "Construction of high fidelity patterns of solution-processed organic light-emitting diodes using surface modified banks by wettability", *The 16th International Meeting of Information Display* (Jeju, Korea, 2016).

3. **J.-H. Suh**, I.-H. Lee, S. Kang, and S.-D. Lee, "Color-separated patterns of quantum dots for high brightness in liquid crystal display", *The 26th International Liquid Crystal Conference* (Kent, OH, USA, 2016).

4. E.-S. Yu, S.-U. Kim, **J.-H. Suh**, J. Kim and S.-D. Lee,

"Dependence of the electro-optical properties of vertically aligned liquid crystal device by domain separation of reactive mesogens", *The 4th SLCP* (Shenzhen, China, 2015).

5. **J.-H. Suh**, B.-Y. Lee, J. Kim, S.-U. Kim, and S.-D. Lee, "Wide-range control of liquid crystal anchoring energy based on siloxane oligomer transfer", *ACLC 2015* (Busan, Korea, 2015).

6. E.-S. Yu, S.-U. Kim, **J.-H. Suh**, J. Kim, and S.-D. Lee, "Control of the anchoring energy in the vertical alignment by a homeotropic alignment agent blended with a reactive mesogen", *The 14th International Meeting of Information Display* (Daegu, Korea, 2014).

7. J. Kim, S.-U. Kim, B.-Y. Lee, **J.-H. Suh**, and S.-D. Lee, "Imprinted lenticular lens array based on liquid crystal for autostereoscopic 2D/3D switchable displays", *The 14th International Meeting of Information Display* (Daegu, Korea, 2014).

8. **J.-H. Suh**, J. Kim, and S.-D. Lee, "Control of liquid crystal pretilt by thermally assisted-transfer of siloxane oligomers during contact printing", *The 25th International Liquid Crystal Conference* (Dublin, Ireland, 2014).

9. S.-W. Lee, Y.-S. Ryu, **J.-H. Suh**, Y Sohn, and S.-D. Lee "Coarsening Nature of Liquid-Ordered Domains in Model Membrane" *KJF International Conference on Organic*

Materials for Electronics and Photonics (Busan, Korea, 2013)

10. Y.-S. Ryu, **J.-H. Suh**, B.-Y. Lee and S.-D. Lee, "Continuous monolayer-bilayer binary membrane array fabricated by hydrophobicity controlled by PDMS transfer method", *Faraday Discussion 161* (London, UK, 2012).

11. S. Kim, Y.-S. Ryu, **J.-H. Suh**, C.-M. Keum and S.-D. Lee "Authorttability gradient surface generated by thermo-transfer printing of poly(dimethylsiloxane)" *The 23rd International Conference on Molecular Electronics and Devices* (Suwon, Korea, 2012).

12. **J.-H. Suh**, Y.-S. Ryu, J.-H. Na and S.-D. Lee "Thermally Assisted Transfer Printing Method for Liquid Crystal Alignment with Multidomain Patterns" *International Symposium on Electronics/Optic Functional Molecules* (Shanghai, China, 2012).

국문 초록

액정 디스플레이는 가벼운 패널 무게를 비롯하여 얇은 두께와 낮은 소비전력으로 인하여 평판 디스플레이 시장에서 각광을 받으며 활발히 연구되어 왔다. 기존 음극선관 디스플레이에 비해 높은 명암비, 균일한 휘도, 그리고 빠른 반응속도를 통해 평판 디스플레이 산업에서 주요한 역할을 해왔다. 그러나, 유기 발광 다이오드와 같은 새로운 경쟁 기술들이 평판 디스플레이 산업에서 발달함에 따라, 광시야각이 표현 가능하고 색 순도를 향상시킬 수 있는 액정 디스플레이 개선 기술이 요구되어 왔다.

본 연구에서는 새로운 액정 디스플레이 소자를 설계하여 감마 왜곡 현상(gamma distortion)을 감소시키고 색 표현 범위를 증대시켰다. 먼저, 광시야각 표현 기술 개발을 위해, 중간 계조에서 액정 분자가 서로 다른 방향으로 정렬하는 멀티 도메인(multi-domain) 제작 기술을 제안하였다. 이를 구현하기 위하여, 액정 분자와 기판 간의 고정 에너지(anchoring energy)를 조절할 수 있는 새로운 액정 배향층을 제작하였다. 다리결합 중합체(cross-linked polymer) 내에

결합되지 못한 소중합체(oligomer)를 기판 위로 전사시켜 기판의 표면 친수성을 변화시켰다. 이와 같이 소중합체가 중합체에서 기판으로 전사되는 기작은 확산에 의한 것으로, 확산이 일어날 때 추가적인 열 처리 공정을 통해서 전사되는 소중합체의 양을 조절하였다. 이때, 열 처리 공정에서의 처리 온도를 변화함에 따라 전사되는 소중합체의 양이 변화하였으며 이를 통해 기판 표면의 표면 에너지가 변화하였다. 실제 액정 분자의 정렬도를 나타내는 선경사각(pretilt angle)과 고정 에너지를 측정해 본 결과, 처리 온도가 변화함에 따라 액정 분자가 수평 배향에서 수직 배향으로 변화하였으며 선 경사각과 고정 에너지 모두 넓은 범위에서 변화하였다.

위 결과를 기반으로, 감마 왜곡 현상을 줄이기 위해 고정 에너지 차이를 기반으로 하는 새로운 멀티 도메인 액정 디스플레이 기술을 개발하였다. 앞서 개발한 액정 배향막을 추가적인 액정 배향막으로 사용하여, 하나의 화소 내부에 서로 다른 고정 에너지를 갖는 두 개의 소화소(sub-pixel)을 제작하여, 서로 다른 임계전압(threshold voltage)를 갖는 멀티 도메인을 제작하였다. 이와 같이 서로 다른 임계 전압을 갖는 멀티 도메인은, 정면과 측면에서 액정 디스플레이를 바라볼 때 생기는 상 지연 효과(phase retardation)를 보상하여 감마 왜곡 현상을 감소 시킬 수 있다. 소중합체 전사를 증대시키기 위해, 자외선-오존 (ultra-violet ozone) 처리를 추가하였으며, 처리시간을 바꾸어 가면서 고정 에너지 조절층의

액정 배향 특성을 실험적으로 분석하였다. 이를 실제 8-도메인(8-domain) 액정 광학 소자 제작에 응용하여, 일반적인 4-도메인(4-domain) 액정 광학 소자와의 실험적인 비교를 통해 본 기술의 응용 가능성을 검토하였다.

이후, 고분자 매트릭스(polymer matrix) 기반의 양자점 발광을 통해 색을 구현하는 새로운 양자점 액정 디스플레이 소자를 제안하였다. 현재까지, 액정 디스플레이를 비롯한 유기 발광 다이오드 디스플레이에 이르기까지 평판 디스플레이 색 재현에 응용하기 위해 다양한 고분자 매트릭스 기반의 양자점 패터닝 기술들이 개발되었으나, 불균일한 발광 특성으로 인해 칼라필터 없이 색 재현하는 것은 불가능하였다. 본 연구에서는, 광경화가 가능하고, 투명한 반응성 메조겐(reactive mesogen)을 고분자 매트릭스로 사용하여 양자점을 고분자 매트릭스 내에 고르게 분포시켰다. 반응성 메조겐과 양자점 간의 혼합 비율을 변화시켜가며 양자점의 발광 특성을 실험적으로 분석하였으며, 기존의 포토-리소그래피(photo-lithography) 공정을 반복적으로 실시하여 한 기판 내에 균일한 발광 특성을 갖는 적색, 녹색, 그리고 청색 패턴을 제작하였다.

마지막으로, 앞서 제작한 양자점 패턴을 이용하여 높은 색 순도를 갖는 새로운 양자점 발광 액정 디스플레이를 제안하였다. 수직 배향 액정 광학 소자에 구동 전압 변화를 통해 광원에서 발생한 빛의 투과도를 조절하고 이를 통해 양자점의

포토루미넌스(photo-luminescence) 발광을 조절하는 소자를 설계하였다. 기존 백색 광과 칼라 필터를 사용하는 기존의 액정 디스플레이, 양자점을 보상층으로 사용하는 청색 광과 칼라 필터를 사용하는 기존의 양자점 디스플레이와의 비교를 통해, 본 연구에서 새롭게 제안된 디스플레이 소자의 색 순도 및 색 표현 범위 확장 가능성을 검토하였다.

결론에서는, 본 연구에서 제안된 광시야각 기술 및 색 재현 기술의 실제 산업 응용 가능성을 검토해보았다. 본 논문을 통해 제시된 새로운 디스플레이 소자 구조와 실험 결과들은 보다 향상된 성능을 갖는 차세대 액정 디스플레이 소자 개발 기술 진보에 이바지 할 것이다.

주요어: 액정, 열 전사 프린팅 기술, 광 시야각 디스플레이, 양자점, 고분자 매트릭스 기반 양자점, 양자점 발광 액정 디스플레이.

학번: 2012-30937